NUREG/CR-3900
Vol. 1

Long-Term Performance of Materials Used for High-Level Waste Packaging

First Quarterly Report, Year Three
April - June 1984

Compiled by D. Stahl, N. E. Miller

Battelle's Columbus Laboratories

Prepared for
U.S. Nuclear Regulatory Commission

GPO Printed copy price: $5.00

NUREG/CR-3900
Vol. 1

Long-Term Performance of Materials Used for High-Level Waste Packaging

First Quarterly Report, Year Three
April - June 1984

Manuscript Completed: July 1984
Date Published: September 1984

Compiled by
D. Stahl, N. E. Miller

Battelle's Columbus Laboratories
505 King Avenue
Columbus, OH 43201-2693

Prepared for
Division of Radiation Programs and Earth Sciences
Office of Nuclear Regulatory Research
U.S. Nuclear Regulatory Commission
Washington, D.C. 20555
NRC FIN B6764
Under Contract No. NRC 04-82-015

ABSTRACT

As part of the Nuclear Regulatory Commission's requirement to assess the Department of Energy's application to construct geologic repositories for storing high-level radioactive waste, Battelle's Columbus Laboratories is investigating the long-term performance of materials used for high-level waste packaging. Devitrification severity of glass waste forms is being studied in terms of volume fraction of crystallization and crystal grain size. Glass-water contact during the heating and cooling periods of glass leaching experiments is being evaluated for its effect on the overall results of the isothermal period. Modeling efforts included the study of possible colloid formation and the change of water chemistry during glass dissolution. The electrochemical properties of container steels were found to be only slightly affected by the groundwater-species concentration, the presence of basalt rock, or the steels' cleanliness or microstructure. Hydrogen-embrittlement susceptibility may increase at expected repository temperatures. Results of the corrosion-modeling effort suggest that radiolysis may significantly affect general-corrosion kinetics. The water-radiolysis model was extended to account for more groundwater species and was used to predict the concentrations of two species in aqueous iron sulfate; results were compared with experimental data. A method was selected for performing uncertainty analyses of waste-package models. Integral experiments have been designed to address the combined effects of repository conditions on the waste package.

This report documents investigations performed during the period April 1984 through June 1984.

TABLE OF CONTENTS

TABLE OF CONTENTS
(Continued)

TABLE OF CONTENTS
(Continued)

LIST OF FIGURES

LIST OF FIGURES
(Continued)

LIST OF FIGURES
(Continued)

LIST OF TABLES

LIST OF TABLES

PREVIOUS REPORTS IN SERIES

NUREG/CR-3405, Volume 1: "Long-Term Performance of Materials Used for High-Level Waste Packaging: Annual Report, March 1982-April 1983."

NUREG/CR-3427, Volume 1: "Long-Term Performance of Materials Used for High-Level Waste Packaging: Quarterly Report, April-June 1983."

NUREG/CR-3427, Volume 2: "Long-Term Performance of Materials Used for High-Level Waste Packaging: Quarterly Report, July-September 1983."

NUREG/CR-3427, Volume 3: "Long-Term Performance of Materials Used for High-Level Waste Packaging: Quarterly Report, October-December 1983."

NUREG/CR-3427, Volume 4: "Long-Term Performance of Materials Used for High-Level Waste Packaging: Annual Report, April 1983-April 1984."

1. INTRODUCTION: PROJECT OBJECTIVES AND APPROACH

The Waste Policy Act of 1982 delegates to the Department of Energy (DOE) the authority for siting, construction, and operation of deep-mined geologic repositories for the disposal of high-level waste and spent fuel. The Nuclear Regulatory Commission (NRC) has the responsibility to regulate the activities of DOE to assure that the health and safety of the repository workers and of the public are adequately protected. Prior to construction, the DOE will submit a license application to the NRC describing in detail the proposed repository. The DOE has been directed to take a multiple barrier approach to the isolation of radioactive wastes with the waste package, the engineered facility, and the natural geohydrologic features of the site being the major barriers. Since NRC's compliance assessment requires the technical capability to understand relevant phenomena and processes relating to the long-term performance of the multiple barriers, the NRC's Office of Nuclear Regulatory Research (RES) has established this waste-package performance program at Battelle's Columbus Laboratories to provide that part of the input to the assessment. As an important aid to this understanding, Battelle is evaluating total system performance which will integrate separate effects and improve the understanding of the long-term performance of waste-package materials. This will also assist in identifying and evaluating research needs.

It is generally accepted that after repository closure the dominant mechanism to cause the release of radionuclides from the repository is groundwater transport. The generally accepted approach to minimizing the release is to provide a number of different barriers to the dissolution and transport of radionuclides by the groundwater. For a deep-mined repository, the geohydrologic features of the earth itself are expected to be a major barrier to the release of radionuclides. The repository site will be selected so that radionuclides will be isolated for very long times. In addition, engineered features of the repository will act as a barrier to the release of radionuclides. The repository will be constructed so as to minimize disturbing the adjacent rock and to accommodate the thermomechanical effects of the emplaced wastes with a minimum of degradation to its geohydrologic properties. Upon closure, the underground openings and shafts to the surface will be backfilled and sealed to minimize groundwater flow paths.

The waste package--which is the center of this study--will be constructed to provide essentially complete containment of the radionuclides through the period of time in which the repository is heated significantly by decaying fission products. After the container is eventually breached by some process, the waste form must remain sufficiently resistant to groundwater attack to provide high retention of the radionuclides and, together with the repository, to control the release of radionuclides for thousands of years. The objective of our research is to provide an improved understanding of the long-term performance of the materials used for the high-level waste package. More specifically, we are identifying those processes that tend to degrade the performance

of the waste-package materials, performing experiments to produce data where data are otherwise lacking on material performance, and analytically modeling the processes to utilize the data to better understand how the processes will affect material's future performance. In addition, we are identifying areas of work that should be performed by DOE to provide missing data which are beyond the resources of the NRC.

1.1 Individual Program Tasks

The program is being conducted in three parallel efforts: waste-form studies, container studies, and integrated system performance studies. A more detailed summary of achievements can be found in the second annual report for this program (NUREG/CR-3427, Volume 4, June 1984, Section 1).

1.1.1 Waste Forms

The waste-form studies are aimed at first describing and modeling those mechanisms that will alter or "age" the waste form during the containment period, and second, identifying and describing those processes that will influence waste-form dissolution after it is exposed to groundwater. The waste-form studies have been largely centered on borosilicate glasses for both defense and commercial high-level wastes; some effort has also been directed toward evaluating spent fuel as a waste form.

In borosilicate glasses, the glass-forming agents can be expected to be tailored to optimize the waste-form properties for each type of high-level waste. After the waste forms are produced, particularly during the very long period of time after disposal while sealed in their containers, they will experience processes that will cause changes. One detrimental effect is devitrification of the glass, which can lead both to new phases with increased solubility and to cracking of the glass (which is detrimental because it allows a greater surface area of the glass to be contacted by the groundwater). A model has been developed to predict the degree of devitrification that will occur from subsequent reheating in the repository after disposal. Another detrimental effect is cracking, which could be induced by the effects of radiation on glass. A study of the radiation effects on glass has revealed no new approach to evaluating this phenomenon experimentally, so we are largely dependent on the existing literature which indicates that radiation produces only a small effect on glass performance.

1.1.2 Container Materials

The container studies focus on processes that can degrade the metallic waste-package container. The objective is to collect data on the parameters that influence the degradation processes, to identify the controlling parameters, and ultimately to model the degradation processes that determine the long-term performance of the container. The material under study is cast low-carbon steel for use in a basalt repository, which is the material currently favored by DOE.

This experiment is in progress and its results will be presented in the next quarterly report.

2.1.2 Crystallinity Influences

Some of the evaluations conducted in the first and second project years indicated that a fraction of crystallinity may be induced by devitrification of the glass. Before undertaking a detailed description of this crystallinity, its detrimental character needs to be determined. The work of Hench and Clark[2.1] showed that volume fractions of crystallinity from 35 to 100 percent could reduce the durability of SRL 131-29.8 percent TDS-3A waste glass to as little as 1/40 of its original durability. They further discussed a mechanism of preferential attack at the glass/crystal interface.[2.2] Therefore two parameters, the volume fraction crystallized and the grain size of the resultant crystals, could influence the corrosion characteristics of devitrified glass. To assess these characteristics, an experiment which exposes two different volume-fractions-crystallized at two different crystal sizes is planned. However, before this experiment can be conducted, a means for generating those specimens is needed.

Heterogenous nucleation is the best means of fixing crystal sizes and volume fractions under isothermal heat-treatment conditions. The occurrence of RuO_2 as a melt insoluble in PNL 76-68 glass, simulated by MCC 76-68, provides an intrinsic nucleation site that should not distort subsequent leaching results. Furthermore, isothermal crystallization experiments by Uhlmann and coworkers[2.3] have shown that time, temperature, and the number of nucleating particles per unit volume determine the volume fraction crystallized.

By choosing different concentrations of nucleating particles, the crystal size may be limited by impingement. For instance, crystal grain diameters of 100 μm and 1 μm should result from respective concentrations of 10^6 and 10^{12} particles per cubic centimeter. These concentrations can be obtained by mixing commercial RuO_2 with MCC 76-68 in weight ratios of 20 mg RuO_2 per gram of glass and 20 μg per gram of glass, if a 0.2 μm mean diameter is assumed for RuO_2.

The temperature range for developing the samples should be between the glass transition temperature for MCC 76-68 (i.e., T_g = 450 C), a temperature at which crystal growth stops, and the liquidus temperature (T_ℓ = 950 C), the temperature at which growth begins. A temperature range of $(T_g + 100\ C) \leq T \leq (T_\ell - 100\ C)$ should be an appropriate starting point.

The isothermal treatment time must also be established. The data of Bickford and Jantzen[2.4] indicate that various defense waste compositions will be significantly devitrified if isothermally treated between 4 and 44 hours at temperatures between T_g and T_ℓ for those glasses. Those glasses are somewhat more resistant to devitrification

to the water-chemistry model, which is a fundamental part of the glass-dissolution model and the general-corrosion model.

The water-chemistry model which we initially developed for our use with our glass-dissolution and corrosion models has intentionally been kept simple. Simplifying assumptions were made and only a limited set of chemical species was used. This set included the basic water species, the species which dominate most natural groundwaters, and certain species which are assumed to result from the corrosion of iron-based metallic containers and from the dissolution of borosilicate glass. Additional species are being incorporated as the model matures. Input to the model includes temperature, oxidation potential, volume of water, and amounts of each of the elements in solution (including those species from the radiolysis code). The water-chemistry model calculates the concentration and activity of each of the water species.

1.2 Overall Program Objectives

In all the program tasks, the ultimate objective is to develop a base of information to assist the NRC in evaluating the performance of the waste package proposed in DOE's license application. A near-term objective is to provide information to allow the NRC to prepare position papers on the information required of DOE for evaluation of DOE's proposed waste package. Of significance here is identifying sensitive parameters affecting the performance of materials and identifying data requirements.

To achieve the above objectives, the waste-form task is providing information to give a better understanding of the release of radionuclides from the waste form, beginning at the time it is first contacted by groundwater through the 10,000-year period defined in the draft EPA Standard. This includes an understanding of the probable physiochemical condition of the waste form when it is contacted by groundwater, as well as the parameters of waste-form composition and environmental conditions which will cause changes from its state at the time of disposal. In addition, we are producing experimental data on the parameters that affect dissolution of the waste form, including composition of the groundwater and environmental conditions. The waste-form dissolution process is also being mathematically modeled to allow analysis of the performance of the waste form under specific input conditions.

The information on the performance of the container materials relates to the required containment period of 300 to 1000 years. The container performance is expected to be most affected by corrosion and hydrogen-attack processes. We are providing information on the parameters of container-material composition, groundwater composition, and environmental conditions that are most significant in these processes. Our studies of cast low-carbon steel in a basalt environment (the container material currently favored by DOE) focus on the susceptibility of the metal to stress-corrosion cracking under repository conditions, because

steel is known to fail by this process in some environments. We are studying the chemical species and environmental conditions that cause cracking to determine whether this mode of failure is expected under credible repository conditions. Our experimental studies on general and localized corrosion, together with our comprehensive general-corrosion model, will assist in evaluating the corrosion-allowance approach for the use of steel as a long-life container.

Modeling efforts in the integrated system performance task are contributing significant information to studies of general corrosion and glass dissolution. These studies require knowledge of the amount and kind of chemical species that may be produced by radiolysis of the groundwater near the waste package as a result of gamma radiation from the enclosed waste. To obtain this information, energy deposition and radiolysis codes are used. The ANISN code is used to calculate the gamma fluxes and energy-deposition rates in and near the waste package over the time after disposal; these have been calculated for commercial high-level waste and for spent-fuel waste forms. The gamma fluxes and energy-deposition rates as a function of time are then used in the water-radiolysis model to calculate the amount and kind of radiolysis products in the groundwater near the waste package. To determine how these radiolysis products may affect the performance of the canister and waste form, it is necessary to determine their chemical activities. These are calculated by the water-chemistry model. The output from the water-chemistry model is the concentration and activity of each chemical species in the groundwater near the waste package. This information is used not only as input to the general-corrosion and glass-dissolution models, but also as a point of reference in directing the experimental efforts in corrosion and dissolution.

2. WASTE FORMS

Waste form experimentation for the third year began in this quarter. As in previous years, experimentation will concentrate on glass waste forms and is based on results of previous experimentation. Experimentation with glasses prepared with real waste will be initiated, as will experimentation with spent fuel.

2.1 Glass Experiments

Four glass experiments are planned for the third year: glass/water contact, crystallinity influences , model validation, and definition of other degradation mechanisms. Experiments with real waste glass and spent fuel are being planned. The goal of each is to develop data that will assist in the evaluation of source terms for radionuclide release to the repository water. The first two experiments, glass/water contact and crystallinity influences, began in the first quarter. The remaining experiments are being planned.

2.1.1 Glass/Water Contact

Some results from the leaching pilot experiment completed in the second project year indicated that spurious data may result from static experiments in which the glass and water are in continuous contact during the heating, isothermal soaking, and cooling periods of an experimental run. Material in solution, either extracted from the specimen or originally present in simulated repository water, may precipitate onto the specimen during cooling from the experimental temperature. Also, reaction with the specimen during heating and cooling periods may introduce anomalies into the data. However, conclusions about experimental conditions usually are drawn from solution chemistry data and surface analyses assuming only an isothermal treatment. Therefore, an experiment has been devised to assess the validity of these assumptions.

In this experiment, a number of samples are in continuous contact with the attacking solution during the entire experiment, while other samples are exposed to the solution only during the isothermal treatment time The experimental matrix is shown in Table 2.1. In all cases, either MCC-1 or MCC-2P protocols are being followed, except for separating some of the samples of glass from the simulated basalt water during the heating and cooling periods.

To accomplish the separation of glass specimen and water, 120-ml acid digestion bombs (Parr Bomb model 4748) were modified to accommodate the glass sample at heights approximately 1/3 of the distance from the bottom or 1/3 of the distance from the top. In all cases, the glass samples, cut to 1 cm cubes and polished to 200 grit SiC, were placed

between two perforated TEFLON* discs, and all the containers were filled with approximately 60 ml or half their volume, of simulated Grande Ronde basalt water. The volume was adjusted to obtain a surface-to-volume ratio of 0.01/mm at the experimental temperature. Some bombs are inverted during the heatup and cooldown periods so the solution contacts the glass during the isothermal period; the other bombs continuously expose the glass to that solution.

Table 2.1. Glass/water contact experimental matrix.

Glass/Water	MCC-1[2]	MCC-2P[3]
Isothermal[1] contact	XXX	XXXX
Continuous[1] contact	XXX	XXXX
Blank[1]	XXX	XXX

(1) X = Replicate samples
(2) 90 C, S/V = 0.01/mm
(3) 190 C, S/V = 0.01/mm.

All containers were placed in two ovens maintained at 90 C and 190 C as determined by a calibrated, type K thermocouple placed in contact with one of the blank containers in each oven. When this thermocouple reached the experimental temperature, the isothermal contact containers were inverted to expose the glass to the basalt water. At the completion of the 28-day exposure period, these containers will be inverted to discontinue contact between the water and the glass samples. They will remain in this position for approximately 1 hour to allow evaporation of surface water; then all bombs will be removed and cooled to room temperature. Once cool, the glass specimens will be removed, weighed, and subjected to surface analyses by appropriate methods such as scanning electron microscopy, secondary ion mass spectrometry, and Auger spectroscopy. After acid digestion, the solution chemistry will be determined.

*TEFLON is a registered trademark of the DuPont de Nemours Company.

This experiment is in progress and its results will be presented in the next quarterly report.

2.1.2 Crystallinity Influences

Some of the evaluations conducted in the first and second project years indicated that a fraction of crystallinity may be induced by devitrification of the glass. Before undertaking a detailed description of this crystallinity, its detrimental character needs to be determined. The work of Hench and Clark[2.1] showed that volume fractions of crystallinity from 35 to 100 percent could reduce the durability of SRL 131-29.8 percent TDS-3A waste glass to as little as 1/40 of its original durability. They further discussed a mechanism of preferential attack at the glass/crystal interface.[2.2] Therefore two parameters, the volume fraction crystallized and the grain size of the resultant crystals, could influence the corrosion characteristics of devitrified glass. To assess these characteristics, an experiment which exposes two different volume-fractions-crystallized at two different crystal sizes is planned. However, before this experiment can be conducted, a means for generating those specimens is needed.

Heterogenous nucleation is the best means of fixing crystal sizes and volume fractions under isothermal heat-treatment conditions. The occurrence of RuO_2 as a melt in oluble in PNL 76-68 glass, simulated by MCC 76-68, provides an intrinsic nucleation site that should not distort subsequent leaching results. Furthermore, isothermal crystallization experiments by Uhlmann and coworkers[2.3] have shown that time, temperature, and the number of nucleating particles per unit volume determine the volume fraction crystallized.

By choosing different concentrations of nucleating particles, the crystal size may be limited by impingement. For instance, crystal grain diameters of 100 μm and 1 μm should result from respective concentrations of 10^6 and 10^{12} particles per cubic centimeter. These concentrations can be obtained by mixing commercial RuO_2 with MCC 76-68 in weight ratios of 20 mg RuO_2 per gram of glass and 20 μg per gram of glass, if a 0.2 μm mean diameter is assumed for RuO_2.

The temperature range for developing the samples should be between the glass transition temperature for MCC 76-68 (i.e., T_g = 450 C), a temperature at which crystal growth stops, and the liquidus temperature (T_ℓ = 950 C), the temperature at which growth begins. A temperature range of (T_g + 100 C) $\leq T \leq$ (T_ℓ - 100 C) should be an appropriate starting point.

The isothermal treatment time must also be established. The data of Bickford and Jantzen[2.4] indicate that various defense waste compositions will be significantly devitrified if isothermally treated between 4 and 44 hours at temperatures between T_g and T_ℓ for those glasses. Those glasses are somewhat more resistant to devitrification

than MCC 76-68 because of their high Al_2O_3 content, so isothermal treatment times of 4 and 44 hours should also suffice for MCC 76-63 glass.

The method of response-surface exploration can be used to develop the time, temperature, and nuclei concentrations that should lead to the required volume-fractions-crystallized and crystal sizes. This method is a statistical design that can be used to find maximum and minimum response conditions without knowledge of exact, functional relationships. For the variables to be explored, a central composite design[2.5] can be used to accommodate quadratic effects in all the variables and should be adequate for the present purposes. This design is presented pictorially in Figure 2.1; the corresponding coordinates are presented in Table 2.2. As previously discussed, they are based on the following initial values of the experimental variables:

Variable	Low	High
T, C	550	850
t, hours	4	44
n, #/cc	10^6	10^{12}

At each condition, the volume-fraction-crystallized and the mean particle size will be determined by standard techniques.

This experiment has begun, and it is expected to be completed in the second quarter. Once these data are in hand they will be used to select conditions for obtaining specimens needed for corrosion testing at different volume-fractions-crystallized and mean crystal diameters.

2.1.3 Future Experimental Work

An experiment to assess the validity of a glass-dissolution model is being planned. This model postulates nuclear-waste-glass dissolution to lie between that of quartz and amorphous silica, as shown in Figure 2.2. An experiment to test this model will involve isothermally treating samples of quartz, amorphous silica, and waste glass specimens for various times. The details of this experiment are partially dependent on the glass/water contact experiment and will be established when that experiment has been completed.

The fourth glass-waste-form experiment is, in reality, a series of experiments intended to address the influence of various environmental factors on glass corrosion. A partial list of accelerating variables is presented in Table 2.3. As with the dissolution-model experiment, this experiment depends in part on the results of the glass/water contact experiment. However, this final series of experiments is in the very early planning stages. Plans should be completed in the second quarter of this project year.

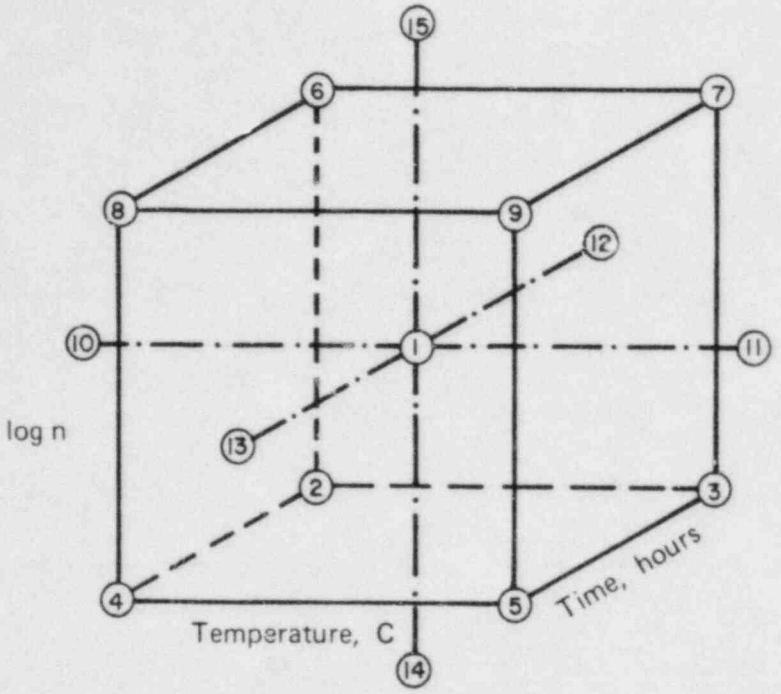

Figure 2.1. Coordinates and levels of central composite design.

Table 2.2. Coordinates and levels of central composite design.

Point	Coordinates	T, C	t, hours	log n
1	(0,0,0)	700	24	9
2	(-1,-1,-1)	610	12	7.25
3	(1,-1,-1)	790	12	7.25
4	(-1,1,-1)	610	36	7.25
5	(1,1,-1)	790	36	7.25
6	(-1,-1,1)	610	12	10.75
7	(1,-1,1)	790	12	10.75
8	(-1,1,1)	610	36	10.75
9	(1,1,1)	790	36	10.75
10	(-1.68,0,0)	550	24	9
11	(1.68,0,0)	850	24	9
12	(0,-1.68,0)	700	4	9
13	(0,1.68,0)	700	44	9
14	(0,0,-1.68)	700	24	6
15	(0,0,1.68)	700	24	12

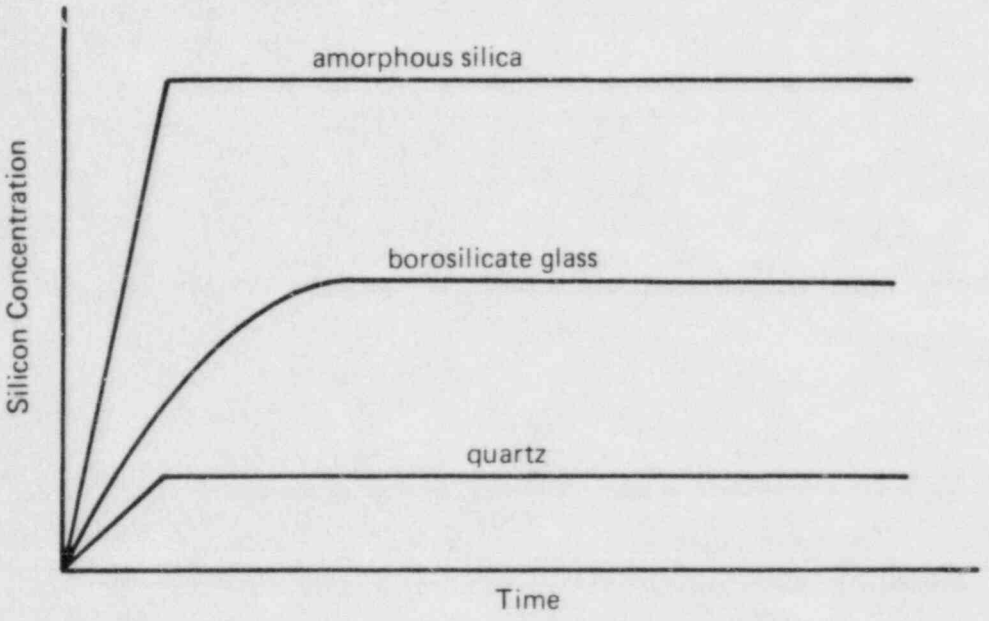

Figure 2.2. Proposed model for glass leaching.

Table 2.3. Preliminary list of factors that may accelerate glass leaching.

Factor	Potential Sources	Postulated Mechanisms for Accelerating Glass Leaching
1. Natural organic acids	Groundwater, packing material, rock	Increases in solubility of nonsiliceous glass components via complexation with polyvalent cations such as metals and transuranics
2. F^-	Groundwater, rock	Complexation with silica (e.g., SiF_6^{2-})
3. Cl^-	Groundwater, rock	Complexation with silica
4. High pH	Ambient groundwater with or without interaction with waste package	Increase in silica solubility via reaction: $H_4SiO_4^\circ \rightleftarrows H_3SiO_4^- + H^+$ which occurs at pH 10.5 and above
5. Eh (redox)	Ambient groundwater with or without interaction with waste package	Solubility of selected glass components may be Eh-sensitive
6. Soft iron	Canister, overpack	Iron silicate precipitation
7. Aluminum	Leached rock and packing material	May lead to aluminum silicate precipitation, analogous to iron silicate precipitation
8. Temperature	Waste package	Silica solubility increases with increasing temperature

2.2 Glass Dissolution/Reprecipitation Modeling

During this quarter, two assumptions were examined. The assumption that the effective rate constant for precipitate growth remained constant during glass dissolution/reprecipitation was revised to take into account the effects of possible colloid formation. In addition, the effect on water chemistry of a time-dependent, rather than a constant, concentration of dissolved silicon-bearing species was examined.

2.2.1 Kinetics of Glass Dissolution/Reprecipitation

In the recently issued Annual Report for the second year of this program,[2.6] results were presented of some initial modeling studies relative to the reprecipitation of dissolved glass species as part of a more stable phase. As discussed therein, the simultaneous occurrence of glass dissolution and precipitate growth takes place when $C_o' < C < C_o$. Here, C is the instantaneous, time-dependent concentration, within a closed volume V of groundwater, of the glass component that controls dissolution. C_o' and C_o are the saturation concentrations of this particular species relative to the precipitate and the glass, respectively. Within this regime, the rate at which C changes with time t was taken as

$$\frac{dC}{dt} = \frac{KS}{V}(C_o - C) + K'(C_o' - C) \qquad (2.1)$$

where K is a rate constant for glass dissolution, S is the surface area of glass exposed to the groundwater, and K' is an effective rate constant for growth of the precipitate.

In the original calculations[2.6], K' was chosen to be time-independent, and the predicted variation of C with t that resulted did indeed exhibit behavior that has been observed experimentally (e.g., nepheline dissolution with gibbsite precipitation, as reviewed by Lasaga[2.7]), i.e.,

- $C\ (t \to \infty) = \text{constant}$
- $C_o' < C\ (t \to \infty) < C_o$

During the past reporting period, calculations were undertaken in which K' was no longer treated as a constant, but rather as an increasing function of time. Such behavior might be expected, for example, for the growth of colloidal particles from solution, which, as they grow, present an increasing amount of surface area to the surrounding groundwater and thus are able to transport the dissolved species from solution at faster net rates. On the other hand, treatment of K' as a constant may be more characteristic of growth of the precipitate as layers on adjacent surfaces, for which the amount of exposed area remains approximately constant.

The particular form assumed for K', at least for the present, was

$$K'(t) = a + b\,(t - t_p) \tag{2.2}$$

where a and b are time-independent parameters (but possibly temperature-dependent, although temperature variations are not being considered here), and the time t_p is defined such that

$$C(t_p) = C_o'$$

Thus, times within the range $t > t_p$ are of interest in solving Equations 2.1 and 2.2. Clearly, the special case for which $b = 0$ corresponds to that which had been previously treated.(2.6)

Equation 2.2 was cast in linear form for simplicity in accounting for a K' parameter that increases with time, rather than for a physically realistic representation of actual reprecipitation kinetics. Unfortunately, however, even the simple form of Equation 2.2 yields results that are rather complex, as compared to the case for which $b = 0$.

Proceeding with the analysis, Equations 2.1 and 2.2 can be combined and expressed in terms of dimensionless variables and parameters to yield

$$\frac{ds}{d\xi} + \gamma\xi s = 1 + (\gamma\xi - 1)r \tag{2.3}$$

where

$$s \equiv C/C_o \tag{2.4a}$$

$$r \equiv C_o'/C_o \tag{2.4b}$$

$$\gamma \equiv b\left(\frac{V}{KS}\right)^2 \tag{2.4c}$$

$$\xi \equiv \frac{1+\beta}{\gamma} + \tau - \tau_p \tag{2.4d}$$

where

$$\beta \equiv \frac{aV}{KS} \tag{2.4e}$$

$$\tau \equiv KSt/V \tag{2.4f}$$

$$\tau_p \equiv KSt_p/V \tag{2.4g}$$

The definitions of s, r, β, τ, and τ_p given here are consistent with those presented in Reference 2.6. The explicit dependence of τ_p upon r is given in Equation 2.20 of that reference.

Equation 2.3 can be easily solved, subject to the initial condition $s(\xi_p) = r$, where $\xi_p \equiv \xi(\tau = \tau_p)$, to yield the rather complex expression

$$s = r + (1-r)\left(\frac{2}{\gamma}\right)^{1/2}\left\{F\left[\left(\frac{\gamma}{2}\right)^{1/2}\xi\right] - F\left[\left(\frac{\gamma}{2}\right)^{1/2}\xi_p\right]\exp\left[\frac{\gamma}{2}\left(\xi_p^2 - \xi^2\right)\right]\right\} \tag{2.5}$$

where F is Dawson's integral, defined in general as[2.8]

$$F(z) = e^{-z^2}\int_0^z e^{u^2}\,du \tag{2.6}$$

Unfortunately, F(z) is not an elementary function; its values must be computed numerically.

Analysis of the properties of $s(\xi)$ is currently in progress. However, one particular feature that can readily be deduced is the behavior of s at asymptotic times, i.e., $\xi \to \infty$. Toward this end, we use a well-known relation[2.8],

$$F(z) = \frac{\pi^{1/2}}{2i} e^{-z^2} \operatorname{erf}(iz) \tag{2.7}$$

together with the asymptotic expansion for the complement of the error function[2.9],

$$\operatorname{erfc}(z) \sim \frac{e^{-z^2}}{z\pi^{1/2}} \left[1 + 0\left(\frac{1}{z^2}\right)\right] \tag{2.8}$$

Equation 2.8 is valid for $z \to \infty$ and $|\arg(z)| < 3\pi/4$. Noting that $\operatorname{erf}(z) = 1 - \operatorname{erfc}(z)$, one can combine Equations 2.7 and 2.8 to obtain

$$F(z) \sim \frac{\pi^{1/2} e^{-z^2}}{2i} + \frac{1}{2z}\left[1 + 0\left(\frac{1}{z^2}\right)\right] \tag{2.9}$$

If z is real,

$$F(z) \sim \frac{1}{2z} \tag{2.10}$$

From Equations 2.5 and 2.10, we obtain

$$s \sim r \tag{2.11}$$

in the limit as $\xi \to \infty$. Consequently, we see from Equations 2.4a, 2.4b, and 2.11 that

$$C \sim C_0' \tag{2.12}$$

as $t \to \infty$. What this means is that as the time becomes asymptotically large, the concentration of the species controlling glass dissolution, within the closed volume of groundwater, gradually approaches the saturation level of that species relative to the precipitate. Of course, such behavior is expected, since from Equation 2.2, K' becomes very large as t increases, and in turn, from Equation 2.1, C must approach C_0' in order to maintain dC/dt at a finite level.

Further examination of the properties of the function $s(\xi)$ will be carried out during the near term. Selected numerical examples will be used to illustrate general features of these properties. The ultimate

goal of these calculations is, of course, to determine effects that reprecipitation has on the overall amount of glass that has dissolved within the groundwater.

2.2.2 Water Chemistry During Glass Dissolution

The water-chemistry model has been used to calculate the changes occurring in water chemistry as waste-form dissolution proceeds and to predict the effects of these changes on the rate of dissolution of a glass waste form. We have assumed that dissolution obeys a linear rate law:

$$\frac{dC}{dt} = k\ (C_0 - C) \tag{2.13}$$

where C is the total concentration of the solubility-limiting element in the solution, t is time, C_0 is the concentration of the solubility-limiting element at saturation, and k is a constant. The definitions of C and C_0 used here are consistent with those used in Section 2.2.1, and the parameter k used here is equivalent to KS/V used in that section. It is assumed that k will be constant for isothermal dissolution of a given waste form. For our calculations, we use dimensionless units and assume k = 1. In this case, the unit of time is the time constant for Equation 2.13. Silicon is assumed to be the solubility-limiting element; all other elements are assumed to dissolve readily compared to silicon (as SiO_2). In addition, it is assumed that the waste form dissolves congruently.

All these assumptions are more or less standard for glass-dissolution calculations. The feature that makes this calculation significantly more realistic than others is that C_0 is not assumed to be constant. Instead, it is assumed that the activity of nonionized silicic acid (H_4SiO_4) is independent of pH and that the increase in silica solubility at high pH is due to ionization. This is in good agreement with experimental data[2.10] on silica solubility.

The composition of the waste form was based on PNL 77-260 glass. PNL 77-260 contains several elements that are not presently included in our water-chemistry model, so we used a simplified glass composition containing oxides of silicon, boron, sodium, and calcium in the mole ratios Si:B:Na:Ca = 1.0 : 0.432 : 0.431 : 0.709.

Two different waters were used for our calculations, pure water and synthetic Grande Ronde basalt groundwater.[2.11] Since not all of the elements in the synthetic groundwater composition described by Jones in Reference 2.11 are included in the water-chemistry model, the composition of the groundwater was modified by lumping sodium and potassium as sodium, and fluorine and chlorine as chlorine. Treating potassium the same as sodium is expected to have a negligible effect on pH calculations, since both NaOH and KOH are strong alkalis. Treating fluorine the same as chlorine is less well justified since HF is a relatively

weak acid while HCl is a strong acid. However, the pH as calculated using this scheme was compared with the pH calculated by a more complete water-chemistry program which did not require lumping of elements, and the difference was about 0.02 pH units.[2.12] This is considered to be sufficiently accurate for our purposes.

The differential equation for glass dissolution (Equation 2.13) is solved by the following conceptual process. From the composition of the initial groundwater, the pH is calculated, and this is used to calculate C_o. The initial rate of dissolution can now be calculated from Equation 2.13. The waste form is allowed to dissolve congruently for a short period of time, thus changing the composition of the groundwater. The process above is then repeated for the modified groundwater composition. In general, it is to be expected that C_o will change with time and that the dissolution rate will not follow a simple exponential curve. This is indeed the case, as shown in Figures 2.3 and 2.4. In the case of pure water, the dissolution rate reaches a maximum at a normalized time of about 0.07. For the synthetic basalt groundwater, however, the dissolution rate drops monotonically from its initial value. The reason for these two very different behaviors can be seen from Figures 2.5 and 2.6. As the waste form dissolves in pure water, its pH rapidly increases from its initial value of 7, and the total concentration of silicon at saturation, C_o, also increases, raising the dissolution rate. In contrast, the pH of the synthetic basalt groundwater drops as the waste form dissolves. That reduces the saturation concentration of silicon, resulting in a lower dissolution rate.

From these results, it is apparent that short-term glass degradation data must be interpreted with caution. In the case of pure water, the theory predicts that the dissolution rate will increase with time, at least at short times. Such experimental data might be incorrectly interpreted as suggesting that the waste form is undergoing catastrophic degradation. In the case of synthetic basalt groundwater, the theory predicts a rapid decrease of the dissolution rate with time. This might lead to an overestimate of the stability of the waste form.

2.3 Radiation Damage and Spent Fuel

A detailed experimental matrix for scoping the influence of various radiation-damage mechanisms on glass corrosion and spent-fuel behavior is presented in Section 4 of this report. Part of the activity in the glass-waste-form effort will be to define an experimental path from the hot-cell experiments to simulation experiments. In this way, corrosion changes induced by the various conditions in the hot cell may be related to possible experimental influences which can be evaluated in subsequent experiments. This effort is in the planning stage.

Experimentation with spent fuel, simulated or real, is not yet clearly defined. Efforts to establish the most worthwhile procedures began in this project quarter. As these procedures become more clearly defined, specific experimental plans will be developed and executed.

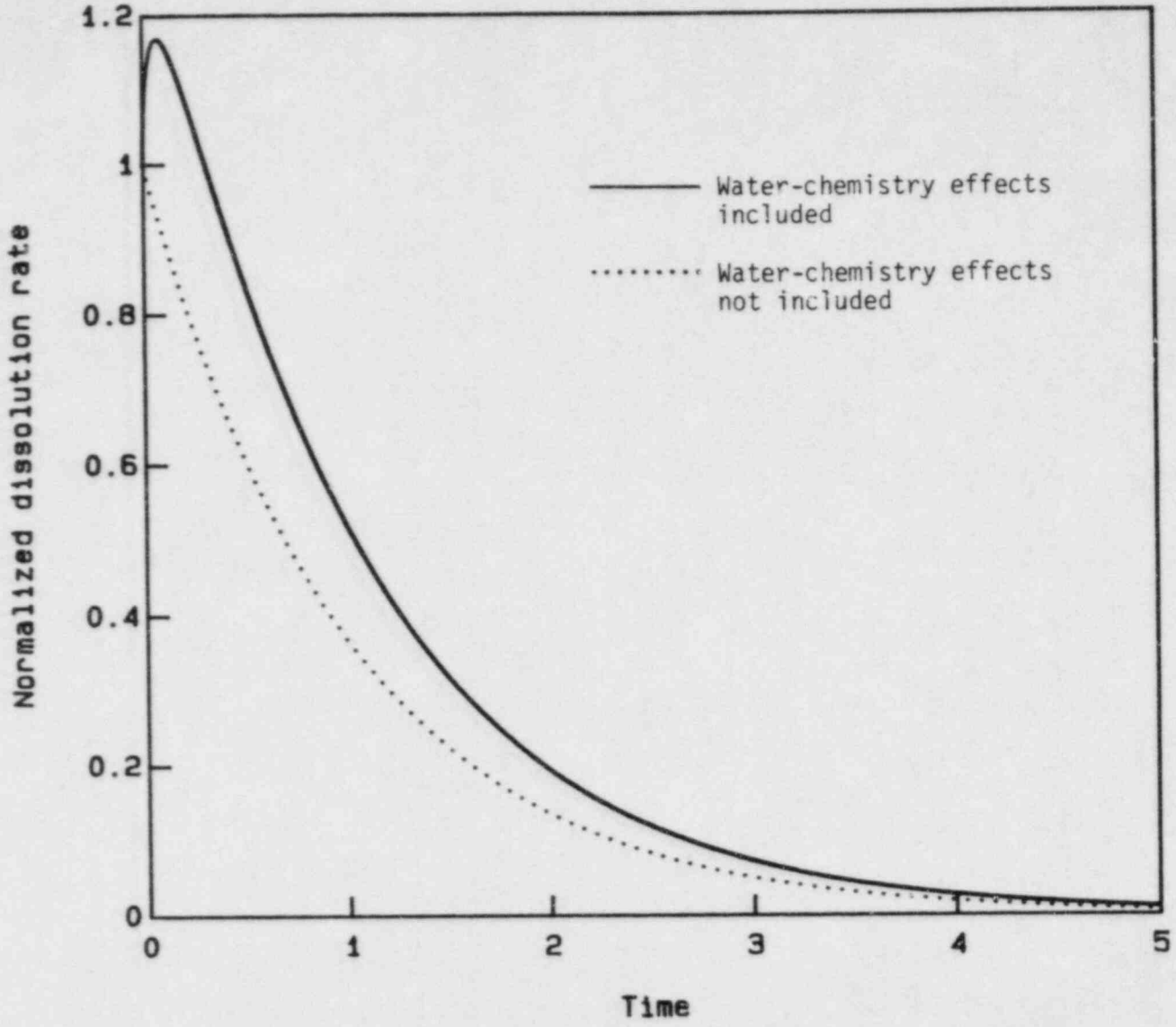

Figure 2.3. Glass-dissolution rate in pure water as a function of time.

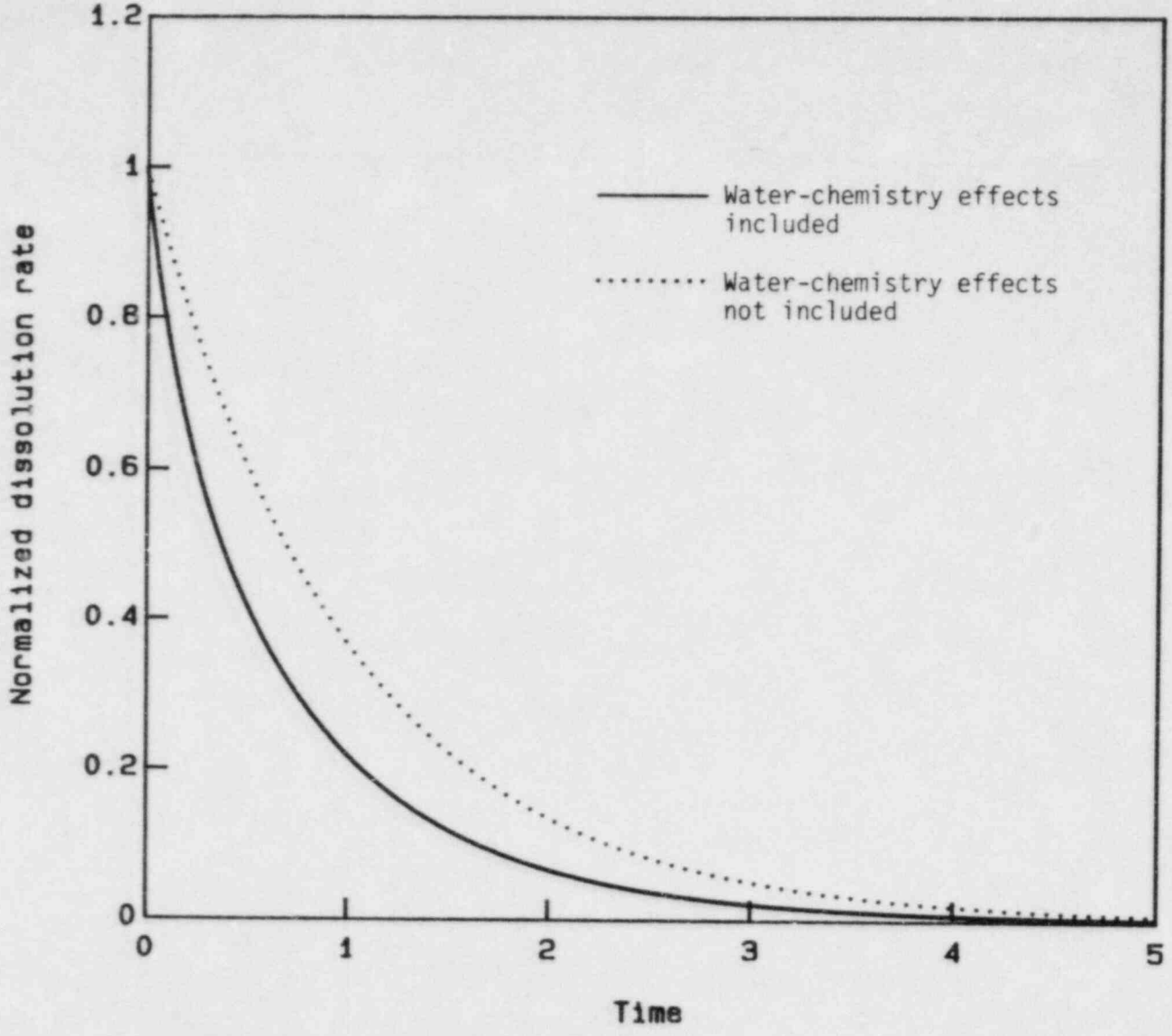

Figure 2.4. Glass-dissolution rate in synthetic basalt groundwater as a function of time.

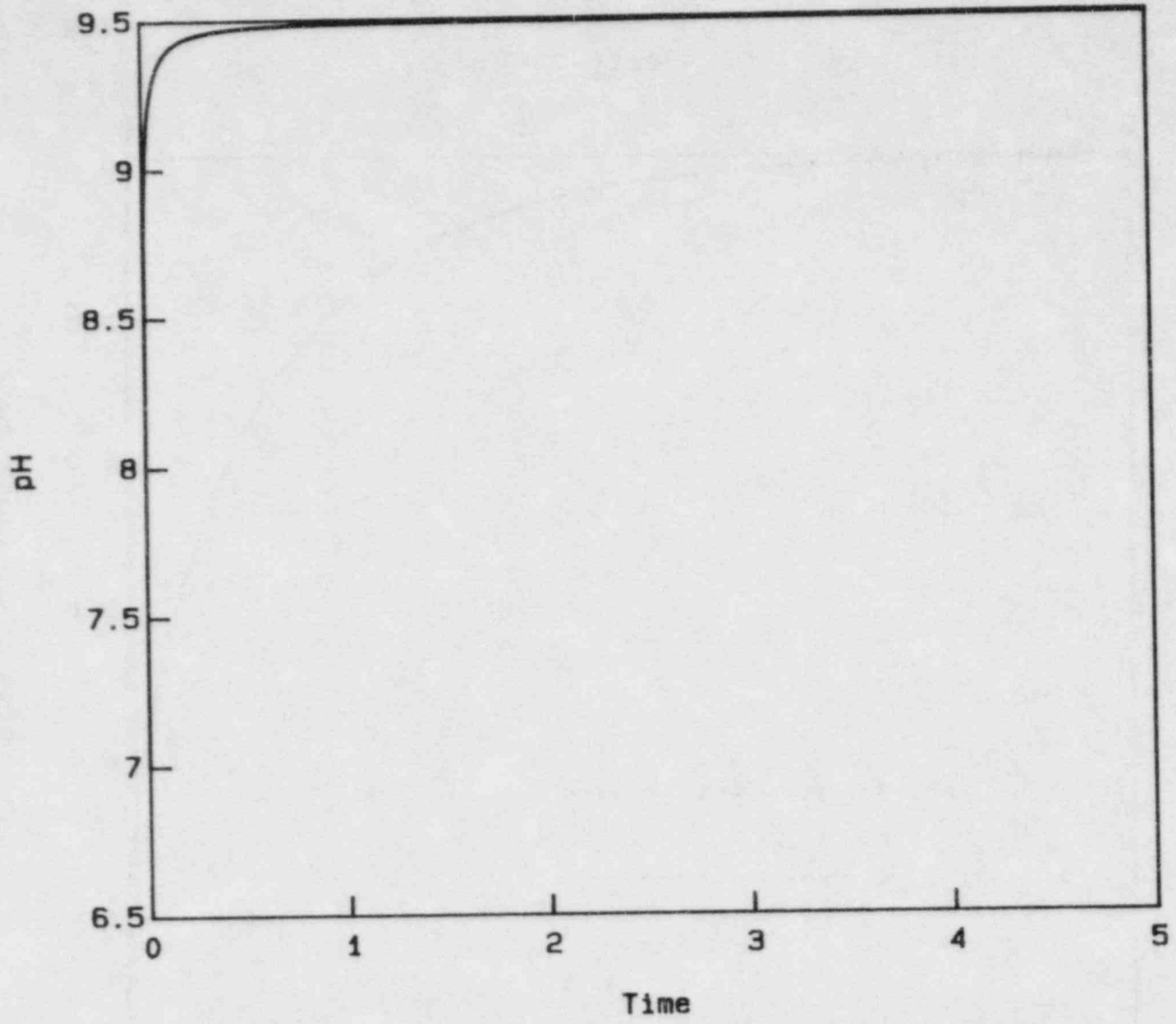

Figure 2.5. pH as a function of time as glass dissolves in pure water.

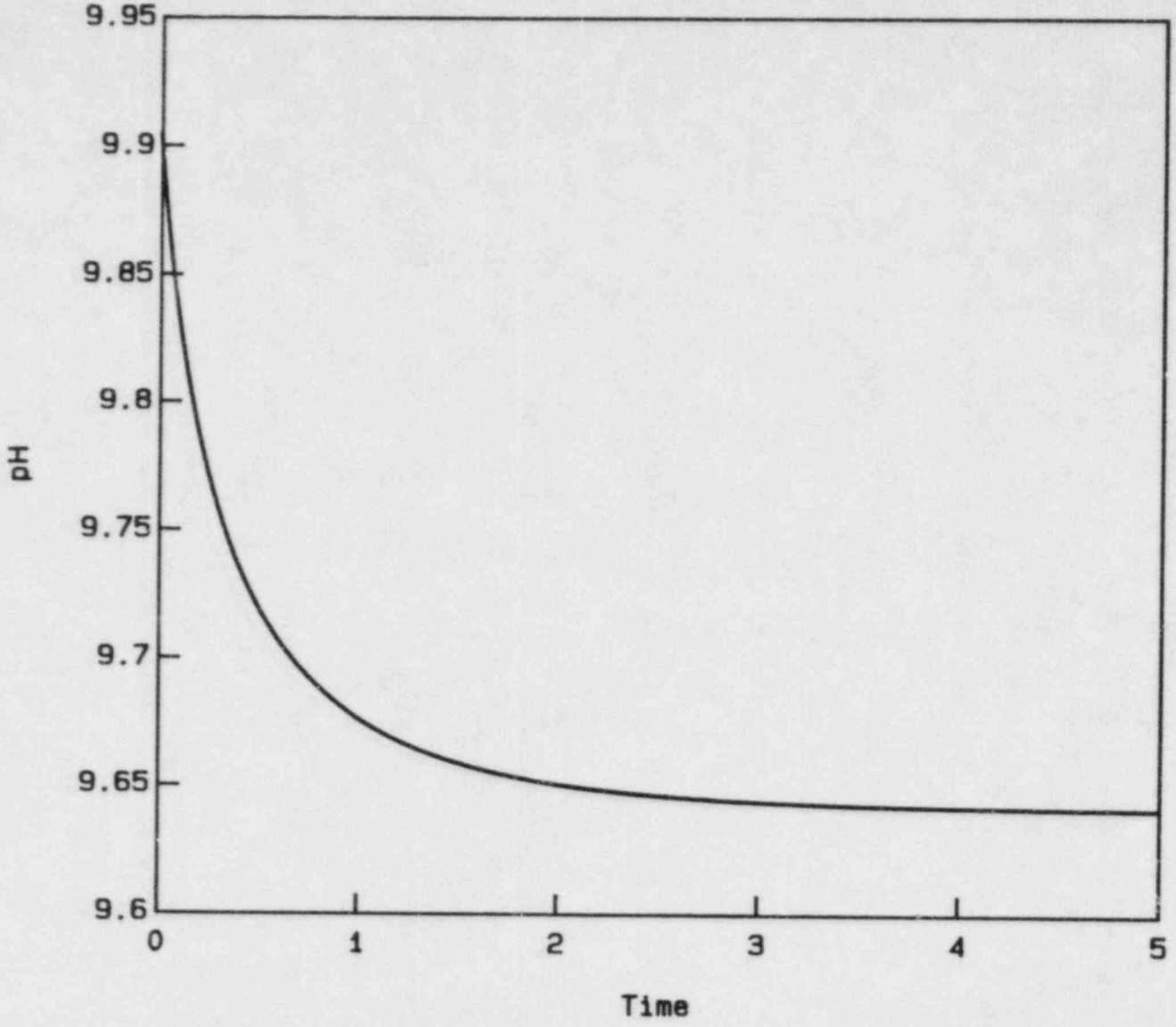

Figure 2.6. pH as a function of time as glass dissolves in synthetic basalt groundwater.

2.4 References for Section 2

(2.1) L. L. Hench and D. E. Clark, "Surface Properties and Performance Prediction of Alternative Waste Forms," report to NRC (Contract NRC-04-78-252) (March 1983).

(2.2) W. J. McCracken, D. E. Clark, and L. L. Hench, "Aqueous Durability of Lithium Disilicate Glass Ceramics," Ceram. Bull. 61 (11), p 1218-1223 (1982).

(2.3) H. Yinnon and D. R. Uhlmann, "A Kinetic Treatment of Glass Formation V. Surface and Bulk Heterogeneous Nucleation," J. Non-Cryst. Solids 44 (1), p 37-55 (1981).

(2.4) D. F. Bickford and C. M. Jantzen, "Devitrification Behavior of Defense Waste Glass," paper presented at Materials Research Society Annual Meeting, (November 1983).

(2.5) C. R. Hick, Fundamental Concepts in the Design of Experiments, Holt, Rinehart, and Winston (1964).

(2.6) 'Long-Term Performance of Materials Used for High-Level Waste Packaging", D. Stahl and N. E. Miller (Compilers), NUREG/CR-3427, Vol 4, BMI-2113 (June 1984), pp. 2-58 ff.

(2.7) A. C. Lasaga, in Reviews in Mineralogy, Vol. 8: Kinetics of Geochemical Processes, A. C. Lasaga and R. J. Kirkpatrick (editors), Mineralogical Soc. of America (Washington, D.C., 1981), pp. 10-11.

(2.8) F.W.J. Olver, Asymptotics and Special Functions, Academic Press, Inc. (New York, 1974), pp. 43-44.

(2.9) W. Gautschi, in Handbook of Mathematical Functions with Formulas, Graphs, and Mathematical Tables, M. Abramowitz and I. A. Stegun (editors), National Bureau of Standards, Applied Mathematics Series-55 (Washington, D.C., 1964), p. 298.

(2.10) G. B. Alexander, W. M. Heston, and R. K. Iler, "The Solubility of Amorphous Silica in Water", J. Chem. Phys., 58, 453, (1954).

(2.11) T. E. Jones, "Reference Material Chemistry--Synthetic Groundwater Composition", RHO-BW-ST-37 P (April 1982).

(2.12) "Long-Term Performance of Materials Used for High-Level Waste Packaging", D. Stahl and N. E. Miller (Compilers), NUREG/CR-3427, Vol. 1 (August 1983).

3. CONTAINER MATERIALS

During this quarter, electrochemical and slow strain rate tests were performed to assess stress-corrosion-cracking susceptibility and pitting in carbon steels under various environmental conditions. Further studies of this type are planned, in addition to pitting-kinetics experiments supporting the development of the pit-propagation model. Work on hydrogen embrittlement has rectified some anomalies in the data obtained during the past project year. Additional hydrogen-embrittlement tests are planned to study the effects on overpack steels of long-term exposure to expected repository temperatures and to assess the embrittlement susceptibility of commercial-purity iron. In the modeling task, the general-corrosion correlation indicates that radiolytic production of oxidizing species can significantly affect general-corrosion kinetics. An improved description of data on pitting-induction time is suggested for use in the pit-propagation model.

3.1 External Corrosion

The objective of the overpack-corrosion effort is to develop an understanding of the corrosion processes which can lead to overpack failure. This objective is being achieved through continued perusal of the relevant literature and experimental evaluation. Accomplishments during this reporting period are described below.

3.1.1 Literature Survey of Stress-Corrosion Cracking

A survey of the literature on "Stress-Corrosion Cracking of Low Strength Carbon Steels in Repository Environments" was performed during the last quarter of project year 1983-1984 and a draft copy of the report was distributed for comments. Comments were received and incorporated in the report and the report is being finalized. The editor of Chemical and Nuclear Waste Management also was contacted and he indicated interest in publishing the report as an article in the journal.

3.1.2 Electrochemical Studies

The objective of the electrochemical studies is to provide information on stress-corrosion cracking and pit initiation of carbon steels in repository environments as influenced by variation in metallurgical and environmental parameters. During the last project year, a matrix of potentiodynamic polarization experiments was started in which the effects of steel composition, structure, and groundwater composition were examined. This matrix is continuing. An effort also was initiated to examine the influence of large compositional variations in groundwater chemistry on electrochemical behavior. The aim of this work is to assess the likelihood that stress-corrosion cracking of carbon steel will occur in repository environments.

3.1.2.1 Metallurgical and Environmental Effects

The matrix of potentiodynamic polarization experiments being performed on cast and wrought steels in simulated basalt groundwater at 90 C was completed. Preliminary analyses of these data indicated that the presence of basalt rock or concentration of the groundwater did not have a major effect on the electrochemical parameters. More detailed analyses indicate small but systematic effects of groundwater chemistry on the electrochemical parameters. Figures 3.1 and 3.2 show that the corrosion potential (E_{cor}) and the potential at the current peak (E_{peak}) shifted to slightly more negative values and the passive current density (i_{pas}) decreased slightly upon increasing the solution concentration. A similar analysis of the effect of leaching of the basalt rock on these parameters indicated no systematic effect on the electrochemical parameters measured. Since the systematic shifts in these parameters were small, their relevance is difficult to ascertain with respect to waste-package performance.

Because variation in the groundwater chemistry had only minimal effects on the electrochemistry, the remainder of the tests in the matrix were performed in a single groundwater composition (referred to in the previous reports as 1X basalt groundwater) which is prepared according to a published procedure[3.1]. The electrochemical studies focused on the effects of steel cleanliness and structure on electrochemical behavior. Two steel compositions were examined, one ("doped" with phosphorus and sulfur) which is comparable to a 1018 composition and one ("clean") having low phosphorus and sulfur (see Table 3.1). These two steels were tested in the as-cast condition and in the hot-rolled condition, giving four combinations. Information on the preparation procedures and characterization of these materials is provided in the 1983-1984 Annual Report[3.2].

Results of polarization tests on the materials at 90 C and a scan rate of 0.6 V/hour in deaerated 1X basalt groundwater are summarized in Table 3.2. The actual curves obtained during this reporting period are given in Figures 3.3 and 3.4. These data show that neither the cleanliness nor the structure of the steel had a pronounced effect on its electrochemical behavior in basalt groundwater.

As an extension of this work, polarization tests were run in duplicate on Ferrovac E in 1X basalt groundwater at 90 C. Ferrovac E is a high-purity iron containing only trace quantities of impurities (see Table 3.1) and represents an upper bound in cleanliness for a ferrous canister material. The results are summarized in Table 3.2 and Figures 3.5 and 3.6. Several features of the data are noteworthy. First of all, two types of behavior are readily apparent. In Specimen 1, the appearance of the polarization curve is similar to that reported for the other steels, exhibiting an active-to-passive transition, a passive region, and definite pitting and protection potentials. Values of the parameters for Ferrovac E were comparable to those previously reported for the other steels (see Table 3.2). On the other

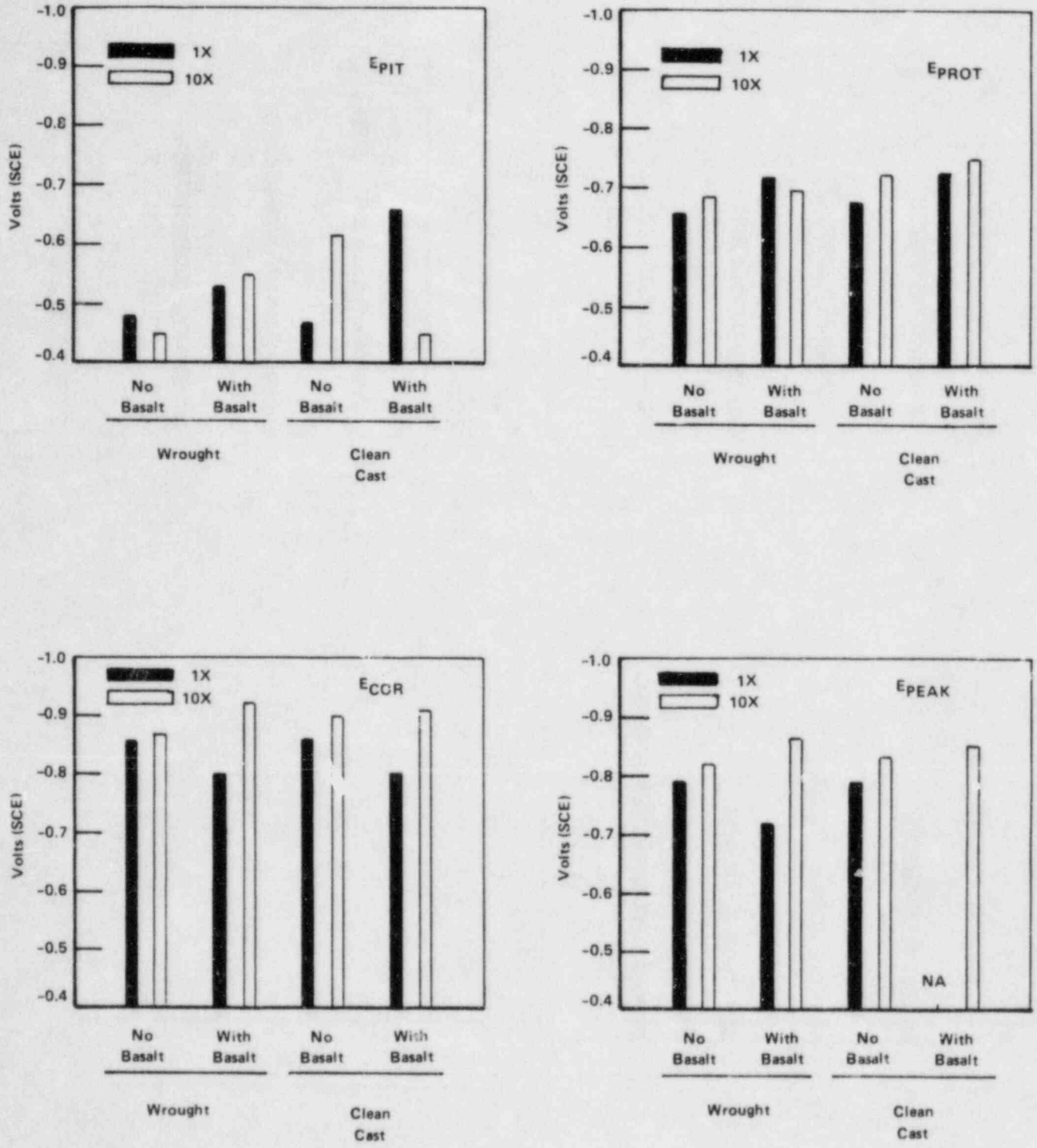

Figure 3.1. Electrochemical potential values taken from potentiodynamic polarization curves for wrought 1018 and clean cast 1018 steel in deaerated simulated basalt groundwater at 90 C.

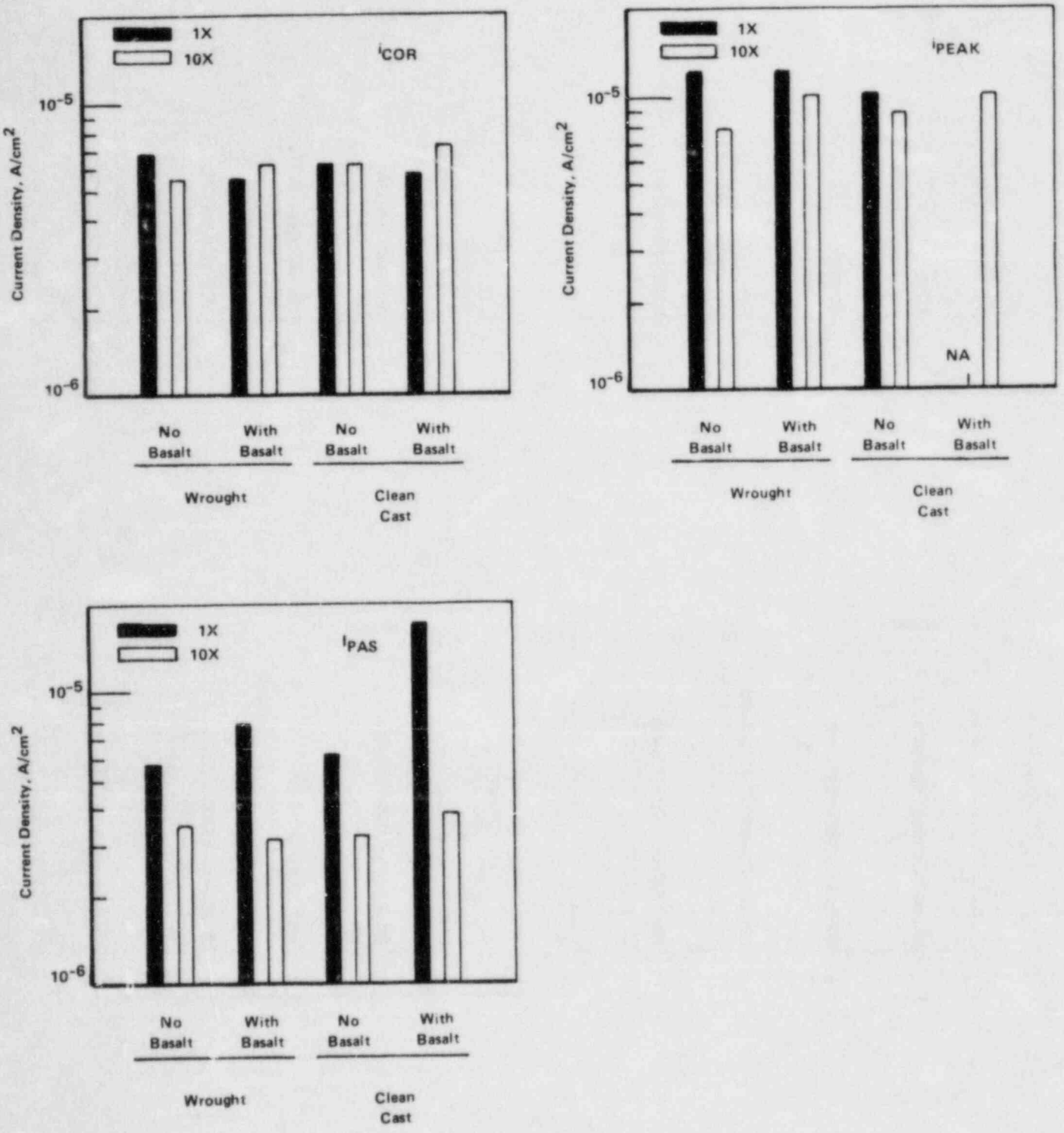

Figure 3.2. Current values taken from potentiodynamic polarization curves for wrought 1018 and clean cast 1018 steel in deaerated simulated basalt groundwater at 90 C.

Table 3.1. Chemical compositions in weight percent of reference steels and steels used in the experimental program.

Element	Proposed DOE Reference Steel	Clean BCL Steel (Actual)	Doped BCL Steel (Actual)	1018 Steel	Ferrovac E
Carbon	0.15-0.20	0.18	0.17	0.15-0.20	0.003
Manganese	0.90 max	0.49	0.55	0.60-0.90	Tr[a]
Phosphorus	0.04 max	0.004	0.029	0.040 max	-
Sulfur	0.045 max	0.002	0.036	0.050 max	-
Silicon	0.60 max	0.30	0.35	-	Tr
Aluminum	-	0.10	0.14	-	Nil[b]
Copper	-	0.006	0.007	-	-
Nickel	-	0.002	0.004	-	Nil
Chromium	-	0.007	0.011	-	Nil
Molybdenum	-	0.000	0.000	-	Tr
Vanadium	-	0.000	0.006	-	-

[a]Tr = trace quantity detected.

[b]Nil = none detected.

Table 3.2. Summary of results of potentiodynamic polarization tests performed on cast and wrought steels in deaerated basalt groundwater at 90 C and a scan rate of 0.6 V/hr.

Material	Structure	E_{cor}, V (SCE)	E_{peak}, V (SCE)	E_{pit}, V (SCE)	E_{prot}, V (SCE)	i_{cor}, A/cm^2	i_{peak}, A/cm^2	i_{pas}, A/cm^2
1018 Steel[a]	Cast	-0.840	-0.745	-0.508	-0.698	3.7×10^{-6}	5.5×10^{-6}	4.6×10^{-6}
1018 Steel	Wrought	-0.859	-0.793	-0.481	-0.659	6.8×10^{-6}	1.2×10^{-5}	5.7×10^{-6}
Clean 1018	Cast	-0.859	-0.793	-0.471	-0.679	6.2×10^{-6}	1.0×10^{-5}	6.2×10^{-6}
Clean 1018[a]	Wrought	-0.859	-0.801	-0.508	-0.669	3.4×10^{-6}	5.2×10^{-6}	4.4×10^{-6}
Ferrovac E (1)[a]		-0.869	-0.764	-0.432	-0.679	6.2×10^{-6}	1.2×10^{-5}	6.2×10^{-6}
Ferrovac E (2)[a]		-0.754	(b)	-0.461	-0.764	1.9×10^{-7}	(b)	4.4×10^{-7}

(a) Polarization curves run during this reporting period.

(b) Specimen's free-corrosion potential was more noble than the potential at maximum current (E_{peak}).

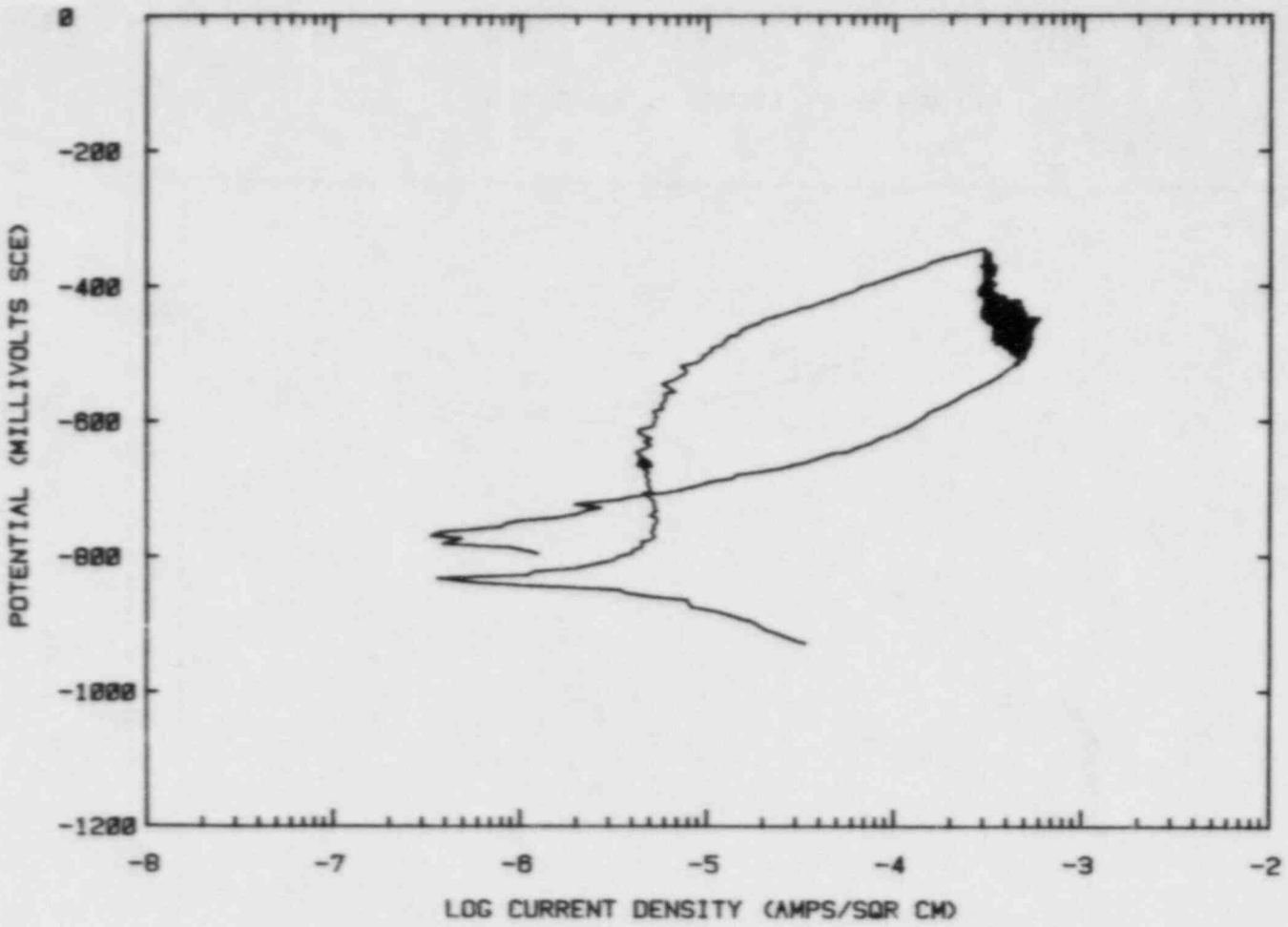

Figure 3.3. Potentiodynamic polarization curve for cast 1018 steel in basalt groundwater at 90 C polarized with a scan rate of 0.6V/hr.

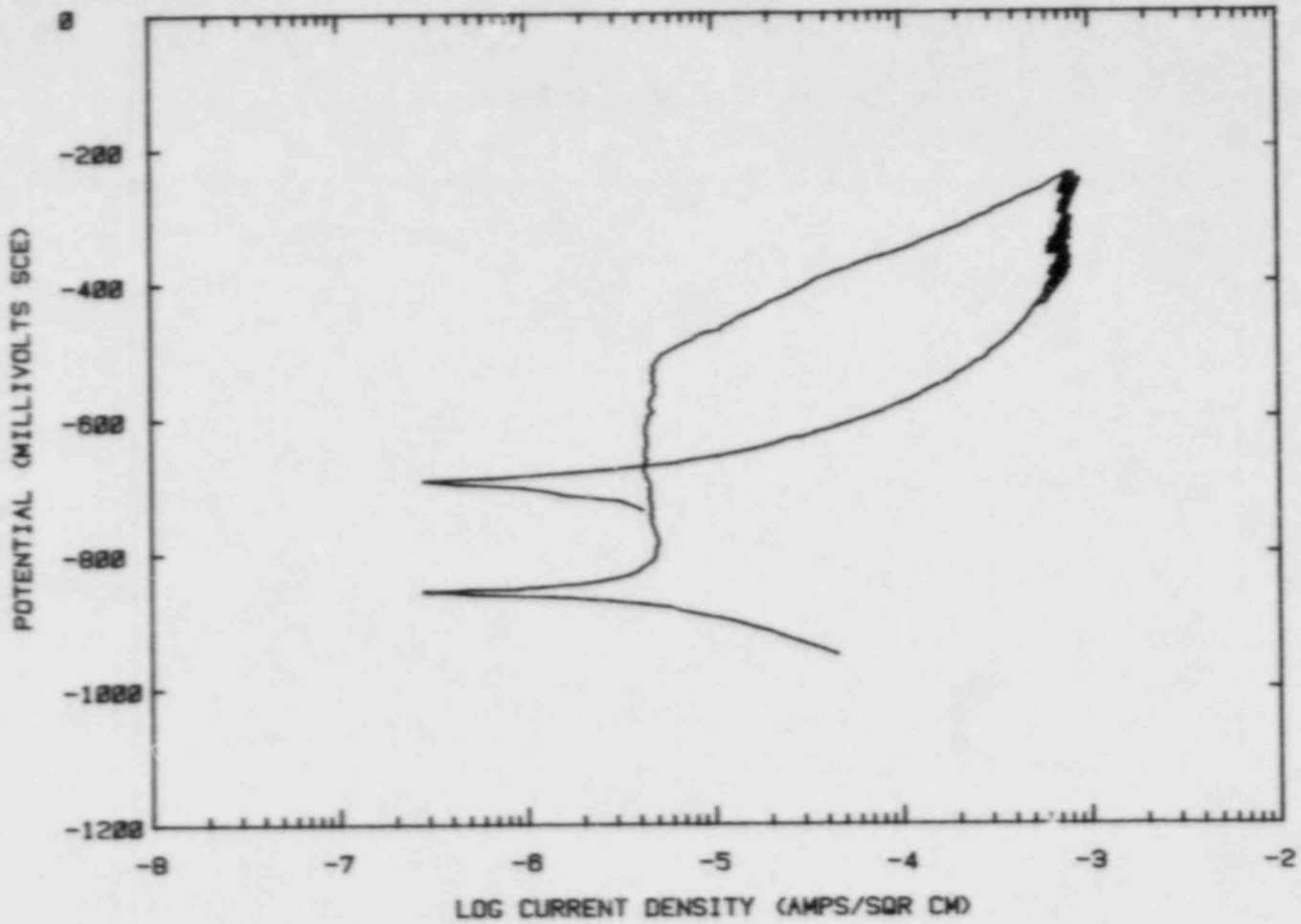

Figure 3.4. Potentiodynamic polarization curve for clean wrought 1018 steel in basalt groundwater at 90 C polarized with a scan rate of 0.6V/hr.

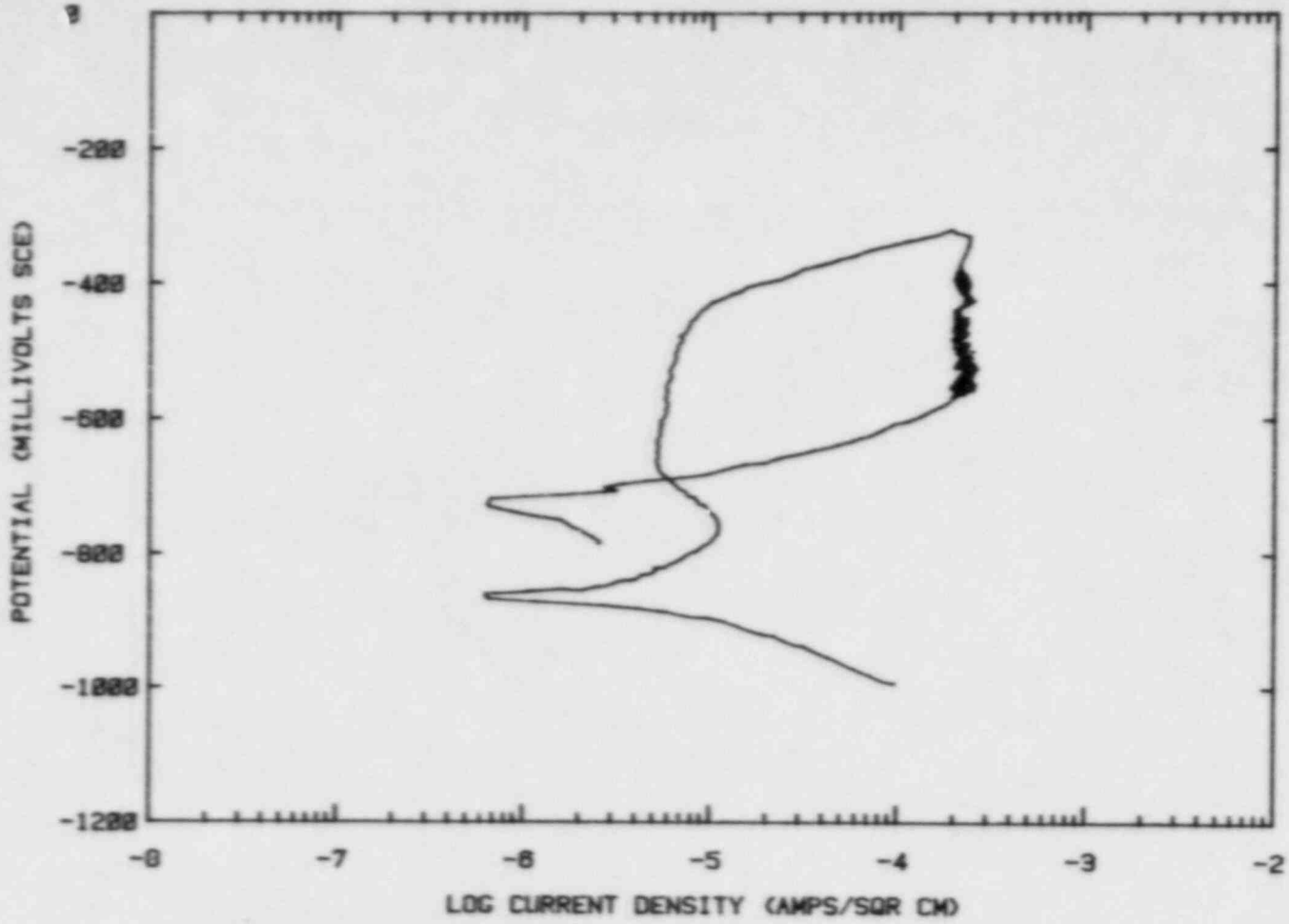

Figure 3.5. Potentiodynamic polarization curve for Specimen 1 of Ferrovac E in basalt groundwater at 90 C polarized with a scan rate of 0.6V/hr.

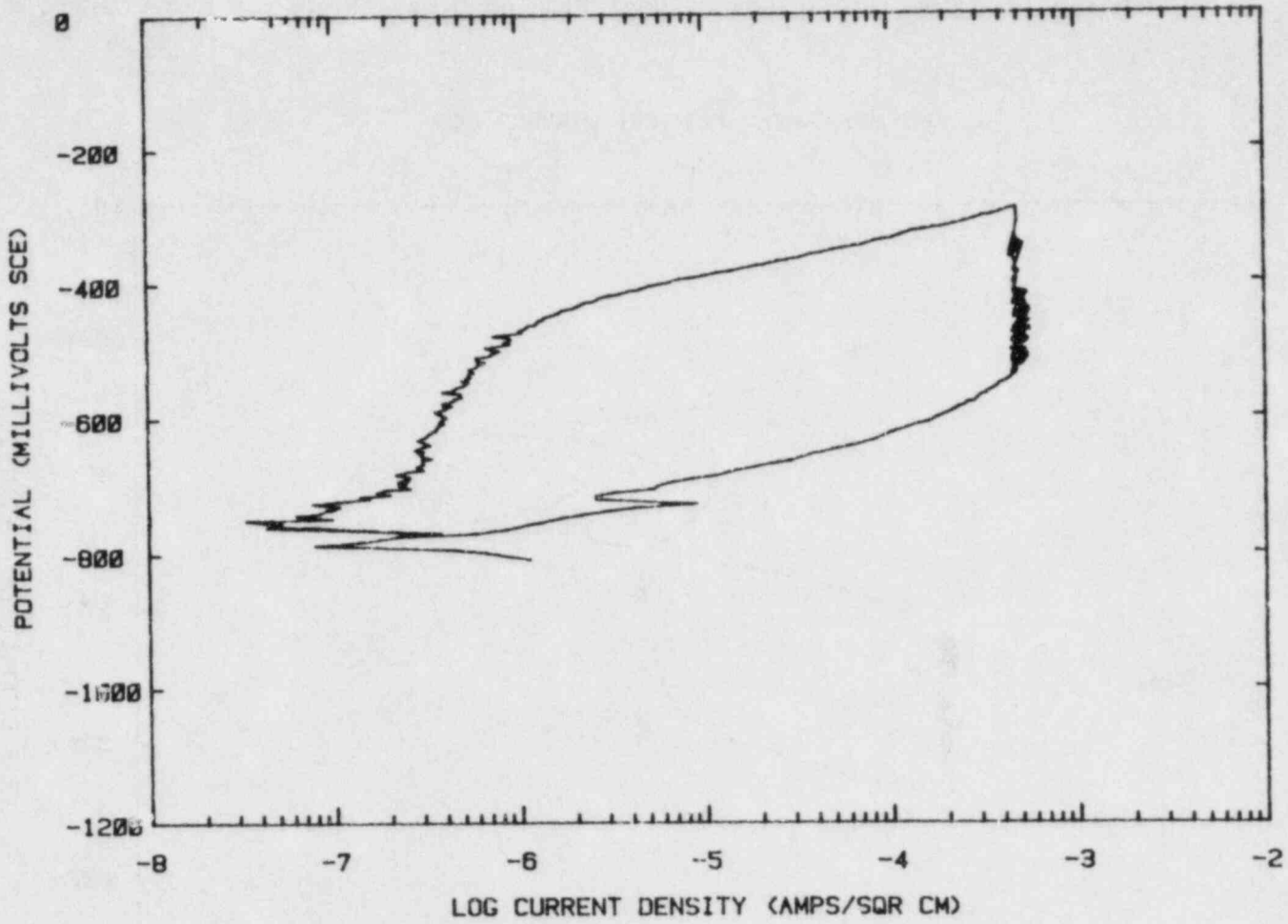

Figure 3.6. Potentiodynamic polarization curve for Specimen 2 of Ferrovac E in basalt groundwater at 90 C polarized with a scan rate of 0.6 V/hr.

hand, Curve 2 does not exhibit an active-to-passive transition or a measurable passive potential range. A pitting potential is evident and hysteresis occurred on the reverse scan, indicating that pitting had occurred on the specimen. The protection and pitting potentials for Curves 1 and 2 were similar, whereas the value for E_{corr} for Curve 2 was more noble than that for Curve 1. The most reasonable explanation for this behavior is that the solution in the cell containing the latter sample was contaminated with trace quantities of air which spontaneously passivated the specimen. Interpretation of the specimen's behavior is somewhat clouded by the occurrence of the spontaneous passivation; in fact, one might mistake this behavior for active corrosion if a reverse scan had not been performed.

The standard procedure for these electrochemical experiments is to allow the specimens to equilibrate in the solution overnight before beginning the polarization experiment. Periodically, during this equilibration period, the specimens of Ferrovac E were visually examined, and evidence of pit initiation was found on the polished surfaces of both specimens. Following the polarization test, the attack on the specimen surfaces appeared to be somewhat greater, as one would expect based on the polarization behavior. Optical photographs of the specimens after testing, given in Figures 3.7 and 3.8, show small distinct pits which were associated with deposit buildup on the specimen surfaces.

In summary, the results of the experimental studies performed this quarter indicate that variation in the composition of the steels from high-purity Ferrovac E to 1018 carbon steel does not have a marked effect on the electrochemical behavior in a simulated basalt repository environment. Since close correlation between electrochemical behavior of steels and pitting and stress-corrosion cracking initiation has been established for many environments, these results may indicate that minor variations in the composition of carbon steel will not have a marked influence on the initiation of either failure mode. Similarily, the use of the more expensive high-purity steel does not appear to be justified. It must be cautioned, however, that this technique does not provide information on propagation rates; thus the effect of minor compositional variations in 1018 carbon steel on pit or crack propagation should be investigated.

In other work, the effect of scan rate on the polarization behavior of several steels was studied in a 1X basalt groundwater at 90 C. These experiments provide information on the most likely potential ranges for stress-corrosion cracking susceptibility of the steels in repository environments. In the fast scan tests (18 V/hour), the curves are generated as soon as the specimen contacts the solution, whereas in the slow scan tests (0.6 V/hr), the specimens are allowed to equilibrate with the solution overnight. The aim of the fast scan polarization tests is to obtain the maximum current density on relatively bare metal surfaces.

20X 6L615

4X 6L614

Figure 3.7. Optical photographs of Ferrovac E Specimen 1 following potentiodynamic polarization testing in deaerated 1X basalt groundwater at 90 C.

20X 6L617

4X 6L616

Figure 3.8. Optical photographs of Ferrovac E Specimen 2 following potentiodynamic polarization testing in deaerated 1X basalt groundwater at 90 C.

Results of these experiments, summarized in Figures 3.9 and 3.10 and Table 3.3, show that passive currents are considerably higher at the faster scan rates than at the lower scan rates, as expected. Empirically, it has been shown that stress-corrosion susceptibility of carbon steel reaches a maximum where the differences in current density between the fast and slow polarization scans are large. On this basis, one would expect that the most likely range for stress-corrosion cracking of carbon steel in basalt groundwater is between -0.78 V and -0.65 V (SCE). However the differences in current between the fast and slow scans are small in comparison to potent cracking systems, and thus one would not expect a high degree of susceptibility to stress-corrosion cracking at 90 C.

A potentiodynamic polarization curve was obtained for wrought 1018 carbon steel in deaerated basalt groundwater at 250 C and a scan rate of 0.6 V/hr. The results, given in Figure 3.11, show that the behavior of the steel at 250 C was qualitatively similar to that observed at 90 C, exhibiting an active-passive transition and definite pitting and protection potentials. Values for I_{cor}, I_{peak}, and I_{pas} were somewhat higher at 250 C than at 90 C. The higher peak current may indicate that stress-corrosion cracking is more likely at 250 C than at 90 C. On the other hand, the hysteresis loop area at 250 C appears to be somewhat smaller than at 90 C, suggesting a greater tendency for pits to repassivate at the higher temperature.

3.1.2.2 Effects of Chemical Species Present in Basalt Groundwater

As discussed above, the active-passive behavior observed for carbon steel in the basalt repository environments is similar to that observed for steels in many potent cracking environments. Although the steels studied do not appear to exhibit susceptibility to stress-corrosion cracking in the groundwater of nominal composition, several potent cracking agents are present in low concentrations in the groundwater. One or more of these species could become concentrated as a result of occluded cell corrosion, heat transfer, or some yet-to-be-defined mechanism over the life of the repository. (In fact, most stress-corrosion failures of practical interest occur in relatively innocuous bulk environments where a potent cracking agent concentrates at local sites. One such example is the caustic cracking of carbon steel boilers, in which the cracking agent, NaOH, concentrates by five orders of magnitude in crevices as a result of local boiling.) Accordingly, it is important to examine the influence of variation in the composition of the groundwater on stress-corrosion cracking susceptibility and to attempt to establish acceptable compositional ranges for the cracking agents that are present.

Because a large number of species and variables must be examined, a full matrix of stress-corrosion cracking experiments would not be practical and is probably not necessary. The approach to be taken in this task is to use potentiodynamic polarization curves to predict stress-corrosion

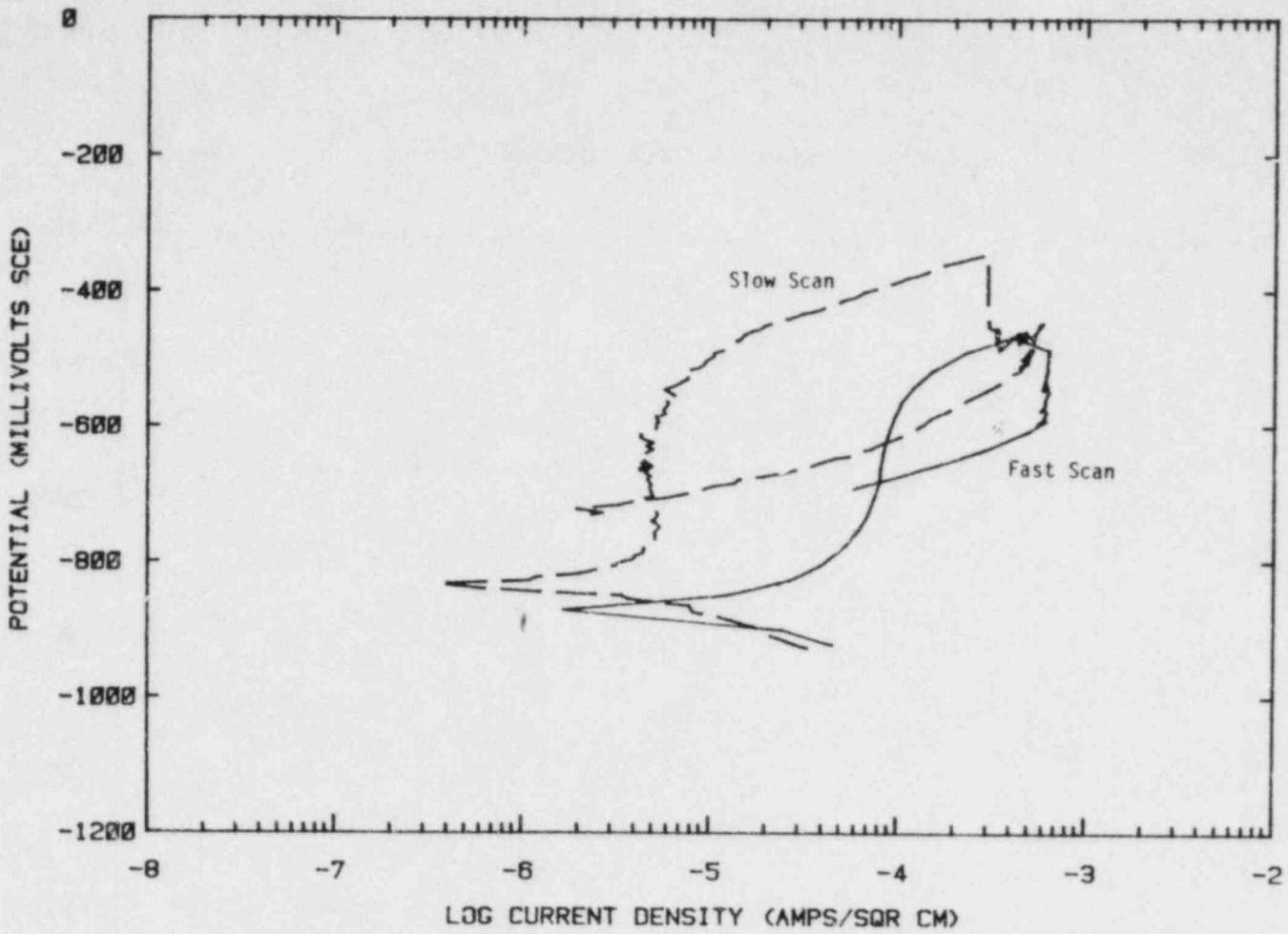

Figure 3.9. Effect of scan rate on the polarization behavior of cast 1018 steel in deaerated basalt groundwater at 90 C.

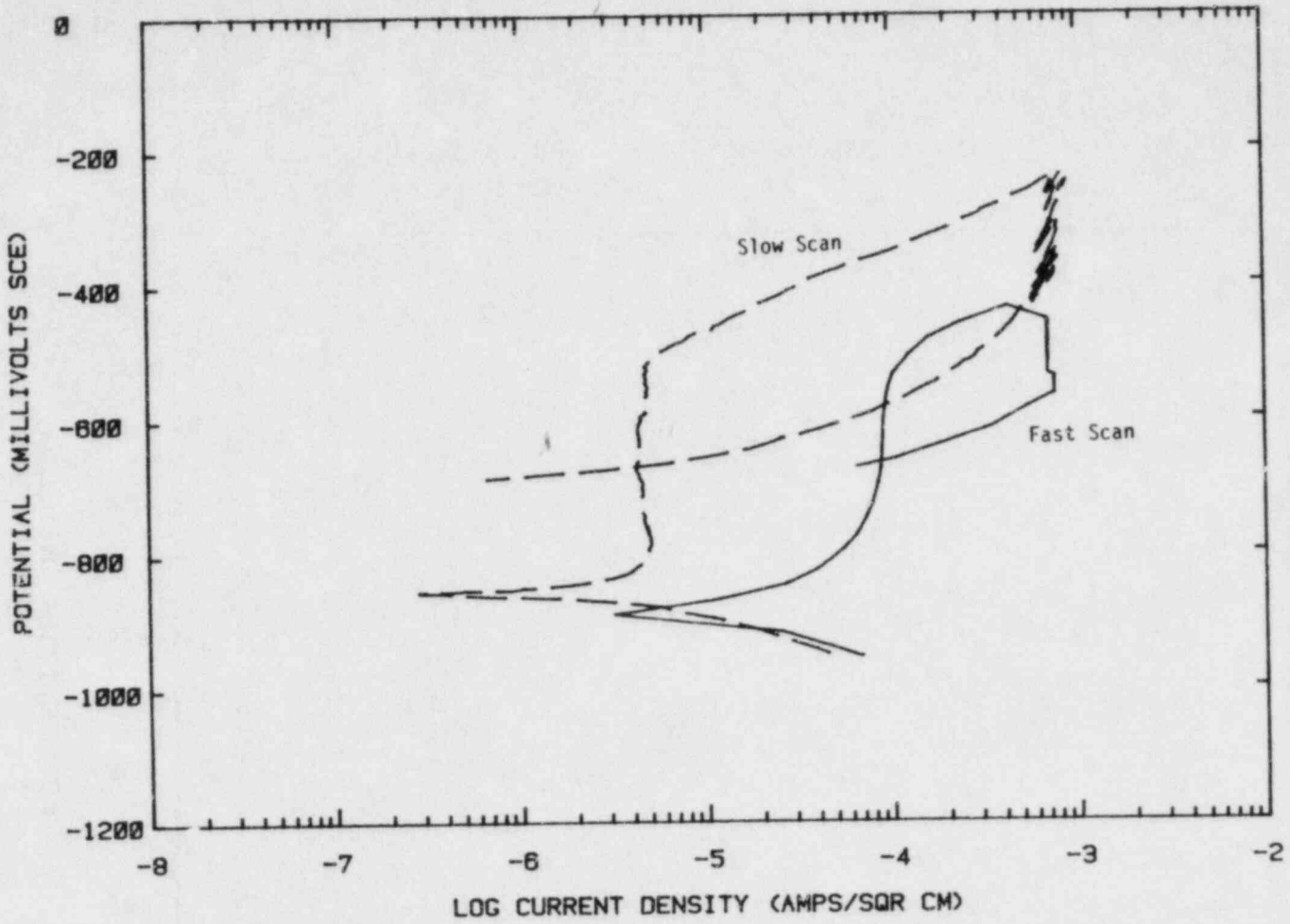

Figure 3.10. Effect of scan rate on the polarization behavior of clean wrought 1018 steel in deaerated basalt groundwater at 90 C.

Table 3.3. Summary of results of potentiodynamic polarization tests performed on 1018 cast steel and clean 1018 wrought steel in deaerated basalt groundwater at 90 C comparing fast scan rate and slow scan rate data.

Material	Scan Rate, V/hr	E_{cor}, V (SCE)	E_{peak}, V (SCE)	E_{pit}, V (SCE)	E_{prot}, V (SCE)	i_{cor}, A/cm^2	i_{peak}, A/cm^2	i_{pas}, A/cm^2
1018 Cast[a]	0.6	-0.858	-0.745	-0.508	-0.698	3.7×10^{-6}	5.5×10^{-6}	4.6×10^{-6}
1018 Cast	18	-0.886	(b)	-0.518	-0.669	1.9×10^{-5}	(b)	8.2×10^{-5}
Clean 1018 Wrought[a]	0.6	-0.859	-0.801	-0.508	-0.669	3.4×10^{-6}	5.2×10^{-6}	4.4×10^{-6}
Clean 1018 Wrought	18	-0.896	(b)	-0.491	-0.649	1.6×10^{-5}	(b)	9.0×10^{-5}

(a) Data repeated from Table 3.2.

(b) Polarization behavior did not exhibit a maximum current peak.

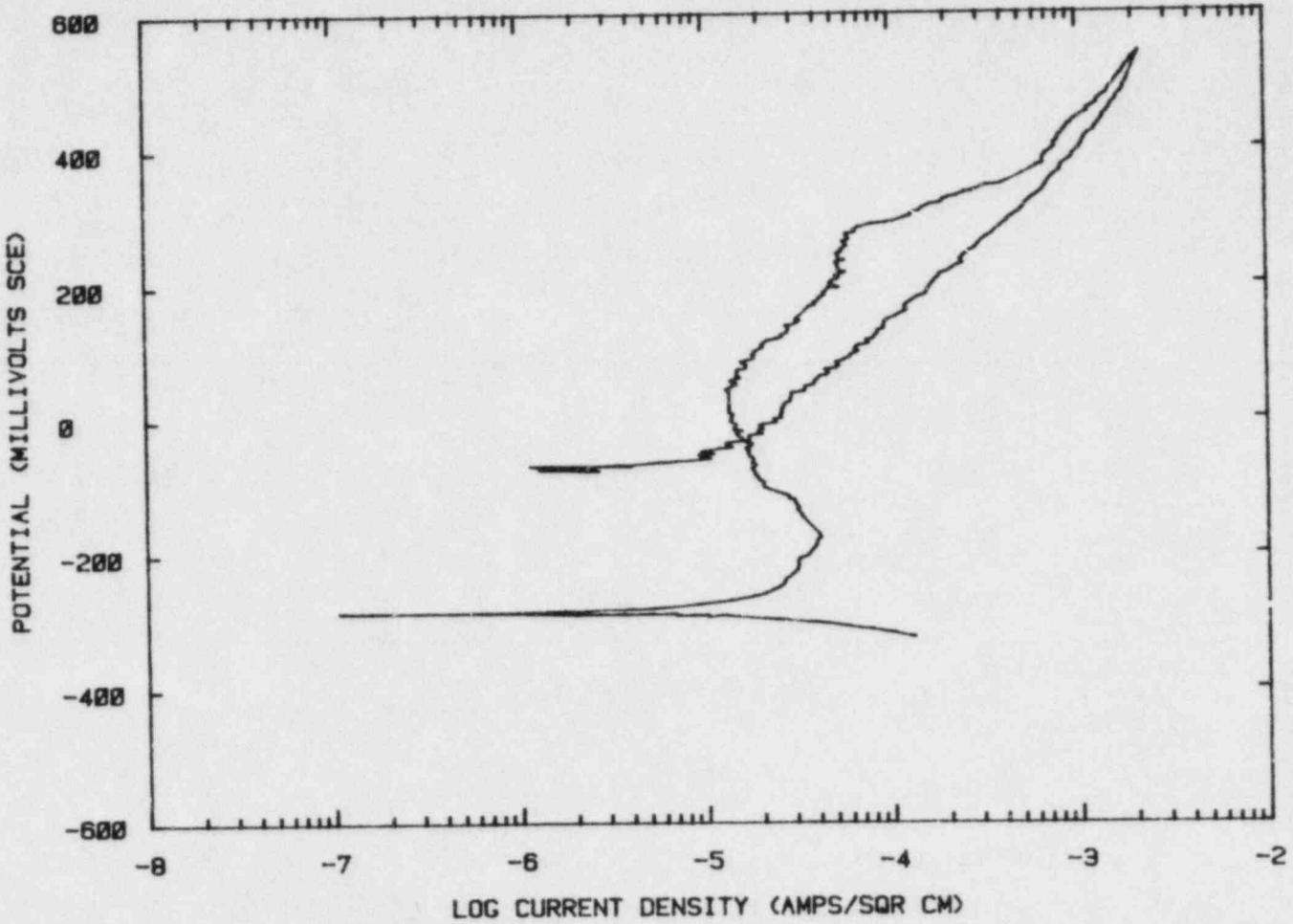

Figure 3.11. Potentiodynamic polarization curve for wrought 1018 steel in basalt groundwater at 250 C with a scan rate of 0.6 V/hr.

cracking tendencies, as described in the literature.[3.3] Polarization curves will be produced at a fast and a slow scan rate, and the difference between the two curves will be used for examining the stress-corrosion cracking tendencies of the steel. To examine the large number of species and variables that may affect these tendencies, a statistical approach is required.

Initially, 15 species or variables were selected for investigation in a screening matrix of experiments. The purpose of the screening test is to determine which of the 15 variables significantly affect stress-corrosion cracking tendencies by estimating the main effect for each variable. For each species, a high and low concentration will be investigated. The low concentration was selected based on the concentration present in typical basalt groundwaters. The high concentration is typically 2 to 4 orders of magnitude higher than the low concentration.

Table 3.4 gives the 15 species and their concentrations selected for examination during the initial 2-level design matrix. These include species present in the groundwater, those that may leach from the backfill, radiolysis products, and species that may intrude into the repository.

Table 3.5 shows typical concentrations which have been reported in the literature for the 15 species being examined in the present experiments, along with the concentrations of other species. Species such as sodium (Na^{+1}), potassium (K^{+1}), calcium (Ca^{+2}), and sulfate (SO_4^{-2}) will also be included in the experimental matrix, but not as controlled variables. The concentration of potassium and calcium will be maintained constant, while sodium and sulfate ions will be used to balance the cation and anion concentrations required for the 15 species to be added as variables. The following are justifications for the concentrations that will be examined in this task.

pH. The high value of pH will be 9.3 and the low value will be 6. A pH of 9.3 is selected based on the pH of the basalt groundwater[3.4] and the knowledge that stress-corrosion cracking in CO_3^{-2}/HCO_3^{-1} is most prominent at pH 9.3.[3.3] A value of pH 6 is selected based on the observation of the decrease in pH found in Reference 3.4.

Cl^{-1}. Chloride significantly affects corrosion and promotes stress-corrosion cracking at high temperature in carbon steel[3.3] and therefore is selected as a variable. The high level will be 100,000 ppm because Cl^{-1} is known to concentrate in crevices and pits or at heated surfaces to extremely high values (500X to 1000X). The low level will be 100 ppm, based on Reference 3.4 (shown in Table 3.5), since it is the low end of the concentration range.

F^{-}. Fluoride is an aggressive species with regard to corrosion of metals. The high level will be 10,000 ppm, which is 200 times the maximum concentration given in Reference 3.4. The low level will be 10 ppm, also based on Reference 3.4. (These values are shown in Table 3.5).

Table 3.4. High and low concentrations of species selected for evaluation in the electrochemical experiments.

	Species	High Concentration	Low Concentration
1.	pH	9.3	6.0
2.	Cl^{-1}	100,000 ppm	100 ppm
3.	F^{-1}	10,000 ppm	10 ppm
4.	Fe^{+2}/Fe^{+3}	Saturation	0.05 ppm
5.	Al^{+3}	1,000 ppm	0.1 ppm
6.	CO_3^{-2}/HCO_3^{-1}	1M	0.001 M
7.	NO_3^{-1}/NO_2^{-1}	1,000 ppm [N]	0.1 ppm [N]
8.	PO_4^{-3}	1,000 ppm [P]	0.1 ppm [P]
9.	$BO_3^{-3}/B_4O_7^{-2}$	1,000 ppm [B]	1 ppm [B]
10.	SiO_3^{-2}	1,000 ppm [Si]	10 ppm [Si]
11.	H_2O_2	100 ppm	0
12.	ClO_4^{-1}	100 ppm	0
13.	O_2	2% (Vapor)	0
14.	CO	1% (Vapor)	0
15.	H_2	80% (Vapor	1%

Table 3.5. Concentrations of species in basalt groundwater or in actual or simulated basalt repository environments.

	Ref. 3.4	Ref. 3.5	Ref. 3.6	Ref. 3.7	Ref. 3.8	Ref. 3.9
1. pH	9.7(5.7)				300 ppm	
2. Cl^{-1}	98-297(500) ppm					
3. F^{-1}	11-42(50) ppm					4%[Fe_2O_3](c)
4. Fe^{+2}/Fe^{+3}	0-0.6(0.5)[Fe^{+2}] ppm	0.009 ppm				18%[Al_2O_3](c)
5. Al^{+3}	0.02(20) ppm	0.007 ppm				
6. CO_3^{-2}/HCO_3^{-1}	4-55/45-118(70/200) ppm					
7. NO_3^{-1}/NO_2^{-1}						
8. PO_4^{-3}		0.2[P] ppm				0.08%[P_2O_5](c)
9. $BO_3^{-3}/B_4O_7^{-2}$	0-1.5(5)[B^{+3}] ppm	1.3[B] ppm				
10. SiO_3^{-2}	30-170(2000)[Si] ppm				30[SiO_2] ppm	59%[SiO_2](c)
11. H_2O_2				0.34 ppm		
12. ClO_4^{-2}						
13. O_2				3.2 ppm	0.5%(b)	
14. CO						
15. H_2				0.02 ppm	76.6%(b)	
Na^{+1}	161-350(500)					2.2%(c)
K^{+1}	3-25(100)					0.7%[K_2O](c)
Ca^{+2}	0.8-10(100)					1.7%[CaO](c)
Mg^{+2}	0-0.2(50)					2.1%[MgO](c)
SO^{-2}	4-197(200)				300 ppm	
S^{-2}	0(100)					
N_2			25 ppm(a)		19.3%(b)	
CH_4			700 ppm(a)		0.3%(b)	
CO_2					2.3%(b)	
E_H	-0.5 to -0.53(+0.2 to -0.4)V_{SHE}					

(a) Measurements at 25 C.
(b) Composition of gas phase for simulated irradiated Grande Ronde basalt groundwater.
(C) Composition of bentonite.

Fe^{+2}/Fe^{+3}. Ferrous (Fe^{+2}) ions are present in the basalt groundwaters at low concentrations (as shown in Table 3.5). Due to the corrosion process, the solution near the canister probably will be saturated with iron ions. With the radiolysis process occurring, ferric ions (Fe^{+3}) also may be present. (The E_H values given in Table 3.5 preclude the presence of Fe^{+3} in the absence of radiolysis.) Ferric ions are oxidizers and as such could affect the corrosion of carbon steel; therefore Fe^{+2}/Fe^{+3} will be included in the matrix. The high level of Fe^{+2}/Fe^{+3} will be saturation and will be added as equal concentrations of Fe^{+2} and Fe^{+3} at levels approximately twice as high as their predicted saturation levels. The low level will be 0.05 ppm based on Reference 3.4 (shown in Table 3.5).

Al^{+3}. Aluminum is known to complex with fluorides and therefore can affect corrosion.(3.9) Aluminum also has been shown to affect pitting properties of stainless steels in ongoing research at Battelle. The high level of Al^{+3} will be 1,000 ppm. The low level will be 0.1 ppm, based on Reference 3.4 (shown in Table 3.5).

CO_3^{-2}/HCO_3^{-1}. Carbonate and bicarbonate are known stress-corrosion cracking agents and are present in basalt groundwater.(3.3) The CO_3^{-2}/HCO_3^{-1} will be added in equal molar quantities. The high level will be 1 M, based on Reference 3.3 and results of studies on pipeline steels performed at Battelle; this level should provide maximum cracking susceptibility. The low level will be 0.001 M, based on the average concentrations presented in Reference 3.4 (shown in Table 3.5).

NO_3^{-1}/NO_2^{-1}. Nitrate and nitrite concentrations have not been reported; however, NO_3^{-1} and NO_2^{-1} are possible radiolysis species, and NO_3^{-1} is a known corrosion inhibitor and cracking agent.(3.3,3.9) Nitrate and nitrite will be added in equal amounts. The high level of NO_3^{-1}/NO_2^{-1} will be 1,000 ppm N and the low level will be 0.1 ppm N.

PO_4^{-3}. Phosphate is present in small quantities in the groundwater(3.4) and also, in the form of P_2O_5,(3.10) Phosphate is a known inhibitor and cracking agent.(3.5) The high level will be 1,000 ppm P, and the low level will be 0.1 ppm P.

$BO_3^{-3}/B_4O_7^{-2}$. Borate is a known corrosion inhibitor and therefore is a potential cracking agent.(3.3,3.9) The high level will be 1,000 ppm B. The low level will be 1 ppm B based on Reference 3.4 (shown in Table 3.5).

SiO_3^{-2}. Silicates are known corrosion inhibitors.(3.3,3.9) The high level will be 1000 ppm Si based on the high possible concentration given in Reference 3.4 (shown in Table 3.5). The low level will be 10 ppm Si based on Reference 3.4 (shown in Table 3.5).

H_2O_2. H_2O_2 is a radiolysis product[3.7] and a strong oxidizer. Reference 3.7 reports that 0.3 ppm H_2O_2 was present after 1000 seconds of exposure at a dose rate of 3.5×10^6 R/hr. The high level will be 100 ppm and the low level will be zero.

ClO_4-1. Perchlorate is a possible radiolysis product and can act as an inhibitor. Although no concentration data are available, the concentration used will be comparable to that for H_2O_2. The high level will be 100 ppm and the low level will be zero.

O_2. Oxygen is a radiolysis product and also may intrude into the repository. It is well known for its effects on corrosion as an oxidizer. The high level of O_2 will be 2 percent in the vapor phase, 4 times greater than the concentration given in Reference 3.8 (shown in Table 3.5). The low level will be zero.

CO. Carbon monoxide was not identified as being present in the groundwater analysis found in References 3.4-3.8, but it is sometimes difficult to differentiate CO from N_2 in mass spectrometry analysis and N_2 was found by this technique.[3.5] Because CO is a potent cracking agent and may be present, it is included in this matrix of experiments. The high level of CO will be 1 percent (in the vapor phase), which is half the CO_2 concentration reported in Reference 3.8 (shown in Table 3.5). The low level of CO will be zero.

H_2. Hydrogen gas may be present in large quantities as a result of radiolysis of groundwater and corrosion reactions: as high as 76 percent in the vapor phase is reported in Reference 3.8 (shown in Table 3.5). The high level of H_2 will be 80 percent and the low level will be 1 percent.

3.1.3 Slow Strain Rate Studies

The objective of the slow strain rate studies is to assess the stress-corrosion cracking susceptibility of carbon steels in candidate repository environments. Specific environmental conditions (solution composition and electrochemical potential) are being selected on the basis of the results of the electrochemical studies and the literature survey, described above.

The HASTELLOY* Alloy C-276 autoclave used for the elevated-pressure slow strain rate tests was modified during this reporting period to accommodate counter and reference electrodes, and two Ag/AgCl reference electrodes were constructed. During this project year, most slow strain rate tests will be performed on hot-rolled 1020 carbon steel. A single slow strain rate test has been performed on a hot-rolled 1020 steel

---

*HASTELLOY is a registered trademark of the Cabot Corporation.

specimen in a 1X basalt groundwater at -250 mV (Ag/AgCl, saturated) and a strain rate of 6×10^{-7} s^{-1}. This potential was selected on the basis of the results of the potentiodynamic polarization experiments performed at 250 C. No cracking was found in the gauge length of the specimen.

3.1.4 Pitting-Kinetics Studies

The objective of the pitting kinetics task is to verify the pit propagation model that was recently developed in the separate-effects modeling effort. The experimental approach consists of exposure of mechanically pre-pitted specimens of hot-rolled carbon steel, with pits having a range of depths and aspect ratios, to a simulated basalt groundwater for up to 8 months. In conjunction with the exposures, an electrochemical pit-propagation monitor is being modified and verified for use in this application. The monitor design currently is being used at Battelle's Columbus Laboratories to study the kinetics of pit propagation in natural-gas-pipeline steels.

During this reporting period, hot-rolled 1018 carbon steel plate, approximately 7.5 cm thick, was ordered and received. Specimens were machined from the plate, and mechanical pits were drilled in the specimens. Each specimen contains pits of a single diameter and three aspect ratios (depth to diameter) of 2, 5, and 10. Pits having four diameters--5.08 mm (0.2 in.), 2.53 mm (0.1 in.), 1.32 mm (0.05 in.), and 0.51 mm (0.02 in)--will be evaluated for 2, 4, and 8 months in aerated and deaerated 1X basalt groundwater at 90 C. During the exposures, free-corrosion potentials of selected specimens will be measured.

3.1.5 Future Work

3.1.5.1 Electrochemical Studies

The statistical design for the electrochemical studies will be continued through the project year. The initial experimental design will consist of 16 experimental tests, which represent a saturated design of resolution III, and 3 center-point tests for which the concentration of each species is controlled at a level between the corresponding high and low values. The center-point tests will be used to estimate the magnitude of error in the data. This resolution III design confounds main effects with 2-factor interactions but does not confound main effects with one another. Ignoring 3-factor and higher interactions, the data from these first 19 tests will be analyzed to identify main effects and 2-factor interactions that are potentially significant in affecting stress-corrosion cracking. Elimination of species may be possible at this point.

Additional tests (including additional center-point tests) will be run for the purpose of separating main effects from the 2-factor interactions. If no species are eliminated after the first 19 tests, 18 additional tests will be required. Two of these would be center-point tests, and the remaining 16 would be repeats of the original 16 non-center-point tests with high concentrations replaced by low

concentrations and low concentrations replaced by high. These tests, combined with the original tests, represent a design of resolution IV which confounds 2-factor interactions with other 2-factor interactions but does not confound the main effects with the 2-factor interactions or with one another. Again ignoring 3-factor and higher interactions, the data from the first 37 tests will allow for the estimation of the main effect of each species free of any 2-factor interactions. In addition, estimates will be obtained for confounded groups of 2-factor interactions. Additional tests may be required to separate 2-factor interactions within significant groups. Elimination of species should be possible at this point.

If the number of deleterious species is relatively small at this stage, a quadratic response surface will be fitted to the data. The first 37 tests will be supplemented by additional tests for which the concentrations of some species will be controlled at the corresponding center-point concentrations. This will transform the original 2-level design into a 3-level design (each species having 3 possible concentrations). The fitted response surface will be used to identify particularly deleterious concentration regions for stress-corrosion cracking. Slow strain rate tests will then be performed to verify the results of the electrochemical test matrix.

In the tests described above, the temperature will be maintained at 90 C. A limited number of additional tests will be carried out at an elevated temperature to assess the effect of high temperature on the experimental results.

3.1.5.2 Slow Strain Rate Studies

During the next reporting period, selected slow strain rate tests will be performed on hot rolled 1020 carbon steel in environments that are selected on the basis of results of the electrochemistry task.

3.1.5.3 Pitting-Kinetics Studies

During the next reporing period, the exposure tests of the mechanically prepitted carbon-steel specimens will be started and initial testing of the electrochemical pit-propagation monitors will begin.

3.2 Hydrogen Embrittlement

During the previous year, experiments were conducted to determine the potential for embrittlement of cast-steel overpacks by hydrogen from corrosion or radiolytic reactions. Although some of the results required verification, those experiments indicated that resistance to cracking could be reduced significantly by hydrogen, particularly in specimens that were annealed after casting. The apparently high sensitivity to embrittlement of annealed specimens suggested that overpacks may become more susceptible to hydrogen embrittlement with service time, because their microstructures change during long-term exposure to repository temperatures.

Work planned for the current year includes: verification of some observations made in the previous year; studies of the susceptibility to embrittlement of cast steels that are heat treated to simulate long-term exposure to repository temperatures (in conjunction with the NRC-sponsored program at Manufacturing Sciences Corporation); and studies of the susceptibility to embrittlement of commercial-purity iron. During this quarter, the verification tests have been completed, and samples of commercial-purity iron have been obtained from Armco, Incorporated.

3.2.1 Verification Tests on Cast Steel

The results of three sets of fracture-toughness tests from the previous year required verification because of inconsistency in the data. The fracture toughness, J_{Ic}, provides an indication of the material's resistance to crack initiation, whereas the tearing modulus, T (given by $T = (E/\sigma_0^2)(dJ/da)$, where E is Young's modulus, σ_0 is the flow stress, and dJ/da is the slope of the J-resistance curve), provides a measure of the material's resistance to unstable crack growth. The data for the annealed "clean" (low sulfur and phosphorus) steel tested in nitrogen were not valid based on ASTM criteria to determine the J-resistance curves. Therefore, two additional tests were conducted in a nitrogen environment on the clean, annealed steel. In addition, the data for the "doped" steel (with sulfur and phosphorus added to levels typical of commercially available steel) in the as-cast condition indicated that the tearing modulus was slightly higher in hydrogen than in nitrogen. Because hydrogen should reduce (or have no effect on) the tearing modulus, those tests were repeated to determine whether this indication was genuine or simply a result of specimen-to-specimen variation in properties. Also, tests with the doped steel in the hot-rolled condition were repeated in hydrogen and in nitrogen.

Table 3.6 presents revised fracture-toughness data that include the results of the new tests. As expected, multiple testing of the as-cast doped steel revealed that the apparent moderate increase in tearing modulus in hydrogen was a result of specimen-to-specimen variation. The tearing-modulus values for that material ranged from 58 to 94 in nitrogen and from 49 to 95 in hydrogen, with little difference in the averages. The fracture toughness, J_{Ic}, also varied widely in both environments. Hydrogen induced a greater reduction of J_{Ic} in the as-cast doped steel than in the as-cast clean steel, although both steels exhibited approximately the same toughness in nitrogen.

The data in Table 3.6 show that in all cases hydrogen reduced the fracture toughness of the steel. Thus, a crack would initiate in an overpack at lower applied stress (or J integral) when hydrogen is present. This observation is consistent with previous studies of hydrogen embrittlement at Battelle and elsewhere, and by itself it would not necessarily indicate that premature failure by hydrogen embrittlement will occur. In many cases, a crack may initiate at low load or J-integral value but then would not propagate, provided that the tearing modulus is sufficiently high to resist further crack advance.

Table 3.6 Revised fracture-toughness data for clean and doped steels.

Steel	Test	Fracture Toughness (J_{IC}), psi-inch	Tearing Modulus $T = (E/\sigma_0^2)(dJ/da)$
		Clean Steel	
As Cast	1000 psig N_2	575	67
	1000 psig H_2	420	72
Annealed	1000 psig N_2	542*	152*
	1000 psig H_2	65	36
Wrought	1000 psig N_2	1,265	117
	1000 psig H_2	65	85
		Doped Steel	
As Cast	1000 psig N_2	658*	77*
	1000 psig H_2	225*	72*
Annealed	1000 psig N_2	245	181
	1000 psig H_2	30	36
Wrought	1000 psig N_2	605*	65*
	1000 psig H_2	185*	73*

*Based on results from new tests.

If the tearing modulus is reduced by hydrogen, unstable crack growth is more likely, and premature failure can occur. The tearing modulus was not significantly lower in hydrogen for the as-cast and wrought conditions; however, a large reduction in tearing modulus was observed for both the clean and the doped steels in the annealed condition. The observation of a significant tearing-modulus reduction in hydrogen for the annealed steels suggests that as microstructures change with time at slightly elevated temperatures, such as those in a repository, sensitivity to hydrogen embrittlement may increase. This possibility will be examined further in the current year in a cooperative effort with the NRC program at Manufacturing Sciences Corporation.

3.2.2 Commercial-Purity Iron

Twelve small laboratory ingots of commercial-purity iron from three heats were provided by Armco, Incorporated, for use in hydrogen-embrittlement and corrosion testing. The ingots were produced with chemical compositions that could be achieved in large quantity using present practice at Armco. The chemical composition of the iron ingots, determined by Armco, are presented in Table 3.7. These ingots currently are being characterized metallurgically, and test specimens are being prepared. In addition, one ingot from Heat V2025 was provided to Manufacturing Sciences Corporation for use in their study of the effects of processing variables on waste-container properties.

3.2.3 Future Work

Hydrogen-embrittlement testing of commercial-purity iron will be initiated during the next quarter. In addition, as cast-steel samples become available from the program at Manufacturing Sciences Corporation, these also will be prepared in the form of compact-tension specimens and tensile specimens and will be tested in hydrogen and inert environments.

3.3 Corrosion Correlations

Work on the corrosion correlations focused on further development and testing of the general-corrosion and pitting-corrosion models. The general-corrosion model was used to calculate the general-corrosion rate as a function of time for three cases: first, with a low value for g (a measure of the local radiolytic-production rate of an oxidizing species) and a low value for ε (the linear gamma-absorption coefficient); second, with a high value for g and a low value for ε; and finally, with high values for both g and ε. The results indicate that general corrosion can be significantly affected by radiolytically-produced oxidizing species. In the pitting-corrosion task, an existing model for the induction time for pitting at an "average" site is used in conjunction with empirical techniques that account for the statistical distribution of induction times about that site. The Weibull distribution is being considered as a flexible way to bring the description of pitting-induction times into accord with experimental data.

Table 3.7. Chemical compositions of commercial-purity-iron samples*.

Heat Number	Content, weight percent												
	C	Mn	Si	S	P	Al	Cu	Ni	Cr	Mo	Cb	Ti	Co
V2023	0.0037	<0.004	0.17	0.0034	0.002	0.004	0.075	0.006	0.046	0.050	<0.002	<0.002	<0.003
V2024	0.0016	<0.004	0.16	0.0027	<0.002	<0.004	0.072	0.026	0.047	0.046	<0.002	<0.002	<0.003
V2025	0.0007	<0.004	0.17	0.0028	<0.002	<0.004	0.076	0.029	0.047	0.048	<0.002	<0.002	<0.003

*Provided by Armco, Incorporated.

3.3.1 General Corrosion

In the recently issued Annual Report for this program[3.11], the results of some sample calculations were presented for a simplified general-corrosion model. The major assumptions inherent in this model were:

- The behavior of one oxidizing species within the groundwater outside the container wall was considered. This species, nominally O_2, was assumed to be radiolytically produced.
- Mass transport of the dissolved species to the container surface occurred via chemical diffusion only, with cylindrical geometry being assumed for the surface.
- Aside from its radiolytic production, the dissolved species underwent no chemical reactions within the groundwater.
- The entire system was isothermal.
- A "maximum-rate" model was used, in the sense that the concentration of the dissolved species at the container wall was taken to be maintained at zero. In this approximation, film-growth kinetics did not, in any way, inhibit the rate of transfer of the species across the metal/groundwater interface.
- The gamma-field intensity, $I(r,t)$, measured at radial distance r from the axis of symmetry at time t, was taken to be

$$I(r,t) = \left(\frac{1}{r}\right) \exp\left[-t - \varepsilon(r-1)\right] \quad , \tag{3.1}$$

where ε is the linear absorption coefficient. In Equation 3.1, the unit of time is the square of the container radius divided by the chemical diffusivity of the species, the unit of distance is the container radius, and the unit of I is clearly its value, in absolute units, at $r = 1$ and $t = 0$.

The local rate of production of the chemical species, being proportional to $I(r,t)$, was expressed as gI, where g is a parameter chosen to be dimensionless, so that the production rate is likewise dimensionless.

The concentration field, $c(r,t)$, characterizing the species, was computed for three different cases, i.e.,

- $g = 1, \varepsilon = 1$
- $g = 10, \varepsilon = 1$
- $g = 10, \varepsilon = 2$

using the following initial and boundary conditions:

- $c(r = 1, t > 0) = 0$
- $c(1 < r < 5, t = 0) = c(r = 5, t > 0) = 1$.

In this manner, effects of increasing the production rate and the linear absorption coefficient were both evaluated.

During the past reporting period, further consideration was given to these same three problems. In particular, the rate of general corrosion was calculated as a function of time for each case. This rate is proportional to the rate at which the oxidizing species is transported across the container surface which, on the basis of this model, is in turn proportional to

$$\frac{\partial c}{\partial t}(r, t)\bigg|_{r=1} \quad .$$

In addition, the total depth of penetration of the corrosion layer into the metal, which is proportional to

$$\int_0^t \left\{ \frac{\partial c}{\partial r}(r,t)\bigg|_{r=1} \right\} dt \quad ,$$

was also calculated for each case as a function of time. The results are illustrated in Figures 3.12 and 3.13. Since we are presently interested only in relative variations of corrosion rates and penetration depths, these quantities are plotted in terms of normalized, dimensionless units, the precise definitions of which are unimportant for present purposes.

The calculated corrosion rates are plotted in Figure 3.12. For the case $g = 1$, $\varepsilon = 1$, the corrosion rate decreases monotonically with time. For the case $g = 10$, $\varepsilon = 1$, which corresponds to a large increase in the production rate of the oxidizing species relative to the previous case (for which $g = 1$), the corrosion rate at any given time is generally significantly higher than the corresponding rate for $g = 1$, $\varepsilon = 1$ calculated at the same time. The corrosion rate even experiences a period during which it increases with time. This behavior results, of course, from the much greater amount of the oxidizing species that is generated for $g = 10$. Finally, the case $g = 10$, $\varepsilon = 2$ illustrates the effect of increasing the linear absorption coefficient by a factor of two. Comparison of the cases $g = 10$, $E = 1$ and $g = 10$, $\varepsilon = 2$ shows that the corrosion rate is indeed reduced by increasing ε, although the resultant curve still lies well above that for the case $g = 1$, $\varepsilon = 1$.

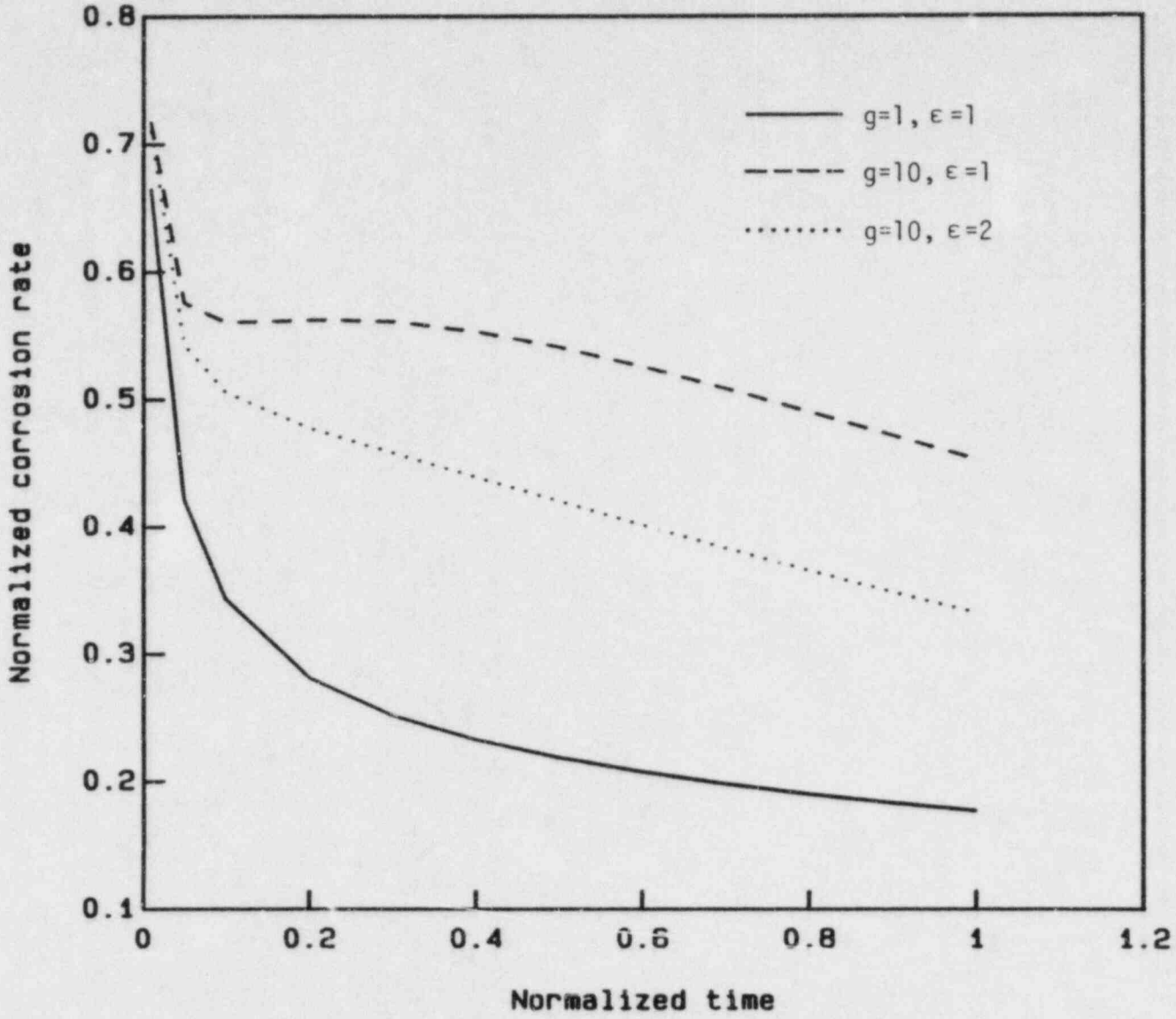

Figure 3.12. Calculated rates of general corrosion as a function of time.

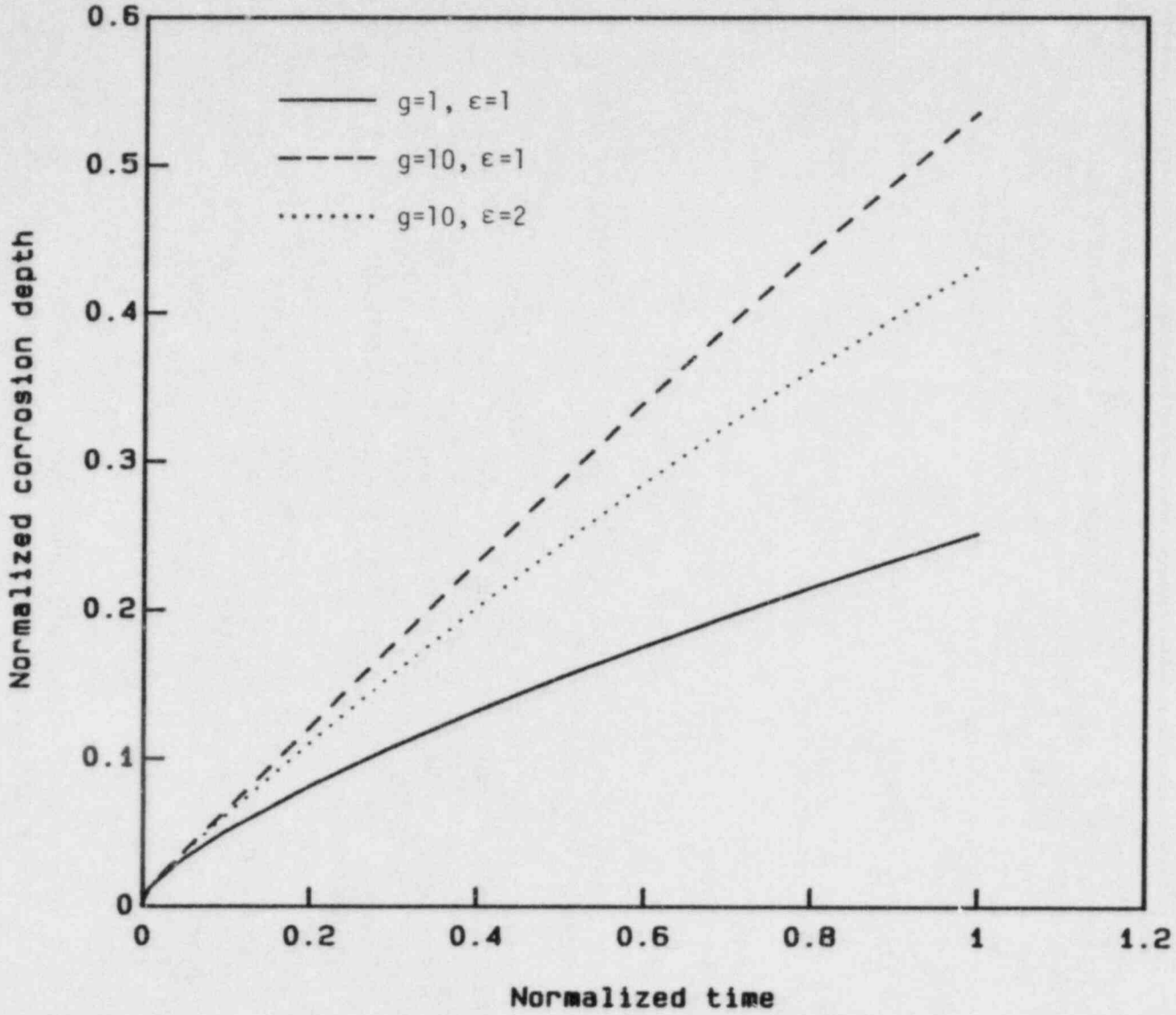

Figure 3.13. Calculated depth of penetration by general corrosion as a function of time.

The corrosion depth calculated for these same three cases is plotted in Figure 3.13 on the same time scale as in Figure 3.12. As would be expected from the results presented in Figure 3.12, the corrosion depth, at a given time, is indeed largest for the case $g = 10$, $\varepsilon = 1$ and smallest for the case $g = 1$, $\varepsilon = 1$.

From the results of this highly idealized analysis, it appears that radiolytic production of oxidizing species could indeed have a significant effect on the overall kinetics of general corrosion. A major objective of this particular task is to quantify further our understanding of this effect through the use of more physically realistic radiolysis models and through the inclusion of film-growth kinetics on the container surface.

3.3.2 Pitting Corrosion

Studies carried out thus far on this program in the area of pitting corrosion have been centered on three principal aspects of the overall process:

- Pit-generation kinetics
- Pit-growth kinetics
- Evolution of the pit-depth distribution.

The greatest emphasis thus far has been placed on the last two aspects, in which substantial progress has been made[3.12].

Our most recent studies of pitting corrosion have dealt with pit-generation kinetics, about which there is still relatively little knowledge. However, it does appear to be possible to make use of existing theoretical models of pit initiation, in conjunction with a more empirical description of the rate at which pits are formed on a metal surface, to develop a physically reasonable description of the overall pit-generation process.

As has already been pointed out[3.12], the approach that would be taken would be to use an existing model[3.13] for the induction time for pitting at an "average" site, and then to account for a statistical distribution of induction times, about that for the "average site", through the application of essentially empirical techniques. The problem then would be to select a statistical distribution that would adequately describe the gross features of pit-generation kinetics.

For example, the time-dependent pit-generation rate, $G(t)$, which is expressed in number of pits per unit area of surface per unit time, may be a "peaked" type. Janik-Czachor and Ives[3.14] described the gross features of such behavior, which are that $G(t)$ rises from zero to a maximum value and then falls to zero once again, using a very simple $\sin^2(0.2t)$ function.

An improved approach to describing the pit-generation rate would be to use a more flexible distribution function, one that could be more readily brought into accord with corresponding experimental data. One such example is the Weibull distribution, which is expressed for our purposes as

$$G(t) = \frac{mN_\infty}{\tau^m}\left(t - t_o\right)^{m-1} \exp\left[-\left(\frac{t-t_o}{\tau}\right)^m\right] \qquad (3.2)$$

and which is applicable for $t > t_o$, with $G(t) = 0$ for $t \leq t_o$. Here, N_∞, m, τ, and t_o are variable parameters, with $m \geq 1$. Clearly,

$$\int_0^\infty G(t)dt = N_\infty \quad ,$$

so that N_∞ represents the total number of pits per unit area achieved at asymptotically large times.

For $m > 1$, the function $G(t)$, given by Equation 3.2, rises smoothly from zero beginning at time $t = t_o$, "peaks" at time t_{max}, which is given by

$$t_{max} = t_o + \tau\left(1 - \frac{1}{m}\right)^{1/m} \quad ,$$

and then decreases monotonically with time, approaching zero asymptotically.

The time t_{max} can be chosen to be the characteristic incubation time, as predicted from first principles[3.13]. Values of N_∞, τ, and m can then be chosen that would yield generation-rate behavior that is consistent with experimental data. Such choices may, however, have to be inferred from pit-depth-distribution measurements, which are more likely to be made than direct measurements of the pit-generation rate itself. Relationships between pit-generation rate and the time-dependent pit-depth distribution have already been established for some elementary cases.[3.12,3.14]

Near-term plans include the application of Equation 3.2, in conjunction with existing pit-growth data for metals, to the prediction of pit-depth distributions as a function of time.

3.4 References for Section 3

(3.1) T. E. Jones, "Reference Material Chemistry--Synthetic Groundwater Composition", RHO-BW-St-37 P (April 1982).

(3.2) "Long-Term Performance of Materials Used for High-Level Waste Packaging", D. Stahl and N. E. Miller (Compilers), NUREG/CR-3427, Vol. 4, BMI-2113 (June 1984).

(3.3) J. A. Beavers, N. G. Thompson, and R. N. Parkins, "Stress-Corrosion Cracking of Low-Strength Steels in Candidate High Level Waste Repository Environments", Topical Report, NUREG/CR-3861, to be published, 1984.

(3.4) "Appendix D: Range of Environmental Parameters", Draft NUREG-1076, ORNL, 1984.

(3.5) Data on Trace Elements from Well DC-6. Personal Communications from Tom Jones to Jeff Means, 1983.

(3.6) W. J. Gray, "Gamma Radiolysis Effects on Grande Ronde Basalt Groundwater", RHO-BW-SA-315 P (presented at the Materials Research Society Symposium-Scientific Basis for Nuclear Waste Management, Boston, MA, November 14-17, 1983).

(3.7) S. A. Simonson, and W. L. Kuhn, "Predicting Amounts of Radiolytically Produced Species in Brine Solution", PNL-SA-11426 (presented at the Materials Research Society Symposium-Scientific Basis for Nuclear Waste Management, Boston, MA, November 14-17, 1983).

(3.8) E. P. Grause, C. Brewster, and P. Soo, "Determination of the Waste Package Environments for a Basalt Repository: Phase 1 - Gamma Irradiation Conditions in the Absence of Methane", BNL-NUREG-24297, Draft Report, (February 1984).

(3.9) G. H. Koch, N. G. Thompson, and J. L. Means, "Corrosion Chemistry of SO_2 Scrubbers Part 1, Trace Elements in FGD Environments and Their Potential Effect on Corrosion of Alloys", EPRI Report to be published on Research Project 1871-6, 1983.

(3.10) NRC Nuclear Waste Geochemistry '83, Proceedings of the U.S. Nuclear Regulatory Commission, Reston, Virginia, August 1983, p. 245.

(3.11) "Long-Term Performance of Materials Used for High-Level Waste Packaging", D. Stahl and N. E. Miller (Compilers), NUREG/CR-3427, Vol. 4, BMI-2113 (June 1984), pp. 3-106 ff.

(3.12) "Long-Term Performance of Materials Used for High-Level Waste Packaging", D. Stahl and N. E. Miller (Compilers), NUREG/CR-3427, Vol. 4, BMI-2113 (June 1984), pp. 3-121 ff.

(3.13) L. F. Lin, C. Y. Chao, and D. D. MacDonald, J. Electrochem. Soc., 128 (1981) 1194.

(3.14) M. Janik-Czachor and M. B. Ives, in Passivity of Metals, R. P. Frankenthal and J. Kruger (Editors), Electrochem. Soc. (Princeton, N. J., 1978), p. 369.

4. SYSTEM PERFORMANCE

One objective of the system-performance task is to develop an improved understanding of phenomena that affect waste-package performance at the system level. This includes phenomena such as those arising through combined effects as well as others which drive the evolution of the waste-package condition.

During the past quarter, our efforts have been directed towards studies of groundwater chemistry, groundwater radiolysis, uncertainty analysis, and the planning of integral experiments. The groundwater-chemistry studies will ultimately provide information on the composition of the aqueous system in the vicinity of waste packages and on how that composition is affected by the presence of the waste package. This information is needed to support other descriptions, such as those of corrosion and radionuclide transport, which will be used to assess the performance of a high-level nuclear-waste repository. The water-radiolysis studies provide information on how the presence of gamma radiation alters the water chemistry in the vicinity of nuclear-waste packages. Such alterations in the water chemistry may affect the long-term performance of the metallic barriers used in waste packages. Radiation-induced changes in the water chemistry may also affect the release rates of radionuclides from waste packages. This may occur through radiation-induced changes in oxidation states which may affect solubilities of radionuclides or groundwater species. These changes may thus affect the waste-package performance measure associated with radionuclide release. Uncertainty analysis studies will provide a quantitative means of assessing the likely range of waste-package performance parameters. This quarter's efforts have been directed towards an examination of various uncertainty analysis techniques. The integral experiments will provide information on several technical issues relevant to waste-package performance.

4.1 Water-Chemistry Studies

The influence of water chemistry on the performance of materials for high-level waste packaging is gaining general recognition among the research community. Degradation of the backfill, the container, and the waste form all will be strongly affected by the composition of the groundwater in contact with these materials. To date, however, it appears that most research efforts either focus exclusively on water chemistry or else concentrate on individual degradation processes neglecting details of water chemistry. Our work is intended to bridge this gap, applying water chemistry to the study of degradation mechanisms.

A complete, quantitative study of the intricacies of water chemistry can be very involved. Our intent, however, is to explore the uses of water-chemistry computer codes as tools that are coupled with descriptions of other phenomena. Accordingly, we are developing and working with a water-chemistry code that is easy to couple with descriptions of other

phenomena. This program is not as sophisticated as existing state-of-the-art water-chemistry codes, but it is sufficiently advanced for our purposes. The code includes the major chemical species, including those derived from the container and waste form as well as the major constituents of natural groundwaters, and it provides a level of detail comparable to that of the descriptions of the degradation mechanisms.

Since water chemistry is being treated as a tool, the results of water-chemistry calculations are reported in the discussions of the processes for which this tool was used. During the current quarter, the primary application of water chemistry was in calculating the kinetics of waste-form dissolution. Some effort was also necessary to adapt our copy of WATEQ to a new compiler version.

Recent results elsewhere[4.1-4.3] indicate that the precipitation of iron silicates and aluminum silicates has a significant effect on the durability of the waste form. At present, our water-chemistry model does not provide adequate treatment of iron and aluminum species. Near-term plans include an effort to improve our treatment of these elements.

4.2 Water Radiolysis Studies

As reported previously[4.4], several investigators have shown that gamma radiation may have adverse effects on the time-to-failure performance measure for metal components which are exposed to water in the presence of a radiation field. These performance issues are being addressed through the corrosion-modeling work described in Section 3.3, the corrosion experiments described in Section 3.1, and the water-radiolysis studies and integral experiments described in this section. One purpose of the water-radiolysis studies is to develop a general description of the gamma radiolysis of groundwaters in the vicinity of nuclear-waste packages. This description will be used to provide water-radiolysis mechanisms and rate constants to the corrosion-modeling effort described in Section 3.3. This work is also being used to provide a description of the composition of the aqueous system in the vicinity of waste-package metallic components to the container-materials task described in Section 3.1. It is intended that this effort will lead to the development of a generalized model for the radiolysis of all candidate groundwaters. This will provide NRC with a tool which can be used to simulate the effects of radiation on aqueous systems. This information can be used as one element of the overall performance assessment of a potential nuclear-waste repository.

Our approach is, first, to develop a description for the radiolysis of pure water which might contain dissolved hydrogen or oxygen. This description is being extended to account for anions and cations which may be present in significant amounts in groundwaters of interest. As this description of groundwater radiolysis develops, it is being benchmarked against experimental data which are available from the literature. As part of this effort, gamma-energy-deposition calculations were performed to determine energy-deposition rates to groundwater and

materials surrounding a waste package. Results of these energy-deposition calculations have been reported previously.[4.4] In addition, several mechanisms for the radiolysis of water were evaluated on the basis of their ability to predict the behavior of water-radiolysis experiments described in the literature. Of these, the mechanism presented by Rosinger and Dixon[4.5] was chosen as the basis for our generalized description of groundwater radiolysis. During this quarter, this description has been extended to account for the presence of iron species in groundwaters. As part of this effort, comparisons are made between predictions of the radiolysis model and measured concentrations of hydronium ions and ferric ions as a function of time for an aqueous iron sulfate system exposed to gamma radiation.

4.2.1 Radiolysis of Groundwaters Containing Iron

A mechanism for the gamma radiolysis of groundwaters containing aqueous iron species is being developed as an extension of the Rosinger and Dixon mechanism[4.6] for the radiolysis of pure water. The reasons for using the Rosinger and Dixon mechanism are described elsewhere.[4.4]

The first step in extending the basic mechanism to include aqueous iron species was to add the elementary reactions for the ferrous and ferric cations given in the mechanism of Christenson and Bjergbakke[4.6]. This mechanism contains 13 reactions describing the oxidation of ferrous ions, the reduction of ferric ions, and the sorption of ferrous ions. These 13 elementary reactions were combined with the 55 reactions of the Rosinger and Dixon mechanism to yield a system of 68 elementary reactions. This system of equations was integrated with respect to time using the MAKSIMA-CHEMIST code[4.7] to simulate an experiment performed by Mathews[4.8]. The data were chosen for a deaerated solution with an initial ferrous ion concentration of 10^{-4} mole per liter. The resulting time dependence of the ferric ion yield showed approximate agreement with Mathews' results,[4.8] as shown in Figure 4.1. However, the hydronium ion concentration calculated with this mechanism was in strong disagreement with the experimental data; this is shown in Figure 4.2, where the hydronium ion concentration gradually increases during the experiment, whereas the calculation shows the hydronium ion concentration quickly decreasing to a very low level, on the order of 10^{-10} mole per liter. The same simulation performed with the entire mechanism of Christensen and Bjergbakke showed very good agreement with the experimental data for the ferric ion concentration but equally poor agreement with the experimental measurements of the hydronium ion concentration. This is shown by the data points represented by circles in Figures 4.1 and 4.2 for the ferric and hydronium ion concentrations respectively.

It was thus necessary to adjust the mechanism so that the hydronium ion concentration would increase. This can be accomplished by increasing the hydronium ion concentration or by decreasing the hydroxyl ion concentration. The latter approach was attempted first by adding the elementary reaction

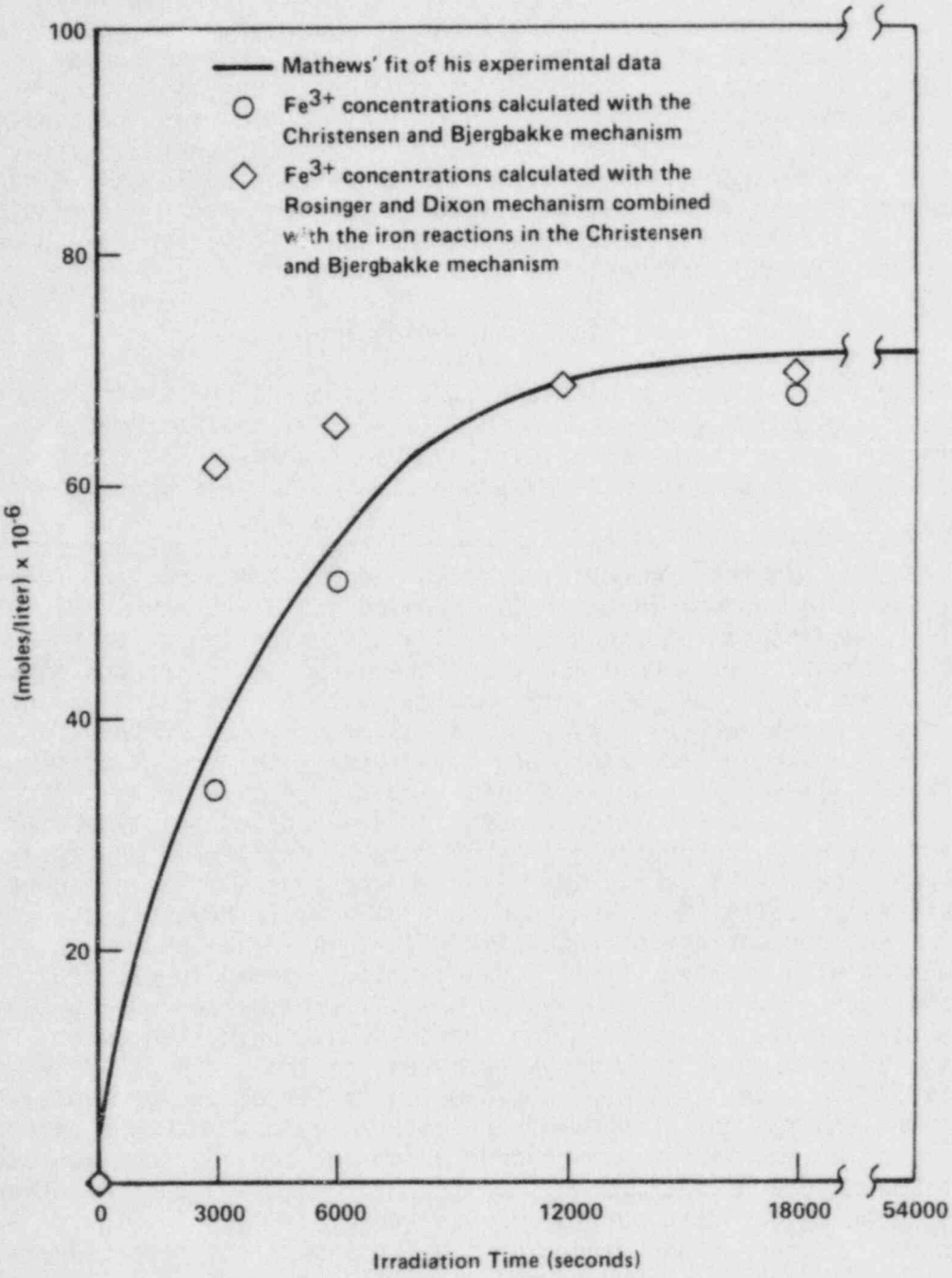

Figure 4.1. Ferric ion concentration as a function of irradiation time, calculated using the basic reaction set modified to include iron (○) and its hydrolysis products (◇).

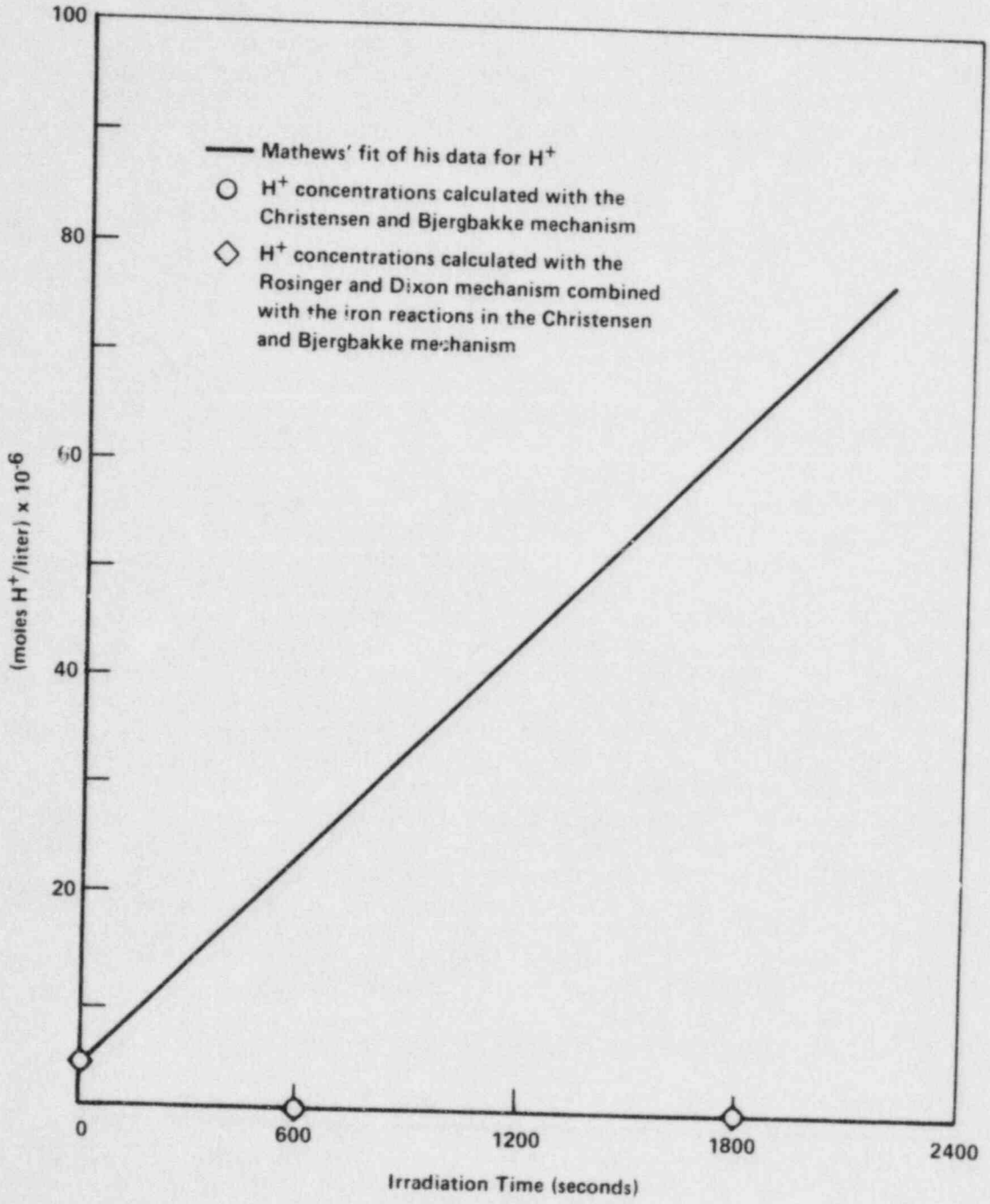

Figure 4.2. Hydronium ion concentration as a function of irradiation time, calculated using the basic reaction set modified to include iron (○) and its hydrolysis products (◇).

$$H + OH^- = e^- + H_2O$$

which is important in systems of high pH[4.9]; but the addition of this reaction had no significant effect on the concentrations calculated for any of the species. The former approach--adding reactions that produce hydronium ion--was then adopted. This was accomplished by adding elementary reactions for the first and second hydrolysis products of aqueous ferric ions. The forward and reverse reactions are:[4.10]

$$Fe^{3+} + H_2O \rightarrow FeOH^{2+} + H^+$$

$$FeOH^{2+} + H^+ \rightarrow Fe^{3+} + H_2O$$

$$FeOH^{2+} + H_2O \rightarrow Fe(OH)_2^+ + H^+$$

$$Fe(OH)_2^+ + H^+ \rightarrow FeOH^{2+} + H_2O$$

The rate constants k_2 and k_{-2} were measured by Hemmes et al[4.11] to be $(6.1 \pm 0.4) \times 10^4$ sec^{-1} and $(8.0 \pm 1.0) \times 10^9$ sec^{-1}, respectively. Hemmes et al also estimated the value of the rate constant k_1 to be 3×10^7 sec-1. The rate constant k_{-1} was estimated from data presented by Sylva[4.10] for the equilibrium constant for the forward and reverse hydrolysis reaction. Data chosen for this estimation were those cited by Sylva for 32 C and an ionic strength of 1.17×10^{-2}. These data were used to estimate a value of 4.7×10^9 sec-1 for k_{-1}. When these reactions were added to the description, the ferric ion concentration was within a factor of 3 of the experimental data. The sum of the ferric ion concentration and the concentration of the first hydrolysis product of the ferric ion showed better agreement with the experimental data than the ferric ion concentration alone. (In actuality, if the first hydrolysis product were present, it would contribute to the observed ferric yield since the experimental measurements were made at 304 nm. Based on the data of Olson and Simonson[4.12], the molar extinction coefficients of ferric ion and the first hydrolysis product of ferric ion are about 120 and 1900, respectively).

The results of calculations that included the first and second hydrolysis products of aqueous Fe^{3+} are shown by the data points represented by diamonds in Figures 4.1 and 4.2. As can be seen in Figure 4.2, the hydronium ion concentration calculated with this system of reactions is too low. Also, the ion product for water is calculated to be 1.8×10^{-8}, which is a significant departure from the desired value of 10^{-14}. When the reactions for the water equilibrium in the absence of radiation were run in a kinetic simulation with the ferric hydrolysis reactions, the ion product for water was observed to be 1.01×10^{-14}. This indicated that the problem was not caused by the hydrolysis reactions themselves.

To provide a reasonable hydronium ion concentration and H_2O ion product, the reactions

$$Fe^{3+} + OH^- = FeOH^{2+} \qquad k = 10^4$$

and $$FeOH^{2+} = Fe^{3+} + OH^- \qquad k = 10^9 \quad ,$$

which are listed in the set of iron reactions in the Christensen and Bjergbakke mechanism, were then removed from the description. This was a reasonable modification because the H_2O concentration is much greater than the OH^- concentration and because these reactions were not among those reported in other kinetic studies of iron sulfate systems. Reactions representing the sorption and desorption of ferrous ion were also removed from the reaction scheme (those reactions involving species identified by Christensen and Bjergbakke as "A"). A radiolysis simulation using this modified mechanism was then run for the conditions used in Mathews' experiment. The ion product for water was now calculated to be 1.01×10^{14}, which is a desired result.

Time-dependent concentrations of various species from this calculation are shown in Table 4.1. Here the H^+ concentration is seen to increase from 4.0×10^{-6} mole per liter at 0 seconds to 2.6×10^{-5} mole per liter, which is much lower than values reported by Mathews. The first and second hydrolysis products for ferric ion level off at about 7.6×10^{-5} mole per liter and 2.2×10^{-5} mole per liter, respectively.

Table 4.1. Concentrations calculated using a modified model.

Time (sec)	H^+ (mole/liter)	Fe^{3+} (mole/liter)	$FeOH^{2+}$ (mole/liter)	$Fe(OH)_2^+$ (mole/liter)
0	4.0E-6	0	0	0
600	1.5E-5	5.58E-8	2.31E-5	1.14E-5
1200	2.16E-5	1.70E-7	5.02E-5	1.77E-5
1800	2.60E-5	2.93E-7	7.32E-5	2.18E-5
3000	2.60E-5	3.09E-7	3.59E-5	2.23E-5
6000	2.60E-5	3.09E-7	3.59E-5	2.23E-5
12000	2.60E-5	3.09E-7	7.59E-5	2.23E-5
18000	2.60E-5	3.09E-7	7.59E-5	2.23E-5

Additional changes were then made to the mechanism to make it more consistent with other mechanisms reported in the literature for ferrous sulfate systems. The following reactions from the Christensen and Bjergbakke mechanism[4.6]:

$$Fe^{2+} + e^- = Fe^{3+} + OH^- + H^- \ *$$

$$Fe^{2+} + H = Fe^{3+} + H^-$$

$$H^- + H_2O = H_2 + OH^-$$

were removed and replaced with the reactions

$$Fe^{2+} + e^- = Fe^{+} + H_2O$$

$$Fe^{2+} + H = Fe^{2+} — H$$

$$Fe^{2+} — H + H^+ = Fe^{3+} + H_2 \quad ,$$

which are cited by Nenadovic et al(4.13). Since the first of these reactions introduces Fe^+ ion into the solution, the assumption was made that this ion would undergo oxidation reactions analogous to those of the ferrous ion. As a first-order approximation, it was assumed that the rates of the Fe^+ oxidation reactions could be estimated from the analogous rates for the ferrous ion oxidation reactions. It was further assumed that the rate constants would vary with the inverse of the radius of the metal ion species. Handbook values of the Fe^{3+} and Fe^{2+} radii(4.14) were listed as 0.64 and 0.75 angstroms respectively. The Fe^+ radius was than estimated, using a linear extrapolation, to be 0.84 angstroms. Using this information, the ratio of the rate constants for the oxidation of Fe^+ ions was estimated to be 0.88.

The final set of reactions which has thus far been added to the Rosinger and Dixon description for the radiolysis of water is listed in Table 4.2. Concentrations of species calculated with this mechanism in a simulation of Mathews' experiment, described previously, are shown in Table 4.3 for selected times after initiation of irradiation. A comparison with measurements made by Mathews is shown in Figures 4.3 and 4.4 for selected iron species and hydronium ions respectively. Figure 4.3 shows that the radiolysis model predicts the presence of several important ferric species, whereas in Mathews' experiment, the assumption was made that only ferric ion is sufficiently concentrated to be measurable by spectrophotometry at 304 nm.(4.8,4.15) However, spectroscopic studies of ferric ion systems show that ferric ion is not the only ferric species which absorbs at 304 nm(4.12,4.16). Based on data reported by Olson and Simonson,(4.12) the molar extinction coefficient for the first hydrolysis product of ferric ion is more than an order of magnitude greater than the molar extinction coefficient for ferric ion at 304 nm. From these data, the molar extinction coefficients are estimated to be approximately 120 and 1900 liter-mol^{-1}-cm^{-1} respectively for these species at 304 nm. Mathews reports measuring a

---

*These equations are shown as they appear in Reference 4.7.

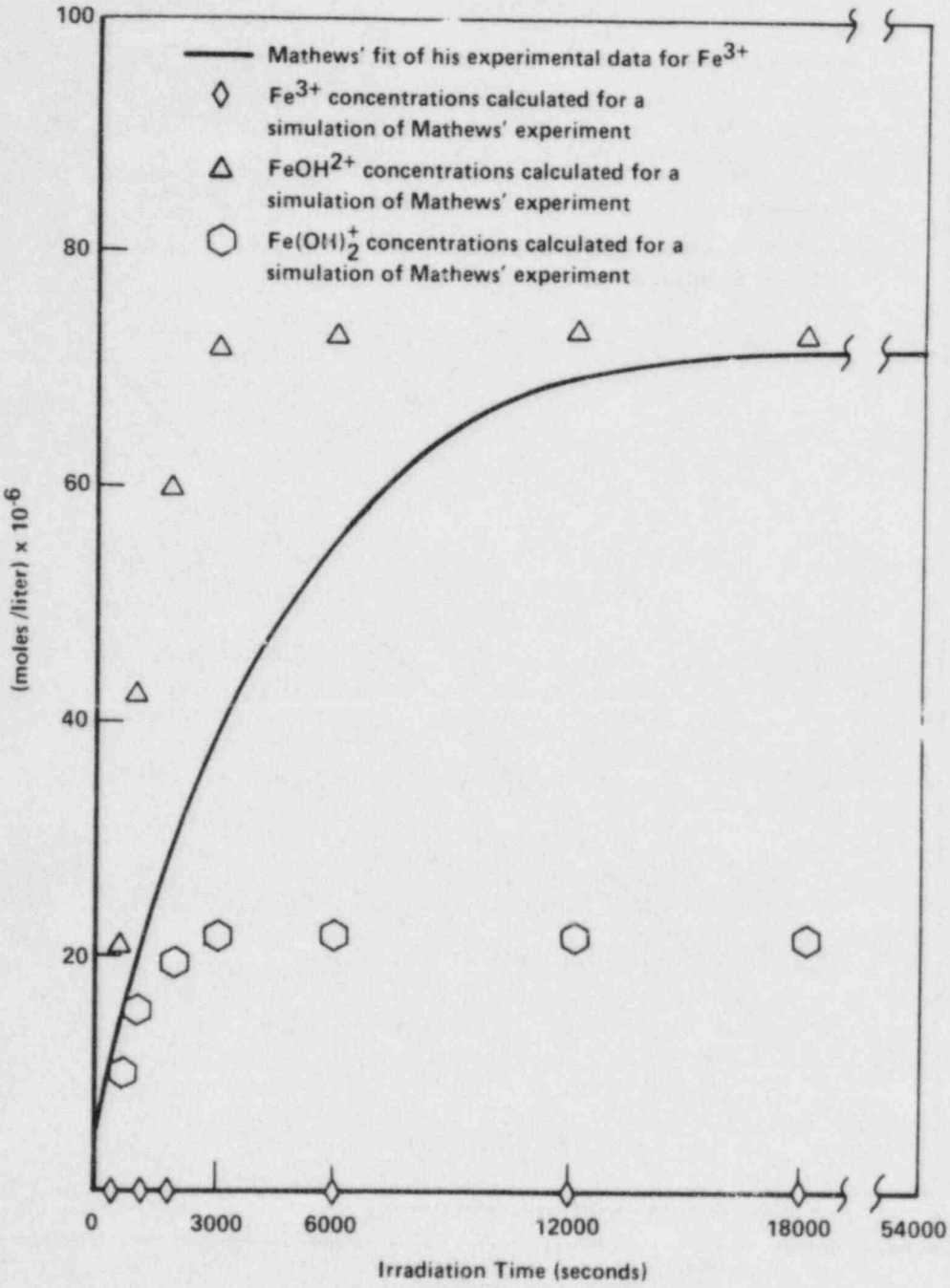

Figure 4.3. Ferric ion, $FeOH^{2+}$, and $Fe(OH)_2^+$ concentrations calculated as a function of irradiation time.

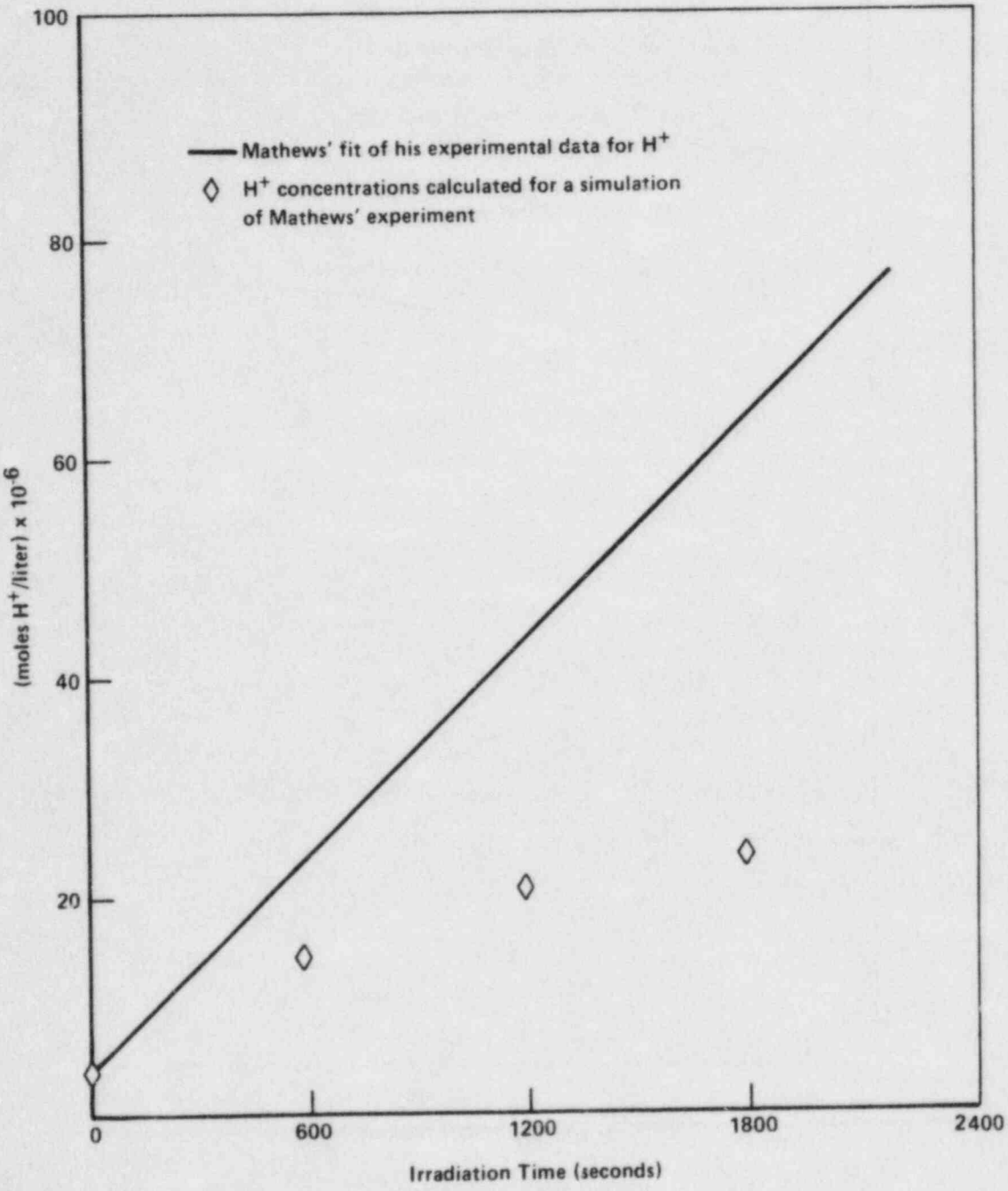

Figure 4.4. Hydronium ion concentration calculated as a function of irradiation time.

molar extinction coefficient of 2180 liter-mol^{-1}-cm^{-1} for ferrous ion solutions which were oxidized to ferric ion solutions with hydrogen peroxide.[4.8,4.15] This high value for the measured molar extinction coefficient indicates that other absorbing species may be present in Mathews' solutions.

Table 4.2. Reactions added to the Rosinger and Dixon mechanism.

Fe^{2+}	+	OH	=	Fe^{3+}	+	OH^-			k = 3.400E+08
Fe^{2+}	+	e^-	=	Fe^+					k = 1.200E+08
Fe^+	+	OH	=	Fe^{2+}					k = 3.000E+08
Fe^+	+	H_2O_2	=	Fe^{2+}	+	OH	+	OH^-	k = 5.290E+01
Fe^+	+	O^{2-}	=	Fe^{2+}	+	$O2^-$			k = 3.520E+08
H	+	Fe^{2+}	=	$Fe^{2+}OH$					k = 1.380E+06
Fe^{2+} — H	+	H^+	=	Fe^{3+}	+	H_2			k = 1.060E+06
Fe^+	+	H	=	FeH^+					k = 1.200E+06
$Fe^{+}H$	+	H^+	=	Fe^{2+}	+	O_2			k = 4.000E+08
Fe^{3+}	+	H	=	Fe^{2+}	+	H^+			k = 1.000E+08
H	+	OH^-	=	e^-	+	H_2O			k = 1.800E+07
Fe^{3+}			=	$FeOH^{2+}$	+	H^+			k = 3.000E+07
$FeOH^{2+}$	+	H^+	=	Fe^{3+}					k = 4.700E+09
$FeOH^{2+}$			=	$Fe(OH)^{2+}$	+	H+			k = 6.100E+04
$Fe(OH)^{2+}$	+	H^+	=	$FeOH^{2+}$					k = 8.000E+09

Therefore, to compare results of our calculations with these experimental data it is necessary to back-calculate the absorption at 304 nm of radiant power by the solutions analyzed in Mathews' experiments. This was done for data reported by Mathews for a deaerated system, assuming a 1-cm path length and an extinction coefficient of 2180 nm. The apparent ferric ion concentration was estimated from the curve which is reported in the literature as a fit of the experimental data. These concentrations and the estimated absorptions are shown in Table 4.4. These data were compared with results of our calculations by estimating the absorptions which would be observed if the solution had the compositions which were calculated. This was determined by taking the sum of the absorption at 304 nm caused by the ferric ion and the first hydrolysis product of the ferric ion. The extinction coefficients used in these calculations are 119 and 1905 respectively, as estimated from data of Olson and Simonson.[4.12] The absorption of radiant power at 304 nm in a 1-cm cell for a solution of a composition calculated by our model and by solutions analyzed by Mathews are shown in Figure 4.5. From this figure, it can be seen that the calculated concentrations of the absorbing species increase more rapidly at short times than is observed in the experimental data. The observed steady states are also approached more rapidly in the calculations than in the experimental data.

Table 4.3. Concentration of all species calculated for a simulation of Mathew's experiment using the Rosinger and Dixon mechanism with the additional reactions shown in Table 4.2.

Time Seconds	e^-_{aq} Moles/L	H^+ Moles/L	OH^- Moles/L	OH Moles/L	H Moles/L	H_2 Moles/L	H_2O_2 Moles/L	HO_2^- Moles/L	HO_2 Moles/L
0.	0.	4.000E-06	2.500E-09	0.	0.	0.	0.	0.	0.
6.000E+02	7.021E-14	1.502E-05	6.731E-10	1.236E-12	2.231E-10	1.561E-05	3.058E-07	3.930E-14	2.302E-16
1.200E+03	5.224E-14	2.050E-05	4.931E-10	1.978E-12	3.141E-10	2.947E-05	2.524E-07	2.396E-14	2.354E-16
1.800E+03	4.533E-14	2.378E-05	4.251E-10	3.587E-12	4.475E-10	3.997E-05	1.913E-07	1.574E-14	2.445E-16
3.000E+03	4.192E-14	2.580E-05	3.918E-10	8.251E-12	6.788E-10	4.737E-05	1.296E-07	9.902E-15	2.711E-16
6.000E+03	4.174E-14	2.592E-05	3.900E-10	8.725E-12	6.974E-10	4.783E-05	1.261E-07	9.597E-15	2.744E-16
1.200E+04	4.163E-14	2.599E-05	3.890E-10	8.678E-12	6.961E-10	4.808E-05	1.263E-07	9.590E-15	2.742E-16
1.800E+04	4.152E-14	2.605E-05	3.880E-10	8.631E-12	6.947E-10	4.834E-05	1.265E-07	9.582E-15	2.740E-16

Time Seconds	O_2^- Moles/L	O_2 Moles/L	H_2O Moles/L	$O_2^=$ Moles/L	O^- Moles/L	O_3^- Moles/L	Fe^{2+} Moles/L	Fe^{3+} Moles/L	$FeOH^{2+}$ Moles/L
0.	0.	0.	5.560E+01	0.	0.	0.	1.000E-04	0.	0.
6.000E+02	7.049E-15	3.059E-14	5.560E+01	1.486E-16	2.272E-23	5.002E-25	6.837E-05	4.842E-08	2.058E-05
1.200E+03	1.212E-14	1.059E-13	5.560E+01	1.262E-16	2.675E-23	3.306E-24	4.071E-05	1.373E-07	4.274E-05
1.800E+03	2.599E-14	2.600E-13	5.560E+01	1.213E-16	4.193E-23	1.400E-23	2.010E-05	2.239E-07	6.010E-05
3.000E+03	1.033E-13	8.916E-13	5.560E+01	1.316E-16	8.905E-23	1.671E-22	5.857E-06	2.927E-07	7.242E-05
6.000E+03	1.168E-13	9.933E-13	5.560E+01	1.327E-16	9.374E-23	9.937E-22	5.253E-06	2.963E-07	7.298E-05
1.200E+04	1.160E-13	9.909E-13	5.560E+01	1.322E-16	9.300E-23	2.661E-21	5.282E-06	2.972E-07	7.300E-05
1.800E+04	1.152E-13	9.885E-13	5.560E+01	1.318E-16	9.227E-23	4.312E-21	5.311E-06	2.980E-07	7.302E-05

Time Seconds	$Fe(OH)^{2+}$ Moles/L	Fe^+ Moles/L	Fe^{2+}—H Moles/L	Fe^+—H Moles/L
0.	0.	0.	0.	0.
6.000E+02	1.045E-05	5.509E-07	1.322E-09	1.054E-09
1.200E+03	1.590E-05	5.174E-07	8.118E-10	1.024E-09
1.800E+03	1.927E-05	3.076E-07	4.925E-10	7.499E-10
3.000E+03	2.140E-05	2.599E-08	2.006E-10	8.901E-11
6.000E+03	2.147E-05	7.511E-09	1.840E-10	2.608E-11
1.200E+04	2.142E-05	7.566E-09	1.842E-10	2.615E-11
1.800E+04	2.137E-05	7.623E-09	1.844E-10	2.623E-11

Table 4.4. Absorbances calculated for the species concentrations calculated in a simulation of Mathews' experiments.

Time (sec)	Fe^{3+} (mole/liter)	$FeOH^{2+}$ (mole/liter)	Calculated Absorbance at 304 nm
600	4.84E-8	2.06E-5	0.039
1200	1.37E-7	4.27E-5	0.081
1800	2.24E-7	6.06E-5	0.114
3000	2.43E-7	7.24E-5	0.138
6000	2.46E-7	2.70E-5	0.139
12000	2.98E-7	7.30E-5	0.139
18000	2.98E-7	7.30E-5	0.139

There is qualitative agreement between the two sets of data, however. A comparison between the calculated hydronium ion concentrations and the observed hydronium ion concentrations for this mechanism and Mathews' data is shown in Figure 4.4, which shows that the calculated values of the hydronium ion concentrations level off at about the same time as the calculated concentrations of the absorbing species. This observation, coupled with the relationship between the ferric ion hydrolysis reactions and the hydronium ion, suggest that an improved description of the hydrolysis reactions may improve the agreement with the calculated hydronium ion concentrations and the calculated absorbances. At present, the agreement between the calculated hydronium ion concentrations and the hydronium ion concentrations reported by Mathews is within one pH unit.

4.2.2 Conclusions

The Rosinger and Dixon mechanism[4.5] for the radiolysis of water is being extended to account for the presence of anions and cations which may be found in groundwaters. Elementary reactions have been added to this mechanism to account for the presence of dissolved iron species. The mechanism developed thus far shows qualitative agreement with data presented in the literature for iron species which absorb radiant energy at 304 nm. The hydronium ion concentrations calculated with this model are within one pH unit of the hydronium ion concentrations observed in an experiment reported in the literature.

4.2.3 Plans for Future Work

In the near term, the description of the hydrolysis of ferric species will be improved through addition of reactions for additional hydrolysis

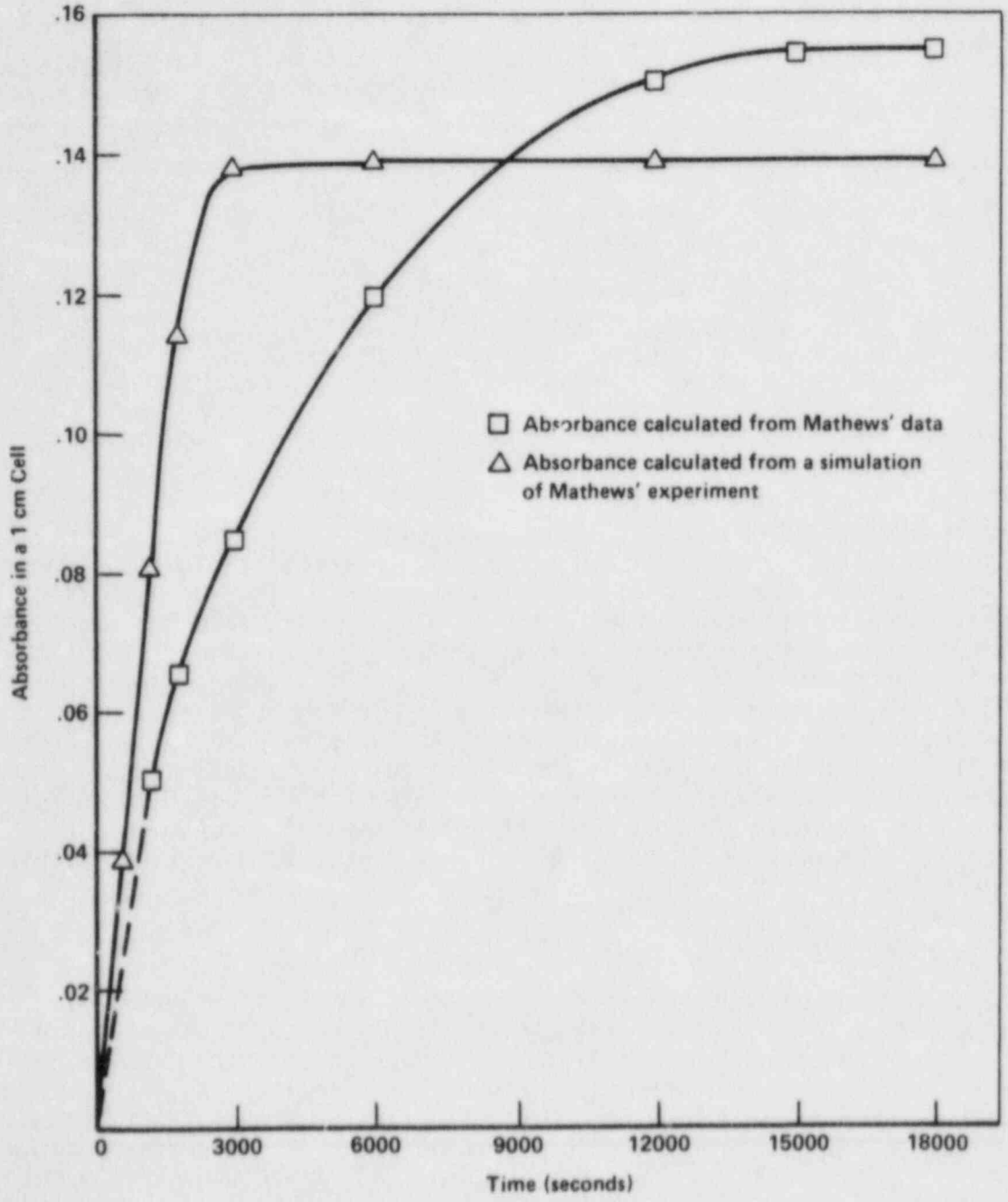

Figure 4.5. Absorption of radiant power at 304 mm in a 1-cm cell for calculated and experimental solution compositions.

products. Additional benchmark calculations will also be performed for simulations of other experiments reported in the literature for the irradiation of ferrous sulfate solutions. Attention will also be given to effects of water chemistry on rate constants used in the radiolysis mechanism which is under development. Longer-term plans call for further extension of the radiolysis description to account for the presence of other anions and cations which may be in groundwaters of potential importance to the disposal of high-level nuclear-waste packages.

4.3 Uncertainty Analysis Methods for Nuclear-Waste-Package Models

This section presents the results of a study to evaluate methods for performing uncertainty analyses of physical models representative of those which are expected to be important in assessing the long-term performance of nuclear-waste-package designs. This evaluation is performed for a simplified, yet realistic, model of a selected physical process which will significantly affect waste-package performance.

The selection of the physical process to be used during this uncertainty analysis evaluation was based on three criteria. First, the physical process should be important to the overall performance of the waste package, yet have large uncertainties in some parameters. Secondly, some data for characterizing these uncertainties should be available for comparison. Finally, if possible, other work should be available for comparison. Based on these criteria, the model for uniform and pitting corrosion which was suggested by Sastre and Pescatore[4.17] was selected.

4.3.1 Corrosion Model

The general form of the corrosion model is given by:[4.17]

$$C_D = (K_u + K_p) \exp(a/T(t))\, O^b\, Cl^c\, t^n$$

$$T(t) = \frac{1}{k}\left(\frac{\alpha}{\pi}\right)^{1/2} \sum_{i=1}^{m} \frac{a_i}{\lambda_i} D(\lambda_i t) + \sum_{j=1}^{R} \frac{d_j}{2\pi k_j L} \ln\left(\frac{d_{j+1}}{d_j}\right) + T_o$$

where C_D is the corrosion depth; $T(t)$ is the time-dependent temperature; K_u and K_p are the uniform and pitting corrosion factors, respectively; O is the oxygen concentration; Cl is the chlorine concentration; t is time; k is the thermal conductivity; α is the thermal diffusivity; d is the diameter of the region; $D(x)$ is the Dawson integral at x; and a, b, c, n, a_i, and λ_i are empirical constants. To check our computer model, the 0.1 to 99.9 percentile spread for the uniform corrosion factor, K_u,

was calculated and compared to the result given in Reference 4.17. The range given in that reference was (0.00147, 676), and the Battelle program found the range to be (0.00157, 636). This range was found to be within the accuracy necessary for this study.

The corrosion model under study requires a total of sixteen inputs, ten of which are random. Table 4.5 gives the distribution type, including constants, with their associated parameters for each of the sixteen inputs. In Table 4.5, the first parameter listed is the value of a constant variable, the lower limit of a uniform distribution, the mean of a normal distribution, and the minimum value of a Rayleigh distribution. The second parameter listed is the upper limit for a uniform distribution, the standard deviation for a normal distribution, and the modal value for the Rayleigh distribution.

4.3.2 Uncertainty-Analysis Methods

The uncertainty analysis methods chosen for study are the ones most widely used in the nuclear power industry: Monte Carlo, Latin Hypercube Sampling (LHS), and Discrete Probability Distribution (DPD) methods. While it is possible to use Monte Carlo methods for the corrosion model used in this study, it is expected that the final model for corrosion and other physical processes (e.g., heat transfer and radiolysis) will require too much computer time if used in a Monte Carlo simulation. Therefore, alternative methods are needed which can accurately approximate the Monte Carlo results.

LHS and DPD methods use an appropriate sampling scheme so that the full sample space required in the Monte Carlo analysis is not needed; thus the computer time is reduced, accompanied by some loss of statistical accuracy. The LHS method, described in Reference 4.18, can be viewed as an extension of quota sampling.[4.19] The DPD method is a form of importance sampling[4.20,4.21].

4.3.3 Results of Uncertainty-Analysis Calculations

Five uncertainty analyses were performed. The first was the Monte Carlo analysis in which 1000 simulations were made. The next two were made using the LHS method in which ten and twenty strata were used. For the final two analyses, the DPD method was used. For these analyses, the standard DPD algorithim cannot be applied unless very few discrete points are used, because even for ten discrete points, a minimum of 2×10^{10} storage spaces are required. We have developed a novel sampling and condensation procedure which alleviates this problem and allows the DPD algorithm to be applied.

Results of the application of each algorithm are shown in Tables 4.6 and 4.7 and in Figure 4.6. Table 4.6 gives a comparison of the LHS results with the Monte Carlo result for the mean corrosion depth, while Table 4.7 gives a comparison of the Monte Carlo and DPD results. As these tables show, both methods provide reasonable approximations to the

Table 4.5. Input data description.

Variable	Distribution Type	Parameter 1(a)	Parameter 2(b)
Rock Parameters			
1. Geothermal Temperature (C)	Uniform	54.0	60.0
2. Thermal Conductivity (W/m/k)	Uniform	1.25	2.50
3. Rock Density (kg/m^3)	Uniform	390.0	2410.0
4. Specific Heat (J/kg/K)	Uniform	820.0	1160.0
Waste Parameters			
5. Waste Age (years)	Constant	0.0	NA
6. Initial Power (kW)	Constant	2100.0	NA
7. Backfill Outer Diameter (m)	Constant	0.686	NA
8. Backfill Thermal Conductivity (W/m/K)	Uniform	0.40	1.40
9. Overpack Outer Diameter (m)	Constant	0.325	NA
10. Canister Wall Thickness (m)	Constant	0.053	NA
11. Canister Length (m)	Constant	4.10	NA
Corrosion Parameters			
12. Pitting Corrosion Factor	Uniform	1.00	6.00
13. Chlorine Concentration (ppm)	Uniform	1.00	101.0
14. Oxygen Concentration (ppm)	Uniform	0.01	3.00
15. Exponent of Time	Normal	0.469	0.0349
16. Uniform Corrosion Parameter (mm/year)	Rayleigh	0.01	118.643

(a)Values given are: lower limit for a uniform distribution, mean value for a normal distribution, minimum value for a Rayleigh distribution, or value for a constant.

(b)Values given are: upper limit for a uniform distribution, standard deviation for a normal distribution, or modal value for a Rayleigh distribution.

Table 4.6. Mean corrosion depth (mm) as calculated by the LHS method.

Year	Monte Carlo	LHS-10	LHS-20
100	15.9	14.1	11.6
200	25.7	22.6	25.8
300	33.8	29.7	32.9
400	40.2	35.5	39.4
500	46.0	41.1	44.5
600	51.6	46.4	49.2
700	56.2	52.1	53.8
800	60.8	57.2	58.2
900	64.9	60.4	62.5
1000	68.9	65.1	66.3

Table 4.7. Mean corrosion depth (mm) as calculated by the DPD method.

Year	Monte Carlo	DPD-10	DPD-20
100	15.9	15.6	15.7
200	25.7	25.1	25.4
300	33.8	33.3	33.0
400	40.2	40.4	39.3
500	46.0	46.5	45.2
600	51.6	51.3	50.6
700	56.2	56.3	55.3
800	60.8	60.6	59.7
900	64.9	64.7	63.8
1000	68.9	68.7	67.9

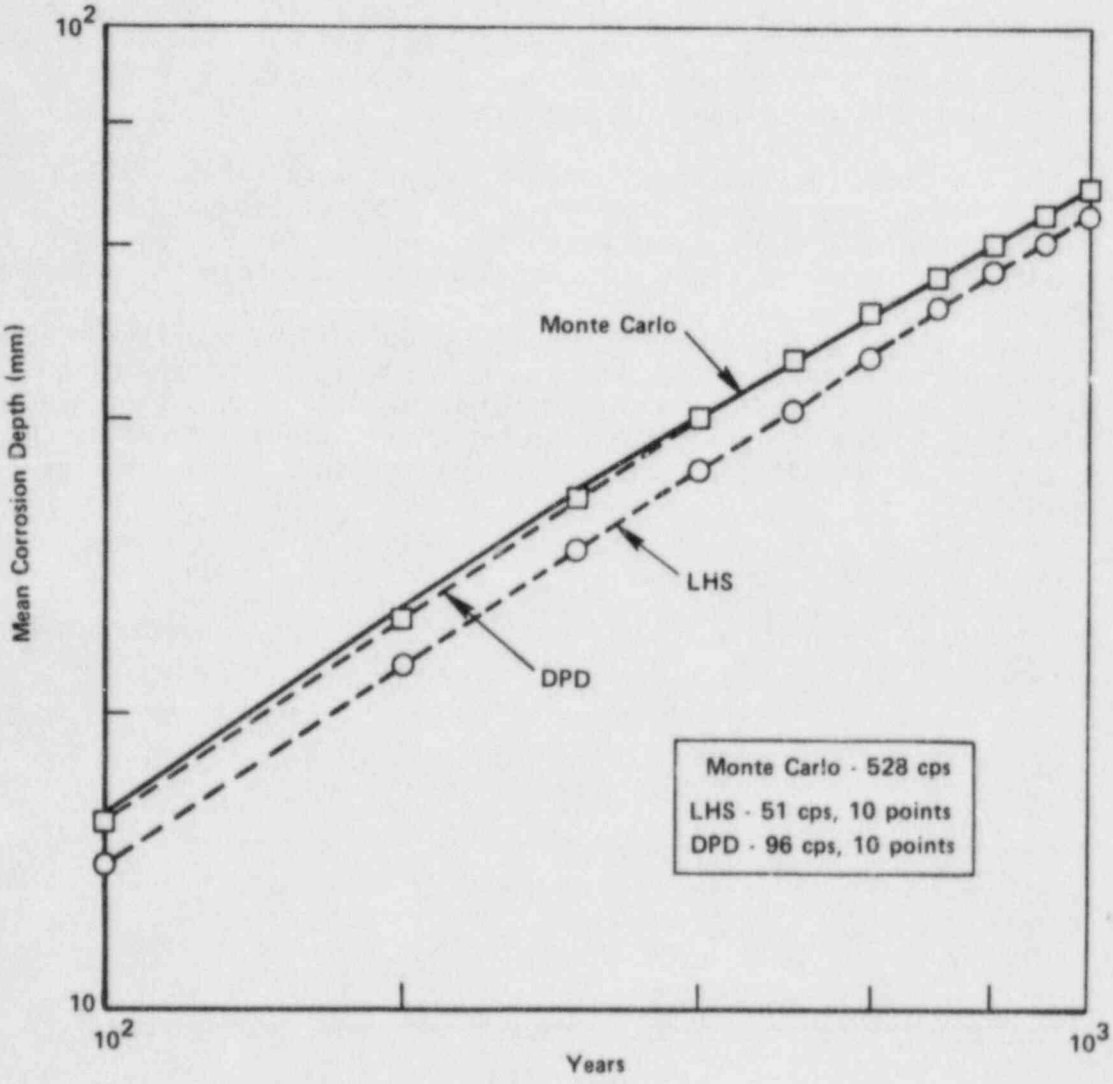

Figure 4.6. Mean corrosion depth calculated by each uncertainty-analysis method.

Processing time is indicated in central processing seconds (cps).

mean; however, the DPD results always provide a closer approximation. Figure 4.6 also indicates the amount of computer time needed to obtain the results using each method; clearly, the LHS and DPD analyses provide an advantage in this respect.

While some indication of the DPD and LHS methods' effectiveness can be obtained from an examination of the mean values, the ultimate goal is to assess each method's ability to indicate the uncertainty in the model. Figure 4.7 presents a plot of the standard deviation calculated by Monte Carlo, DPD, and LHS analysis. From this figure, it is obvious that the DPD method of analysis does considerably better than the LHS method in predicting the standard deviation, which is one measure of the uncertainty in the response of the model.

Table 4.8 gives results of percentile calculations for the DPD-20 and LHS-20 cases, together with the Monte Carlo result at year 1000. As the figures show, the DPD overestimates the spread. The DPD analysis does predict the tenth and ninetieth percentile value within the accuracy of the Monte Carlo result, while the LHS result only falls within the range of the ninety-fifth percentile value. Given the poor performance of the LHS prediction for the other values examined, it is not believed that this result is an indication of anything other than good fortune. Additionally, in the analysis, the response is the corrosion depth, and therefore an overestimate of the spread represents a conservative result.

Table 4.8. Percentile estimates from each of the uncertainty methods.

Percentile	Monte Carlo Value	DPD Value	LHS Value
5	38.07	33.22	49.15
10	43.45	43.62	50.14
90	96.16	96.45	88.68
95	103.9	116.7	104.6

4.3.4 Conclusions

The conclusion reached by this study is that the uncertainty analysis of waste-package models should be performed using DPD methods when a Monte Carlo analysis is not possible. In this study the DPD analysis using 20 discrete points was a factor of 2.3 faster than the Monte Carlo analysis, while the 20-strata LHS run was a factor of 8.2 faster.

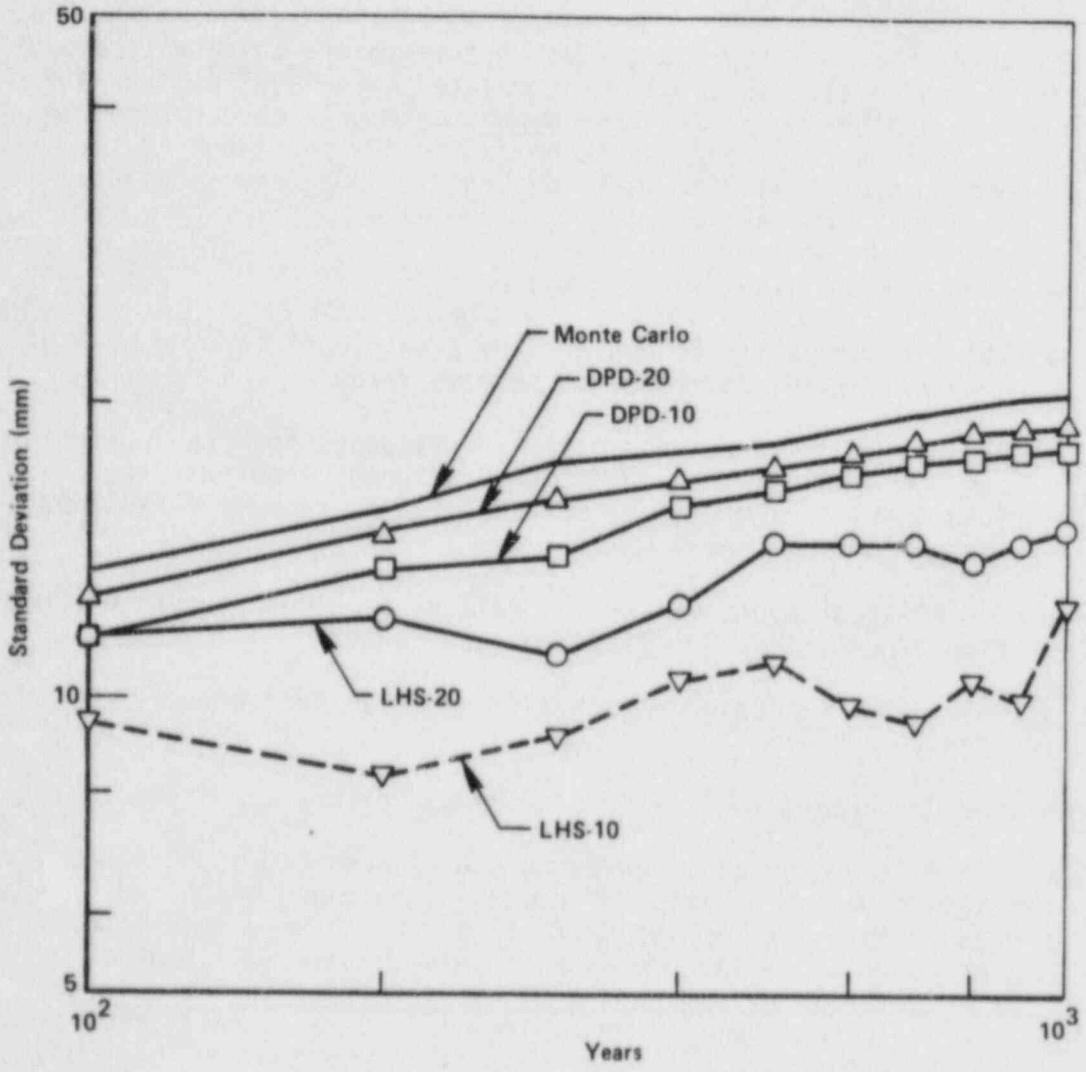

Figure 4.7. Standard deviation of the corrosion depth predicted by each uncertainty-analysis method.

However, given the increased accuracy of the DPD results over the LHS results, DPD methods must still be preferred.

4.3.5 Near Term Plans

No further work is planned for this year.

4.4 Integral Experiments

The integral experiments are a series of experiments which will employ high-level radioactive waste glass, simulated high-level radioactive waste glass, and spent fuel. These experiments will be performed in a radiation field and will address technical issues pertinent to the system performance of nuclear waste packages. Among the technical issues which will be addressed are:

- What are the significant combined effects?
- Is it conservative to neglect the presence of barrier remnants when evaluating radionuclide release rates?
- Are radionuclide release rates for releases from the waste package under in-situ conditions different from existing laboratory determinations of radionuclide release rates from waste-form materials?
- Do different types of barrier failure-openings lead to different time-dependent radionuclide release rates?
- Does gamma radiation affect waste-package performance significantly?
- How does spent fuel perform under repository conditions?

An approach using integral experiments has been chosen because there are many possible combined effects and because the issues are broad. Information gleaned from the combined-effects experiments--observations of reaction products and measurements of release rates--will provide a basis for prioritizing issues and combined effects. The experiments will also provide measurements of radionuclide release rates from spent fuel and high-level-waste glass, as well as information on the mobilities of specific radionuclides in the waste-package environment.

The measurements of release rates are also expected to provide a qualitative evaluation of how release rates are affected by:

- Barrier failure mode
- Radiation fields
- Packing material
- Waste form.

Among the parameters which will be studied in these experiments are:

- Waste form (spent fuel and waste glass)
- Canister failure modes
- Flow rate.

4.4.1 Technical Issues

4.4.1.1 Significant Combined Effects

The use of a predictive methodology for waste-package performance in the licensing process will require a degree of confidence that all important degradation processes are accounted for either explicitly or implicitly in the models. One difficulty, however, is that there are many possible combined effects, and the significance of many possible combined effects is not well understood. The purpose of these experiments is thus to simulate a waste-package environment to provide evidence on what combined effects are important and should be studied in greater detail. This information will be obtained in post-test analyses of the surfaces and interfaces of the materials used in the experiments. For example, if a surface product is observed with a composition indicative of both the metallic barrier and packing materials, it will then be assumed that evidence for an interaction has been observed. This observation would then serve as a partial justification of further basic research and modeling of this interaction. The role of the integral experiments with respect to combined effects is therefore to help prioritize the need for detailed knowledge and models of combined-effects processes. This information will be useful to NRC when evaluating a license application, because it will provide a partial basis for evaluating whether the applicant has adequately addressed an appropriate subset of combined effects and issues.

These experiments are not intended to provide detailed information on the combined-effects processes. They are intended to be scoping experiments that will provide a qualitative basis for identifying those combined-effects processes which might realistically be expected to occur and for prioritizing further research on combined effects.

4.4.1.2 Effect of Barrier Remnants on Release-Rate Assessment

When evaluating release rates of radionuclides from breached waste packages, the effect of any remaining barrier components and corrosion products on the release rate must be considered. Different types of barrier failures (e.g., pitting and cracking) may have different effects on the release rate and hence may affect descriptions such as that used in the WAPPA code where the diffusion coefficient for release to the packing material from the waste form is scaled by the fraction of the barrier area which is failed.[4.22] Corrosion products remaining from barrier-degradation processes may also affect radionuclide release rates by altering the porosity of the surrounding media and thereby affecting

diffusion coefficients. They may also act as agents for physical or chemical sorption of radionuclides, and they may interact chemically with the radionuclides. It will also be necessary to account for effects of corrosion products on local water chemistry.

To address these issues, several experimental tests and post-operation analyses are planned. The effects of barrier failure modes on release rates will be addressed by comparing the releases and release rates associated with different types of small-scale simulated breached canisters (e.g., cracked, pitted, or closure-weld failed), with account taken of the fractional area of the breach. Post-operation analyses of the surfaces, interfaces, simulated corrosion products, and packing material will provide information on interactions between these materials and the released radionuclides.

4.4.1.3 Comparison of Laboratory and In-Situ Release Rates

Radionuclide release rates measured in these experiments on borosilicate-glass and spent-fuel waste forms will be compared with data available in the literature. Experiments which do not have packing material downstream of the waste form will be used to address this issue, since only the release from the waste package and its remnants is of concern. Packing material will be present on the upstream side of the simulated waste package to help provide a suitable aqueous environment.

4.4.1.4 Effect of Failure-Opening Type on Release-Rate Assessment

Experiments will be performed with a variety of canister failure openings. The release rates measured for each of the simulated failure modes will be compared. To facilitate comparison of the release rates, packing material will not be placed downstream of the simulated waste package. Differences in release rates normalized to surface area of the simulated breach may indicate an effect of differing failure openings. Post-operational analyses of the waste-package surfaces will provide additional indications of whether different failure openings cause significant differences in local water chemistry. This may be indicated by differences in the surface composition of the waste-package surfaces in the breach areas for the various simulated failure openings.

4.4.1.5 Effect of Gamma Radiation on Waste-Package Performance

The integral experiments will be performed in a gamma field. The dose rate to the groundwater for these experiments will be 100 R/hr, which is representative of the dose rate to groundwater at the surface of a waste package for borosilicate-glass waste forms at 100 years after reprocessing.

Effects of gamma radiation on the performance of the waste package will be evaluated through post-test examination of corrosion samples placed in flowing simulated groundwater in the radiation field. The corrosion specimens will include a prepitted section of cast steel with machined pits of various depths and diameters, U-bend cast-steel and stainless-steel specimens, and a galvanic-corrosion specimen.

4.4.1.6 Performance of Spent Fuel Under Repository Conditions

These experiments will include four tests with spent fuel. Three of these tests will use failed spent-fuel sections, and one test will be performed with an isolated fuel pellet. All the tests will employ flowing simulated basalt groundwater which has been modified by packing material. Two of the tests with failed spent fuel will also employ simulated corrosion products, basalt, and packing material. Release rates measured in these tests will be compared with release rates for spent fuel in aqueous systems measured by other investigators. Burnup effects will not be addressed in these scoping tests.

4.4.2 Experiments

Integral and control experiments will be performed on radioactive high-level waste glass, simulated PNL 76-68 waste glass, failed spent fuel, and a spent fuel pellet. These tests will be performed in a radiation field representative of that on the outer surface of the waste package. Anoxic basaltic groundwater modified by packing material will be delivered to each test section. Some time-dependent release measurements will be made, followed by post-operation analyses.

4.4.2.1 Apparatus

A sketch of the apparatus is shown in Figure 4.8. Simulated anoxic groundwater is delivered through a cartridge containing basalt rock followed by a cartridge containing packing material. The fluid then enters the manifold system of a 25-channel peristaltic pump. The pump delivers the fluid through independent pump heads to each of 23 different test sections located in an oven in a hot cell. Fluid will then flow from each test section to independent on-line collection ports which will be maintained under an argon cover to prevent back-diffusion of air into the system. The collection ports will be located outside the hot cell and will permit on-line fluid samples to be taken.

Acquisition of equipment and materials for the apparatus has been initiated. Scoping experiments are underway to define the flow path flow-related problems which might arise.

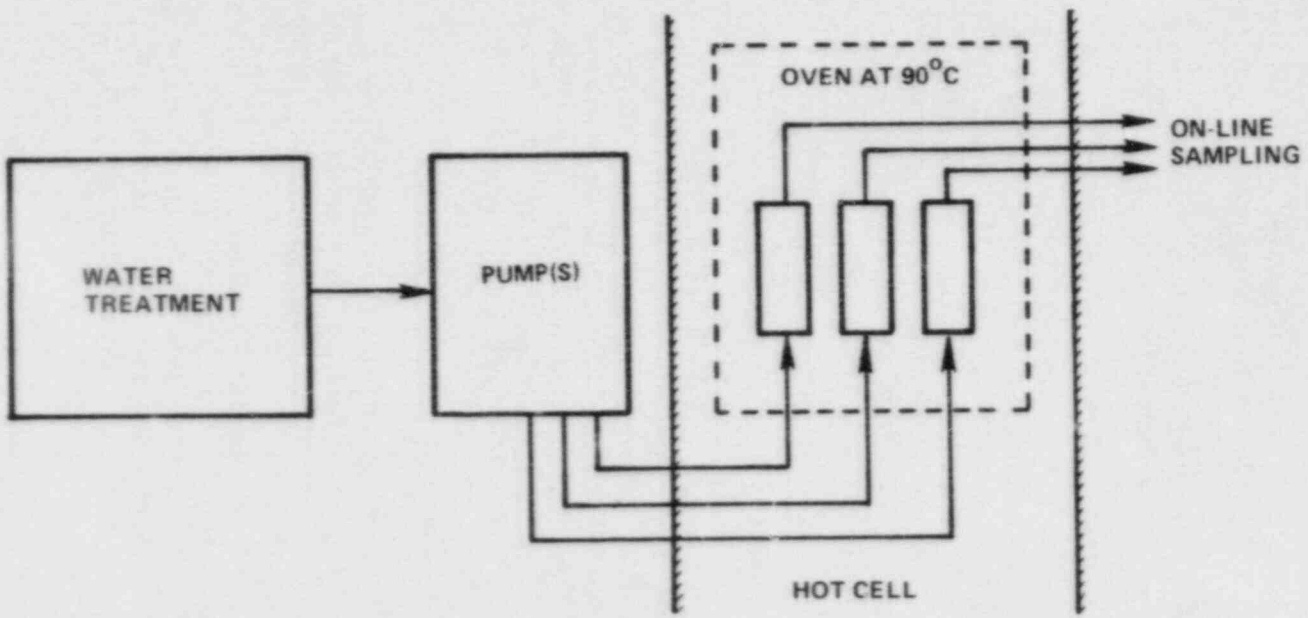

Figure 4.8. Schematic of apparatus to be used in integral experiments.

4.4.2.2 Analysis

Both on-line and post-test analyses will be performed.

The on-line analyses will be performed on fluid effluents taken from individual test trains. These specimens will be analyzed for their gamma-emitting radionuclides by gamma spectroscopy. General elemental analyses will be performed with inductively-coupled argon plasma techniques. If solid phases are observed, the fluid can be filtered with membrane filters and the residue can be examined by such means as scanning electron microscopy. On selected samples, total alpha activity will be measured, and some specific alpha-emitting nuclides will be identified. The radionuclide release data based on the fluid effluent will be presented as total releases for each test section and as releases normalized to exposed surface area of waste form in each test section. These data will be presented as current concentrations and estimated cumulative releases. At the conclusion of the experiments, attempts will be made to integrate the total release from waste forms for selected test sections by summing the inventories of radionuclides in the lines and sorbed on materials. The current concentrations will be presented as a direct function of time, and the cumulative releases will be presented versus time and square root of time.

Following the experiments, post-operation analyses will be performed on samples of components, surfaces, and interfaces removed from the test sections. These analyses will include gamma spectroscopy and a variety of surface techniques including anastigmatic secondary ion mass spectrometry, Auger, electron spectroscopy for chemical analysis, scanning electron microscopy, and electron microprobe.

4.4.3 Near Term Plans

In the near term, the apparatus will be assembled as components are received. Scoping studies will be continued during this period to identify and resolve problems which might arise during the planned experiments.

4.5 References for Section 4

(4.1) C. Q. Buckwalter and L. R. Pederson, "Inhibition of Nuclear Waste Glass Leaching by Chemisorption", J. Am. Ceram. Soc., 65, 431-436, 1982.

(4.2) G. L. McVay and C. Q. Buckwalter, "Effect of Iron on Waste-Glass Leaching", J. Am. Ceram. Soc., 66, 170-174, 1983.

(4.3) A. Barkatt, et al, "Aluminosilicate Saturation as a Solubility Control in Leaching of Nuclear Waste-Form Materials", in "Materials Characterization Center Workshop on Leaching Mechanisms of Nuclear Waste Forms", J. E. Mendel (Compiler), PNL-4382 (August 1982).

(4.4) "Long-Term Performance of High-Level Waste Packaging", D. Stahl and N. E. Miller (Compilers), NUREG/CR-3427, Vol. 4, BMI-2113 (June 1984), Section 4.

(4.5) E.L.J. Rosinger and R.S. Dixon, "Mathematical Modeling of Water Radiolysis: A Discussion of Versions", AECL-5958 (1977).

(4.6) H. Christensen and E. Bjergbakke, "Radiolysis of Groundwater from HLW Stored in Copper Canisters", SKBF-KBS-TR-82-02 (1982).

(4.7) M. B. Carver, D. V. Hanley, and K. R. Chaplin, "MAKSIMA-CHEMIST: A Program for Mass Action Kinetics Simulation by Automatic Chemical Equation Manipulation and Integration Using Stiff Techniques", AECL-6413 (1979).

(4.8) R. W. Mathews, "The Radiation Chemistry of Aqueous Ferrous Sulphate Solutions at Natural pH," Aust. J. Chem. 36 (1983) 1305-17.

(4.9) B.H.J. Bielski and J. M. Gebicki, "Species in Irradiated Oxygenated Water," Advances in Radiation Chemistry, ed. M. Burton and J. L. Magee, V. 2, Wiley-Interscience, 1980.

(4.10) R. N. Sylva, "The Hydrolysis of Iron (III)", Rev. Pure and Appl. Chem., 22 (1972) 115-32.

(4.11) P. Hemmes et al., "Kinetics of Hydrolysis of Ferric Ion in Dilute Aqueous Solution", J. Phys. Chem. 75 (1971) 929-32.

(4.12) A. P. Olson and T. R. Simonson, "The Hydrolysis of Ferric Ion", J. Chem. Phys. 17 (1949) 1322-25.

(4.13) M. T. Nenadovic et al., "Pulse Radiolysis Studies of Iron (I) in Aqueous Solutions", J. Chem. Soc., Dalton Trans. 4 (1980) 586-9.

(4.14) R. C. Weast, ed., Handbook of Chemistry and Physics, CRC Press, (1974) p. F-198.

(4.15) R. W. Mathews, "Effect of Solute Concentration and Temperature on the Ceric-Cerous Dosimeter", Radiation Research 55 (1973) 242-55.

(4.16) E. Rabinowitch and W. H. Stockmayer, "Association of Ferric Ions with Chloride, Bromide, and Hydroxyl Ions (A Spectroscopic Study)", J. Amer. Chem. Soc. 64 (1942) 335-47.

(4.17) C. Sastre and C. Pescatore, "Draft Technical Statement of Waste Package Reliability", NUREG-0997R (November 1983).

(4.18) M. D. McKay, W. J. Conover, and R. J. Beckman, "A Comparison of Three Methods for Selecting Values of Input Variables in the Analysis of Output from a Computer Code", Techometrics, 21, No. 2 (1979).

(4.19) H. A. Steinberg, "Generalized Quota Sampling", Nuclear Science and Engineering, 15 (1963).

(4.20) S. Kaplan, "On the Method of Discrete Probability Distributions in Risk and Reliability-Application to Seismic Risk Assessment", Risk Analysis, 1, No. 3 (1981).

(4.21) R. E. Kurth and D. C. Cox, "Discrete Probability Distributions for Probabilistic Fracture Mechanics", to be published in Risk Analysis (1984).

(4.22) INTERA Environmental Consultants, "WAPPA: A Waste Package Performance Assessment Code", ONWI-452 (April 1983), p. 149.

5. QUALITY ASSURANCE

Quality assurance surveillance of the various program activities continued during the quarter. One new procedure, WF-PP-26.1 Revision 0, was prepared and approved while two others, WF-PP-11 and -14 were revised to Revision 1. One other procedure, WF-PP-27, was revised two times during the quarter to Revision 4 to reflect changes in testing requirements. As of this date there are 34 approved QA procedures and two approved work instructions for the program.

A summary of the program procedures which are being used to conduct the experimental program is given in Table 5.1. Included is the procedure number, the current revision number, the title, and the status.

Quality assurance surveillance activities will continue. Procedures will be revised and new ones prepared as necessary to meet program requirements.

Table 5.1. Status of NRC waste packaging program QA procedures.

Procedure No.	Title	Status
WF-PP-1 Revision 0	Procedures for Record Keeping and Documentation for NRC Waste Form System Model Development	Approved
WF-PP-5 Revision 0	Procedures for Record Keeping and Documentation for Separate Effects Model Development	Approved
WF-PP-10 Revision 0	Laboratory Procedure for Preparation of Glasses for NRC Waste Form Project	Approved
WF-PP-11 Revision 1	Laboratory Procedures for Preparation of Teflon-Leach Containers	Approved
WF-PP-14 Revision 1	Laboratory Procedure for Leaching Glass Samples	Approved
WF-PP-16 Revision 0	Laboratory Procedure for Operating the Orton Dilatometer	Approved
WF-PP-20 Revision 0	Procedure for Determining the Corrosion Rates of Alloys at High Temperatures	Approved
WF-PP-25 Revision 0	Procedure for Preparation of Carbon-Steel Casting	Approved
WF-PP-26 Revision 0	Procedure for Preparation of Steel Hydrogen-Embrittlement Test Specimens	Approved
WF-PP-26.1 Revision 0	Procedure for Preparation of Hydrogen-Embrittlement Test Specimens from Steel or Iron Samples	Approved

Table 5.1. Continued.

Procedure No.	Title	Status
WF-PP-27 Revision 4	Procedure for J-Testing Compact Tension Specimens	Approved
WF-PP-28 Revision 1	Procedure for Performing Tension Tests of Steel Specimens	Approved
WF-PP-29 Revision 0	Procedure for Conducting Hydrogen-Absorption Experiments	Approved
WF-PP-30 Revision 0	Laboratory Procedure for Preparation, Cleaning, and Evaluation of Titanium Grade-12 Specimens for Corrosion Studies of the Overpack Performance for the NRC Waste Packaging Program	Approved
WF-PP-31 Revision 0	Laboratory Procedure for Preparation, Cleaning, and Evaluation of Cast and Wrought Carbon Steel Specimens for Corrosion Studies of the Overpack Performance for the NRC Waste Packaging Program	Approved
WF-PP-32 Revision 0	Procedure for Preparation of Brine A for Corrosion Testing Under Simulated Repository Conditions	Approved
WF-PP-33 Revision 0	Procedure for Preparation of Simulated Basalt Groundwater Solution	Approved
WF-PP-33.1 Revision 0	Procedure for Preparation of Basalt Rock for Use in Corrosion Studies for the NRC Waste Packaging Program	Approved
WF-PP-34 Revision 0	Procedure for Preparation of Simulated Tuff Groundwater Solutions	To be Written

Table 5.1. Continued.

Procedure No.	Title	Status
WF-PP-35 Revision 1	Procedure for Performing Autoclave Exposures for Corrosion Tests in Simulated Brines	Approved
WF-PP-35.1 Revision 0	Procedure for Performing Autoclave Exposures for Corrosion Tests in Simulated Brines Using Sealed Internal Canister	Approved
WF-PP-36 Revision 0	Procedure for Performing Stagnant Autoclave Exposures for Corrosion Tests in Simulated Basalt or Tuff Groundwaters	Approved
WF-PP-37 Revision 0	Laboratory Procedure for Preparing Polarization Resistance Specimens, Performing Polarization Resistance Measurements and Evaluating Polarization Resistance Data	Approved
WF-PP-37.1 Revision 0	Laboratory Procedure for Performing Eh and Corrosion Potential Measurements in Autoclave Exposures in Simulated Basalt and Tuff Groundwater	Approved
WF-PP-37.2 Revision 0	Laboratory Procedure for Determination of the Polarization Behavior of Metal Specimens at Ambient Pressure	Approved
WF-PP-38 Revision 0	Procedure for Preparing and Evaluation of U-Bend Specimens for Stress Corrosion Studies of Overpack Materials for the NRC Waste Packaging Project	Approved
WF-PP-38.1 Revision 0	Procedure for Performing and Evaluating 3 Point Bend Beam Specimens for Stress Corrosion Studies of Overpack Materials for NRC Waste Package Program	Approved

Table 5.1. Continued.

Procedure No.	Title	Status
WF-PP-39 Revision 0	Procedure for Preparing, Testing and Evaluating Crevice Corrosion Specimens of Titanium Grade-12 and Cast Steel	Approved
WF-PP-40 Revision 0	Laboratory Procedures for Preparation, Cleaning, and Evaluation of Thermogalvanic and Heat-Transfer Specimens	Approved
WF-PP-41 Revision 0	Laboratory Procedures for Determination of Corrosion Rates Under Heat-Transfer Conditions	Approved
WF-PP-42 Revision 0	Laboratory Procedure for Determination of Thermogalvanic Corrosion Rates	Approved
WF-PP-43 Revision 0	Procedure for Welding Titanium Grade-12 Plate for Use in Corrosion Studies of Overpack Materials for NRC Waste Isolation Project	Approved
WF-PP-44 Revision 0	Procedure for Welding Cast and Wrought Steel Specimens	To be Written
WF-PP-45 Revision 0	Laboratory Procedure for Preparing and Evaluating Slow Strain-Rate Specimens and for Performing Slow Strain-Rate Tests	Approved
WF-PP-45.1 Revision 0	Laboratory Procedures for Performing Slow Strain-Rate Tests Under Potentiostated Conditions	Approved
WF-PP-46 Revision 0	Procedure for Preparation of Titanium Grade-12 Corrosion Specimens with Metallic Iron Embedded in the Surface	Approved

DISTRIBUTION LIST

Office of Regulatory Research
Division of Radiation Programs and Earth Sciences
Mail Stop 1130 SS
U.S. Nuclear Regulatory Commission, Washington, D.C. 20555

Attn: Division Director/Deputy Director
E. F. Conti, Chief, Waste Management Branch
F. A. Costanzi
J. R. Randall
M. B. McNeil
K. S. Kim, Project Manager (15)

Division of Waste Management, NMSS
Mail Stop 623 SS
U.S. Nuclear Regulatory Commission, Washington, D.C. 20555

Attn: Division Director/Deupty Director
Chief, Engineering Branch
E. A. Wick
M. Tokar
K. C. Chang
Document Control Center

Advisory Committee on Reactor Safeguards
Mail Stop H-1016
U.S. Nuclear Regulatory Commission, Washington, D.C. 20555

Attn: Waste Management Subcommittee
R. C. Tang

Battelle's Columbus Laboratories
505 King Avenue
Columbus, Ohio 43201-2693

Attn: D. Stahl, Program Manager (50)

DISTRIBUTION LIST (Continued)

Martin A. Molecke
Sandia National Lab.
Albuquerque, NM 87185

Neville Pugh
National Bureau of Standards
Washington, D.C. 20234

Nicholas Grant
Department of Metallurgy
Massachusetts Institute
of Technology
Cambridge, MA 02139

Jerome Kruger
Corrosion Section
National Bureau of Standards
Washington, D.C. 20234

Tae-Moon Ann
Brookhaven National Lab.
Upton, NY 11973

Don J. Bradley
Waste Package Programs
Battelle Pacific Northwest Labs
Richland, WA 99352

Allen G. Goff
Oak Ridge National Laboratory
P.O. Box X
Oak Ridge, TN 37830

Lynn Hobbs
Department of Materials Science
Massachusetts Institute of
Technology
77 Massachusetts Avenue
Cambridge, MA 02139

Richard E. Westerman
Pacific Northwest Lab.
P.O. Box 999
Richland, WA 99352

Thomas D. Chikalla
Pacific Northwest Lab.
P.O. Box 999
Richland, WA 99352

John Crandall
Savannah River Lab.
Aiken, SC 29808

Edward J. Hennelly
Savannah River Lab.
Aiken, SC 29808

Arthur A. Bauer
Office of Nuclear Waste Isolation
Battelle Memorial Institute
505 King Avenue
Columbus, OH 43201

Michael Smith
Basalt Waste Isolation Projects
Rockwell Hanford Operation
Richland, WA 99352

Kenneth Russell
Department of Materials Science
and Engineering
Massachusetts Institute of
Technology
Cambridge, MA 02139

Robert H. Doremus
Materials Engineering Department
Rensselaer Polytechnic Institute
Troy, NY 12181

David C. Kocher
Oak Ridge National Lab.
P.O. Box X
Oak Ridge, TN 37830

Stanley Wolf
DOE/BES
Washington, D.C. 20585

Neville Moody
Sandia Livermore Lab.
Livermore, CA 94550

Donald E. Clark
ONWI
Battelle Memorial Institute
505 King Avenue
Columbus, OH 43201

DISTRIBUTION LIST (Continued)

Martin Seitz
Argonne National Lab.
Argonne, IL 60439

Martin J. Steindler
Argonne National Lab.
Argonne, IL 60439

Donald G. Schweitzer
Brookhaven National Lab.
Upton, NY 11973

Peter Soo
Brookhaven National Lab.
Upton, NY 11973

David Martin
Iowa State University
Ames, IA 50011

Harold Wollenberg
Lawrence Berkeley Lab.
Berkeley, CA 94720

Nestor Ortiz
Sandia National Lab.
Albuquerque, NM 87185

Pedro B. Macedo
Catholic University of America
Washington, D.C. 20064

Robert Williams
Electric Power Research Institute
P.O. Box 10412
Palo Alto, CA 94301

William P. Reed
U.S. Department of Commerce
National Bureau of Standards
Washington, D.C. 20234

Ray Walton
U.S. Department of Energy
Washington, D.C. 20545

John E. Mendel
Materials Characterization Center
Pacific Northwest Lab.
Richland, WA 99352

Larry Hench
University of Florida
Gainesville, FL 32611

Davis E. Clark
University of Florida
Gainesville, FL 32611

Joseph Mascara
MS 5650 NL
U.S. Nuclear Reg. Comm.
Washington, DC 20555

Ken W. Stephens
The Aerospace Corp., Suite 400
955 L'Enfant Plaza, S.W.
Washington, DC 20024

Robert S. Dyer
Office of Radiation Programs (ANR-461)
U.S. Environmental Protection Agency
401 M Street, S.W.
Washington, DC 20460

Lorenzo Ricks
Office of Energy Research
U.S. Department of Energy
Washington, D.C. 20545

Larry Evans
Armco Research Center
703 Curtis Avenue
Middletown, OH 45043

Woody Swope
Armco Stainless Steel Division
P.O. Box 1697
Baltimore, MD 21203

M. John Plodinec
Savannah River Laboratory
Aiken, SC 29808

Dennis R. Floyd
Manufacturing Sciences Corp.
711 Walnut Street
Boulder, CO 80302

NRC FORM 335 (11-81) U.S. NUCLEAR REGULATORY COMMISSION

BIBLIOGRAPHIC DATA SHEET

1. REPORT NUMBER (Assigned by DDC)
NUREG/CR-3900, Vol. 1

4. TITLE AND SUBTITLE (Add Volume No., if appropriate)
Long-Term Performance of Materials Used for High-Level Waste Packaging, First Quarterly Report, Year Three April - June 1984

2. (Leave blank)

3. RECIPIENT'S ACCESSION NO.

7. AUTHOR(S)
Compiled by D. Stahl and N. E. Miller

5. DATE REPORT COMPLETED
MONTH: July YEAR: 1984

9. PERFORMING ORGANIZATION NAME AND MAILING ADDRESS (Include Zip Code)
Battelle's Columbus Laboratories
505 King Avenue
Columbus, Ohio 43201-2693

DATE REPORT ISSUED
MONTH: September YEAR: 1984

6. (Leave blank)

8. (Leave blank)

12. SPONSORING ORGANIZATION NAME AND MAILING ADDRESS (Include Zip Code)
Division of Radiation Programs and Earth Sciences
Office of Nuclear Regulatory Research
U.S. Nuclear Regulatory Commission
Washington, D.C. 20555

10. PROJECT/TASK/WORK UNIT NO.

11. FIN NO.
B6764

13. TYPE OF REPORT
Quarterly

PERIOD COVERED (Inclusive dates)
April-June 1984

15. SUPPLEMENTARY NOTES

14. (Leave blank)

16. ABSTRACT (200 words or less)

Devitrification severity of glass waste forms is being studied in terms of volume fraction of crystallization and crystal grain size. Glass-water contact during the heating and cooling periods of glass leaching experiments is being evaluated for its effect on the overall results of the isothermal period. Modeling efforts included the study of possible colloid formation and the change of water chemistry during glass dissolution. The electrochemical properties of container steels were found to be only slightly affected by the groundwater-species concentration, the presence of basalt rock, or the steels' cleanliness or microstructure. Hydrogen-embrittlement susceptibility may increase at expected repository temperatures. Results of the corrosion-modeling effort suggest that radiolysis may significantly affect general-corrosion kinetics. The water-radiolysis model was extended to account for more groundwater species and was used to predict the concentrations of two species in aqueous iron sulfate; results were compared with experimental data. A method was selected for performing uncertainty analyses of waste-package models. Integral experiments have been designed to address the combined effects of repository conditions on the waste package.

17. KEY WORDS AND DOCUMENT ANALYSIS

17a. DESCRIPTORS

High-level waste
Waste package
Waste form/container/overpack

17b. IDENTIFIERS/OPEN-ENDED TERMS

18. AVAILABILITY STATEMENT
Unlimited

19. SECURITY CLASS (This report)
Unclassified

21. NO. OF PAGES

20. SECURITY CLASS (This page)
Unclassified

22. PRICE
$

105-M